Superparamagnetic Iron (III) Oxide Nanoparticle Polymer (SPIONP): Fabrication and Properties

by

Jia Zhuo (Cheryl) Cheng

MSc Research

Department of Electronics

University of York

July 2012

Abstract:

It has been found that the magnetic ground state of nanoparticles can be heavily influenced by the size and macrostructure of the particles, which behave significantly differently from the bulk materials. To obtain superparamagnetic iron particles, co-precipitation technique is applied. Seven different samples (S1-S7) are fabricated under varied conditions by changing the pH value or the reaction temperature. In order to determine the size and properties of the SPIONs manufactured, different electron microscopes and VSM (Vibrating Sample Magnetometers) are applied. S6, which is fabricated at 60℃ with pH value 2.75, has the most stable and ideal morphological and magnetic properties.

The idea of producing an elastic magnetic polymer by mixing superparamagnetic iron oxide particles and silicone sealant, Methyltriacetoxysilane and Ethyltriacetoxysilane, termed SPIONP (Superparamagnetic Iron Oxide Nanoparticle Polymer) is proposed to investigate if the distance between the particles can be changed due to the strain applied to enhance their interaction (by direct exchange interaction or dipole interaction) so that they become ferromagnetic or ferrimagnetic. A particle concentration of 30% of the SPIONP pellets was found as the critical locus of particle interaction. The VSM result shows a reduced magnetization after compression. The deformation of the pellets results in a change of distance between the SPIONs in the silicone matrix, which strongly influences the dipole interaction, in another word, the magnetic properties could be altered by stain change of SPIONP.

List of Contents

List of Tables:

List of Illustration:

Acknowledgements:

This thesis would not have been possibly accomplished without the guidance and the help of my supervisor, Prof. Yongbing Xu who contributed and extended his valuable assistance in the preparation and completion of this research. I will never be able to forget his sincerity, inspiration and encouragement.

Also, Dr. Martin Robinson for his unselfish and kindest support as my thesis adviser;

Secondly, I would like to express my deepest gratitude to several individuals;

Dr. Iain Will, who has always been there offering his generous consultation and support to me; Mr Charan Panesar, who has shown me an incredibly talent of crafting ability with making all our designs real and assembled VSM from scratch; Mr Cong Lu and Mr James Sizeland who have both spent remarkably long time to help me with all the TEM and SEM work. Mr Nicholas Maltby, who set up the whole labview software system of VSM and always encouraging me; Mr Er Liu and Miss An Ding, for their care and attention; Mr Shuo Zhao, for his generous help on 3-dimension Graphs.

Besides, I also want to acknowledge Prof. Kevin O'Grady to generously give me permissions to access to his VSM in physics department and has given me a number of suggestions about my research; and also his supporting staff and students, Dr. Alejandro Gomez Roca, Nick and Robbet who have given me instructions on preparing samples and taking test on VSM.

Last but not the least, my family, my friends in Electronics department and the omnipresent God, for giving me the strength finish this work.

Declaration:

This thesis is a result of all author's research work regarding to the topic. No part of this thesis has been published or submitted for publication.

The author declare that this work does not infringe upon anyone’s copyright nor violate any proprietary rights and that any ideas, techniques, quotations, or any other material from the work of other people included in this thesis, published or otherwise, are fully acknowledged in accordance with the standard referencing practices.

Chapter 1: Introduction

1.1 Introduction

Magnetic nanoparticles are widely applied in diverse technological industries such as recording media, biomedical applications, environmental sensors etc. The study of the properties of magnetic nano-scale particles is one of the most essential focuses of material physics, medicine, biological and environmental sciences. *Nanoparticles are defined as particles with size in the range of 1 to 100 nm at least in one of the three dimensions.* [1] **[(R. Nagarajan, T. Alan Hatton,, September 19, 2008)]** Research shows that their distinguishing characteristics and unique behavior are due to the tremendous surface area and inequable magnetic properties compared to the bulk materials. Scientists have begun to synthesize new materials to satisfy different demands in various applications of industry and biomedical engineering.

One of the key components in making new materials or applications is to understand the magnetic properties of nanoparticles. "*The properties of materials composed of magnetic nanoparticles are a result of both the intrinsic properties of the particles and the interactions between them.*"**2 (Kodama, 1999)** Superparamagnetism and ferromagnetism are two of the forms of magnetisms that appear in nanoparticles, and these need to be understood before any further theoretical explorations are made.

The magnetic polymer is a functionally complex material synthesized by adding magnetic nanoparticles to polymers including silicone and plastic. It is widely used in aeronautical engineering, from the automotive industry, computational techniques to

photocopiers. The magnetic polymer is gradually replacing conventional sintered magnets in the fields of copier developer rollers, fuser rollers, automotive instrumentation and robot-controlled components.

1.2 General Properties and Production of Magnetic Particles

1.2.1 Ferromagnetism

Ferromagnetism is the mechanism that generates permanent magnets, and ferromagnets form one of the most important classes of functional materials. They have high permeabilities and retain their magnetization while exposed to a magnetic field even after it is removed. Common ferromagnetic materials are iron (Fe), cobalt (Co) and nickel (Ni). The electronic spins of unfilled d-bands spontaneously align parallel to one another inside a domain below a critical temperature, T_C (Curie).

A hysteresis loop is apparently one of the best ways to distribute the magnetic properties of ferromagnets (**Fig. 1**). As shown below, when the field strength H approaches a certain point and the saturation magnetization, M_S, is reached, the magnetization will not increase any further no matter how strong H is. When H is reduced to zero, the magnetization of the material is maintained at M_S at first, and then slowly decreases to the isothermal remanent magnetization, M_{rs}. The coercive force, or Coercivity, is "the intensity of the applied magnetic field required to reduce the magnetization of that material to zero after the magnetization of the sample has been driven to saturation." [3] **(Livingston, 1981)**

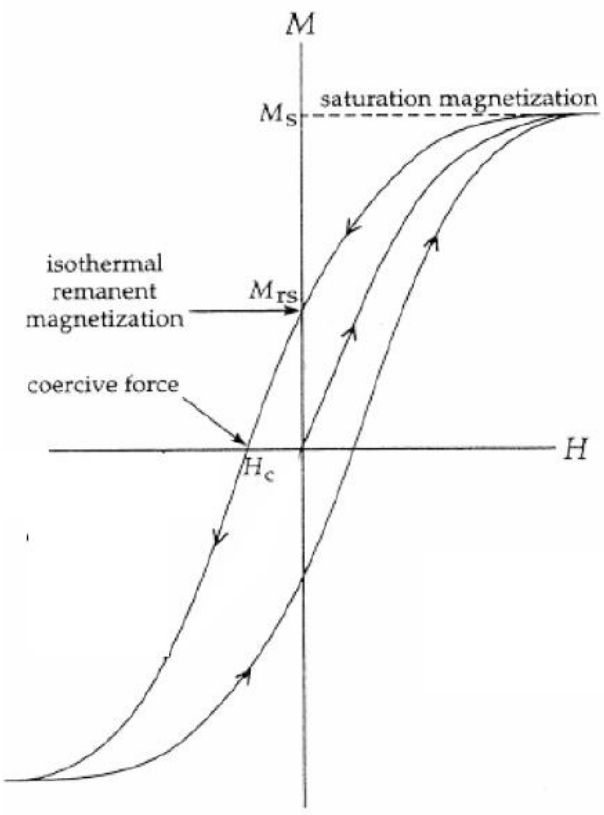

Figure 1: hysteresis loop of a ferromagnetic material, where M is the magnetization; H is the magnetic field applied; MS is the saturation magnetization; HC is the coercive force. [Source: [4]**(Anon., 2007)**]

The applications of ferromagnetic materials can be found everywhere in our daily lives for example, from electromagnets, transformers, magnetic recording materials, permanent magnets, to inductance cores. There will be a detailed discussion of these in the following chapters.

1.2.2 Superparamagnetism

Scientists have been making magnetic metal materials with small dispersions since the 1930s.[5] [**(Shih, 1931)**], however the first and actual nano-sized particle modelization was achieved about a decade later, in the late '40s. During the modelization, it was considered that the magnetic moment would follow an Arrhenius law, with a characteristic relaxation time τ, which was only solved by Néel in 1949. [6][(L. Néel, 1949)] "He supposed that each nanoparticles was formed by rigidly aligned spins that rotate coherently during magnetization reversal, considering the case of uniaxial anisotropy when the energy barrier is much larger than the thermal energy of the system." [7] [(M. Knobel, 2008)]

Superparamagnetism appears in tiny ferromagnetic or ferrimagnetic nanoparticles which are single-domain. In sufficiently small magnetic atoms, the energy needed to get into the magnetic domain is larger than the energy needed to maintain its single domain. If there is no external magnetic field applied, the overall magnetization is zero and the time of magnetization of the nanoparticles is longer than that of the *Néel Relaxation Time*. That is to say, these nanoparticles are in a superparamagnetic state. In the meantime, they can be magnetized and appear to be paramagnetic but with a much higher susceptibility if an external magnetic field is applied.

The relationship between temperature and volume of the particles for superparamagnetism is proportional, that is, to be superparamagnetic, a higher temperature must be reached for larger particle size.

$$\mathbf{K_u V = K_B T}$$

Superparamagnetism normally occurs below the Curie temperature of the material. The difference between ferromagnetism and superparamagnetism can be illustrated by the following. (**Fig. 2**)

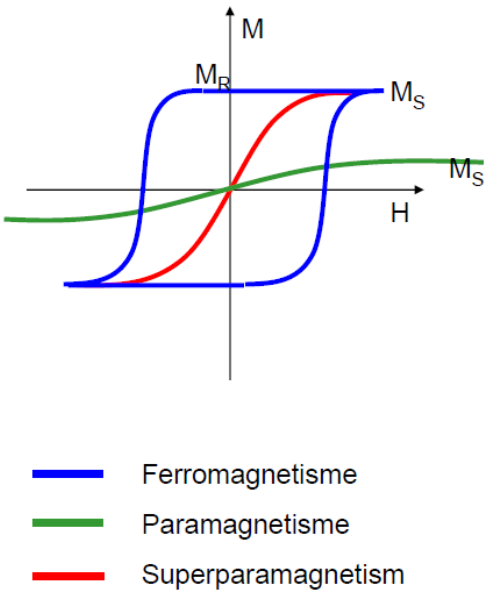

Figure 2: Superparamagnetic materials have very high saturation magnetization, MS, and no remanence MR=0 8 [Source: [4] **(Anon., 2007)**]

The general applications of superparamagnetic materials are: ferrofluids, superparamagnetic clustering, imaging (MRI), magnetic separation (cell, DNA) and medical treatments (targeting drug delivery). A detailed introduction to applications will be given in the next section.

1.3 Objective

The aim of the experiments is to produce an elastic magnetic polymer by mixing superparamagnetic iron oxide particles with silicone sealant (Methyltriacetoxysilane and Ethyltriacetoxysilane) and measuring them in VSM to investigate whether the distance between the particles can be changed to influence their interaction (by direct exchange interaction or dipole interaction), i.e., whether the magnetic properties of SPIONP could be altered by the stain.

There are two main steps in producing the elastic Superparamagnetic Iron Oxide Nanoparticles Polymer (SPIONP). The first and most fundamental one is to obtain nano-size iron (III) particles by using the co-precipitation technique. Details of production and the instrument setup will be given in Chapter 5 along with the corresponding measurements of the properties of the particles.

Chapter 2: Applications of Magnetic Particles and Literature Review

Magnetic particles are widely utilized in a broad range of applications. Particles with different magnetic properties, sizes, surface characteristics, structures and shapes are demanded in different fields of industry/applications. Recent research shows that the main applications of magnetic particles, including resonance imaging, magnetic recording media, drug targeting, biomedical treatment and environmental applications are developing rapidly.

2.1 Biomedical Application and Literature Review

Superparamagnetic particles are used in the following two biomedical applications:

- Detection: MRI (Magnetic Resonance Imaging)
- Treatment: Hyperthermia, Drug delivery [8] **[(A.S.Teja, 2009)**

MRI is a very powerful imaging method which is also widely used in clinical medicine. Superparamagnetic iron oxide nanoparticles (SPIONPs) coated with hydrophilic polymers, such as poly(oligo(ethylene oxide) monomethyl ether methacrylate) (POEOMA), accumulate in tissues after injection and lead to the enhancement of proton relaxation compared to neighboring tissues. [9] **[** (J.K.Oh, 2011)] Being the core contrast agents in the in vivo MRI process, SPIONPs allow the determination of diseased tissue

among healthy ones. (**Fig.3)** Basically, the smaller-sized particles with a more hydrophilic surface will have a longer plasma half-life and lead to easier elimination of the SPIONPs in blood circulation.[10] **(Mornet S, 2004)**

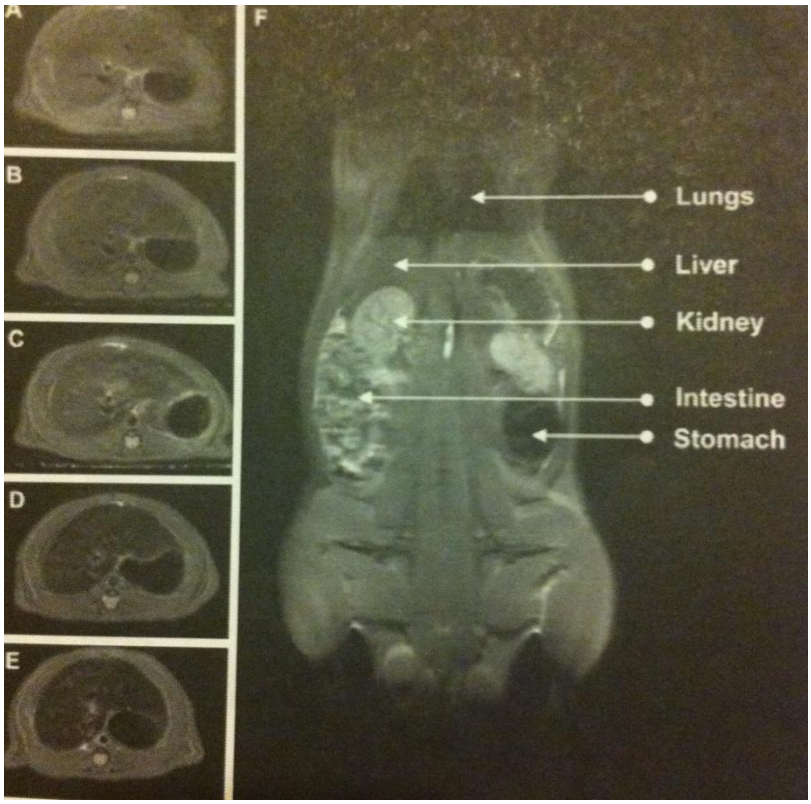

Figure 3: MR images of a live rat after injection of a solution containing SPIONPs coated with hydrophilic polymer (d=10 nm). Left images show liver selections measured at (A) 0 min, (B) 15 MIN, (C) 1 hr, (D) 2 hrs, and (E) 6 hrs. (F) shows a coronal section of the body. [Source: [11] **(Lutz-f, 2006)**.]

Functionalized SPIONPs are also applied in drug delivery and hyperthermia, the cancer therapy. Polymer- or protein-coated particles with attached drugs are injected and led through the body by supplying an external magnetic field. After being stabilized in the cell, the drugs are released upon the collapse of micellar aggregates in the cell. The primary requirements for drug delivery techniques are: stability for prolonged

circulation, controllable release of therapeutics, non-toxicity to cells and high loading efficiency [11]. In practice, the size of the active magnetic core is about 2-3 nm whereas, with coating, it reaches a size of around 10 nm.

Similar to the first processes in drug delivery, SPIONPs are injected into the human body and translocated to the tumours. By utilizing the magnetic properties of SPIONPs, under the condition of exposure to an alternating external magnetic field, tumour cells can be heated up to forty-five degrees where they are irreversibly damaged due to a higher sensitivity than healthy cells. The external magnetic field provides energy for both the magnetic moments and the dissipated thermal energy which increases the temperature of the tumour cells. The heating rate depends on the size of the SPIONPs.

2.2 Environmental Applications and Literature Review

The Earth is now suffering serious consequences from global environmental issues. Human beings have to face all kinds of pollution and severely impacted ecosystem change. The biggest challenge for scientists is how to detect the pollutants, improve the environment and in the meantime, prevent it from becoming worse. Many environmental applications involve not only magnetic nanoparticles but also other complex nanostructures.

Water purification: The water crisis has become a big issue due to global warming, increasing drought areas and severe water pollution. The limited available natural water resource is contaminated by industrial wastewater streams and sewage water release.

Metal-oxide nanoparticles **(Fig. 4)**[12] are well utilized in nanoparticle enhanced filtration as water-purification catalysts and redox active media [14]. In addition, CNT (carbon nanotubes), dencrimers and zeolites are the other three major groups of nano materials.

Figure 4: Metal-Oxide nanoparticles used to enhance the contaminated water filter [Source: **[12] (Nora & Diallo, 2005-10-01;)**]

Why are nanoparticles such a good medium during the water purification process? Their massive "surface area, electronic, shape-dependent optical and catalytic properties" **[13](Obare & Meyer, 2004)** can explain this question. Titanium dioxide (TiO_2) was commonly used to purify both organic and inorganic pollutants in the past due to its capability of being both an oxidative and a reductive catalyst during the decontamination process. **[14] (Chitose, et al., 2003)** In recent years, **[15] (Nurmi, 2005)** introduced a different technique which involves combining nano zero valent iron (Fe^0) and bimetallic iron particles, to create a medium that could aid in the detoxification of organic and inorganic pollutants in aqueous solutions.

Environmental detection and sensor monitoring: With highly developed satellites providing monitoring and detection, remote sensing and image processing has become

very popular to help environmental scientists to understand both macro and micro pollution situations on the ground. The newly launched nanotechnology based on NO_x sensors[16] **[(Vaseashta & Marshall Univ., 2006)],** is now able to acquire extremely accurate data, even the concentration of the pollutant on the ground by detecting radiation signals generated by the nanoparticles in the sensor of the satellite's band. Associated software such as ER Mapper™ is then capable of calculating a series of cluster algorithms based on the images.[15] The Terra ASTER Satellite (**Fig.5**) has been introduced to obtain high spatial resolution images.

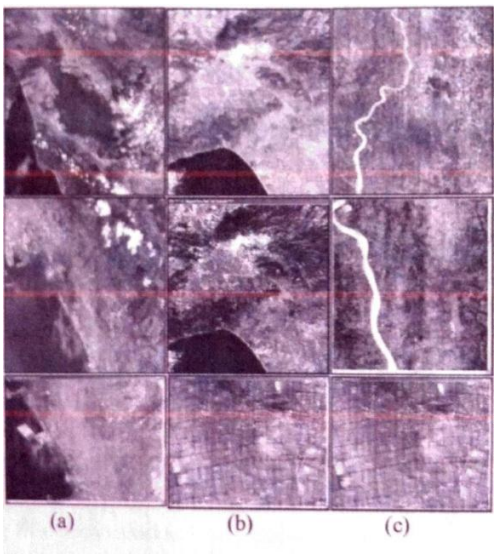

Figure 5: Above images shows three Terra ASTER Satellite images of smog and pollution. (a) Los Angles; (b) San Francisco; (c) Calcutta [Source:[16] **(Vaseashta & Marshall Univ., 2006)**]

In these images, the scattering of the pollutant (aerosols and particulates) in the atmosphere is clearly shown. By monitoring the concentration of the aerosol layers, appropriate measures could be developed to improve the environmental issues.

2.3 Magnetic polymers

The magnetic polymer is as introduced in the introduction a new material synthesized by mixing magnetic particles with polymers .

One of the most important applications of magnetic polymers is drug delivery. Thermo sensitive magnetic polymer (*N*-isopropylacrylamide polymer) particles are used as contactless controllable drug carriers to deliver drugs and are also applied in tumour tissue imaging.[17] **(Detlef Müller-Schultea, 29 April 2005)**

To accomplish drug delivery, the *N*-isopropylacrylamide polymer beads are synthesized using a water-in-oil suspension polymerization technique [18] **(Müller-Schulte, 2003.)** The following flowchart shows the basic process of polymer bead preparation. **(Fig.6)**

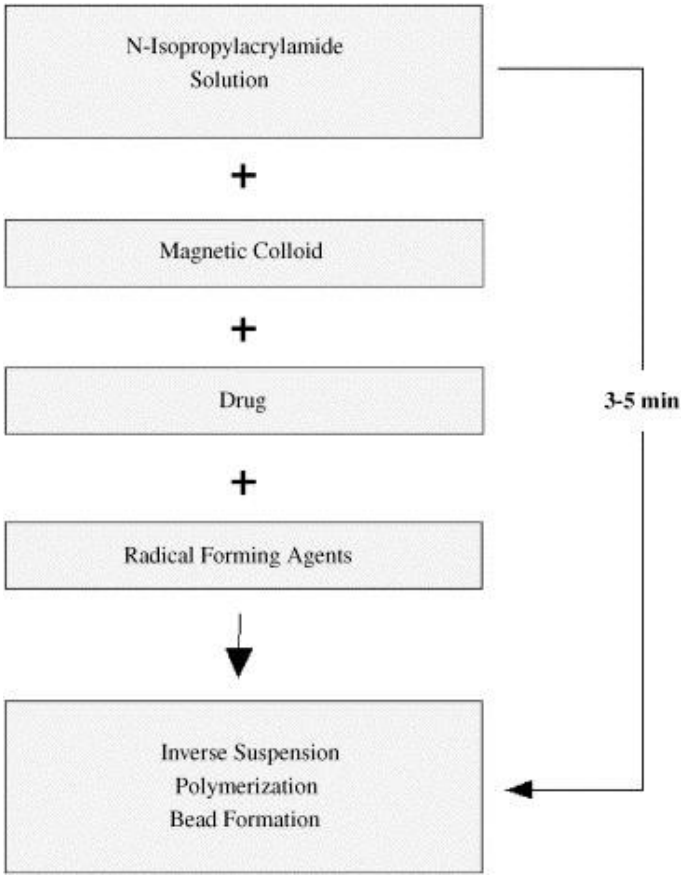

Figure 6: Schematic of drug delivery [Source: [17] **(Detlef Müller-Schultea, 29 April 2005)**]

As is stated in [17] **(Detlef Müller-Schultea, 29 April 2005)**; *"The spherically shaped N-isopropylacrylamide micro- and nanocarriers are simultaneously encapsulated together with magnetic colloids using a newly developed inverse suspension polymerisation technique, which for the first time provides a basis for an in vivo contactless controlled drug release,"* which shows a perfect bioactive capacity to achieve drug release.

There are numerous other applications of magnetic polymers, especially in the biomedical field and sealing industry. Exploration of more new materials synthesized by magnetic polymers needs to be undertaken, however, the main disadvantage is the long processing time.

Chapter 3: Experimental Techniques

3.1 Fabrication Techniques

Fabrication plays an important role in the application of nanoparticles. It is a large topic involving both chemical and physical processes, and often a combination of both. Various types of nanofabrication techniques and methods have been discovered but all have their limitations. Understanding the processes of fabrication will definitely help in the study of and research into the magnetic properties of nanoparticles.

3.1.1 Lithography

The most fundamental method used in fabrication is lithography, including a few steps of a related process; resist coating of unpatterned substrate or film, removal of the resist solvent and improving adhesion by using a soft-bake of resist, exposure to a radiation source with a mask on, and development to obtain various depth profiles in the resist. Afterwards, pattern transferring can be achieved by applying different types of etchings and depositions, which are introduced later. **(Fig. 7)**[19]

The resist used in spin-coating of the substrate is dissolved in an organic liquid solvent. The polymer chain is either (a) broken in the resist after adequate radiation exposure (positive), or otherwise, (b) cross-linked (negative).

Generally, the developed resists are hardened before etching. Wet or dry etching is applied when transferring the pattern from the resist to an unpatterned film whereas post-deposition or electrodeposition is applied on pattered resist by lift-off. The major

difference between wet and dry etching is that wet etching mainly involves chemical processes and occasionally electrochemical processes to dissolve the material, whereas in dry etching, both physical and chemical processes are implemented such as ion milling, plasma etching, and reactive ion etching. Lift-off is another way of fabricating the developed resists by laminating post-deposition on patterned resist. **[Fig.7 (c)]** This process involves lifting off a much thicker layer of developed film along with a thin layer of film on top of the resist. Thus, by making a sharp, clean break-off of the film at the edge of the resist, the leftover portion that directly deposits on the substrate surface during the resist striping can be obtained. Hence, it is preferred to have resists developed with "undercut edge profiles, as well as directional deposition techniques".[19] Notice that the resist thickness is generally much larger than the height of the lift-off material. One of the most commonly used growth techniques is electrodeposition, a technique that depends on temperature and pressure. When a current is supplied and passed through, material would be deposited from an electrolyte during the electrodeposition process. Compared to the lift-off technique, electrodeposition is easier to operate and more effective. This technique can produce fabricated materials with a larger height (up to the thickness of the resist) and a variety of geometries.

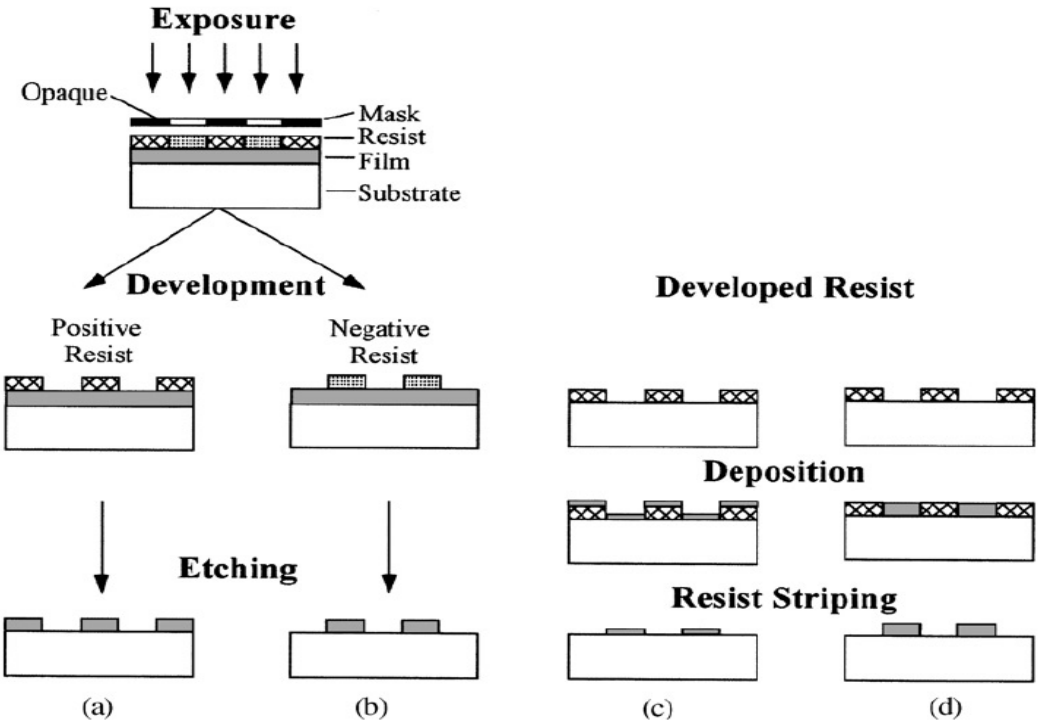

Figure 7: Schematics of lithography process for (a) positive and (b) negative resists in conjunction with (a), (b) etching, (c) lift-off and (d) electrodeposition 9[Source: (J. I. Mart ń, January 2003)]

Materials can be fabricated by combining alternative pattern transferring processes with different lithography techniques. Depending upon the source of exposure, various lithography techniques are termed, for example, electron beam lithography, x-ray lithography, interference/holographic lithography, etc.

Lithography is not the only method used to obtain nanoparticles or nanostructures. There are also other techniques, such as step growth methods, and focused ion beam milling.

Step growth methods: This particular method is usually used to fabricate nanostructures by depositing magnetic material on a step-shaped substrate. The created

step shape is a double-edged sword, being both the advantage and the disadvantage of this technique as it limits the nanostructure.

Focused ion beam milling: A beam of ionized inert gas can perform the perfect magic of fabrication. This technique is widely used to produce tiny nanostructures such as nanoparticles up to few nanometers. When ions are energized and collide with the surface atoms of the magnetic material, the ejection of atoms can lead to the milling. Apparently, electromagnetic lenses can control the size of the resulting nanostructure, which makes this technique more accurate and flexible in fabricating a range of structures. However, the main disadvantage is the long processing time.

3.1.2 Chemical Synthesis

Wet chemical synthesis is based on colloidal precipitation in chemical solutions. The reaction takes place on a molecular scale which involves temperature and pH value control. Multitudinous morphologies (spheres, nanorods, nano pyramids, etc.) and particle sizes can be obtained by changing different parameters of the reaction conditions, such as growth kinetics, magnetic field strength and reaction temperature. **[20](Ni Xiaomin & Zhang Dongen, 2004)**

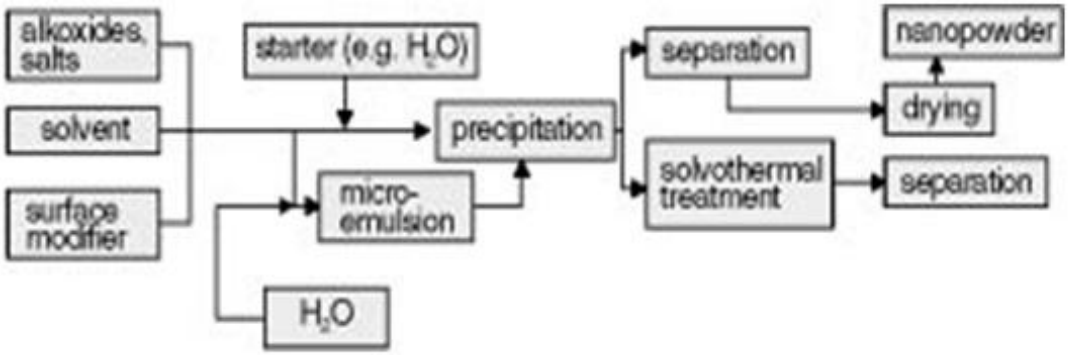

Figure 8: Flowchart showing the general process of wet chemistry synthesis of nanoparticles [21] **(Schmidt, 2001)**

As illustrated above, alkoxide salts dissolved in solvent (eg. De-ionised water) are mixed with micro emulsion and then undergo thermal treatment. Nanoparticles start to be precipitated, separated and eventually dried out.

The chemical reaction that occurs during the precipitation is shown below (fig.)

XRY = bifunctional molecule, SCA

X = binding grouping (β-diketones, complex formers, reactive silanes, acids etc.)

R = ≡ Si -, hydrocarbon groupings

Y = reactive and non-reactive or functional groupings (complex formers, acids, bases, epoxides, double bonds, aryl or alkyl groupings)

Figure 9: The surface modifying and chemical reaction of common chemical synthesis of nanoparticles [21] **(Schmidt, 2001)**

Under particular circumstances, well-structured crystalline clusters of nanoparticles with extremely small size (less than 10 nm) can be fabricated easily by using wet chemistry synthesis. For example, using the co-precipitation technique:

Co-precipitation technique to produce iron (III) oxide nanoparticles: An aqueous solution of ferrous sulphate (Fe 2+) and an aqueous solution of ferric sulphate (Fe 3+) are mixed in a particular molar ratio. Alkaline solution is slowly dropped into the mixture until the pH approaches 10 with mechanical or magnetic stirring. Black slurry precipitation is produced immediately when ammonia is added. After a long period of vigorous stirring, hydrochloric acid is added to create a pH of 3. The precipitation is rinsed with acetone and D.I. water after the production and dried at 60 ℃ in the heating cabinet.

3.2 Measurement Techniques

In order to determine the size and properties of the SPIONs manufactured, different electron microscopes are applied. SEM (scanning electron microscopy) and TEM (transmission electron microscopy) are widely used in this field. Basically, electrons have very short wavelengths, which can be coupled with each other to produce electron microscope images. Both SEM and TEM can produce high resolution images and provide spatially resolved information, distribution maps and data processing. TEM can even procure atomic scale information and achieve single-atom sensitivity. Generally speaking, both TEM and SEM have layouts of an electron probe, condenser lens, specimen holder, focusing lens, magnification lens connected to a CCD camera and data

display instruments. The electron probe that generates the E-beam is characterized as high intensity, high radiation and high energy. Specimen interactions with the E-beam generate signals and achieve localization. The signals are then captured, focused, detected and finally recorded by the different functional lenses, CCD camera, hence displayed by computer lab view software.

VSM has a different function compared to TEM and SEM. The magnetic properties of the vibrating samples can be tested and plotted into a hysteresis loop.

3.2.1 SEM

SEM (scanning electron microscopy) is widely used when testing bulk samples (nm to μm to mm) due to its flexibility in a multispectral environment. The sample preparation is reasonably fast and minimally invasive. The imaging gives direct access to complex native surfaces in three dimensional phases.

Before fabricating SPIONs, to become familiar with the morphologies and basic characteristics of iron oxide particles, larger particles sized 1-7 μm are used to synthesize an iron oxide particle polymer**. (Fig.10)**

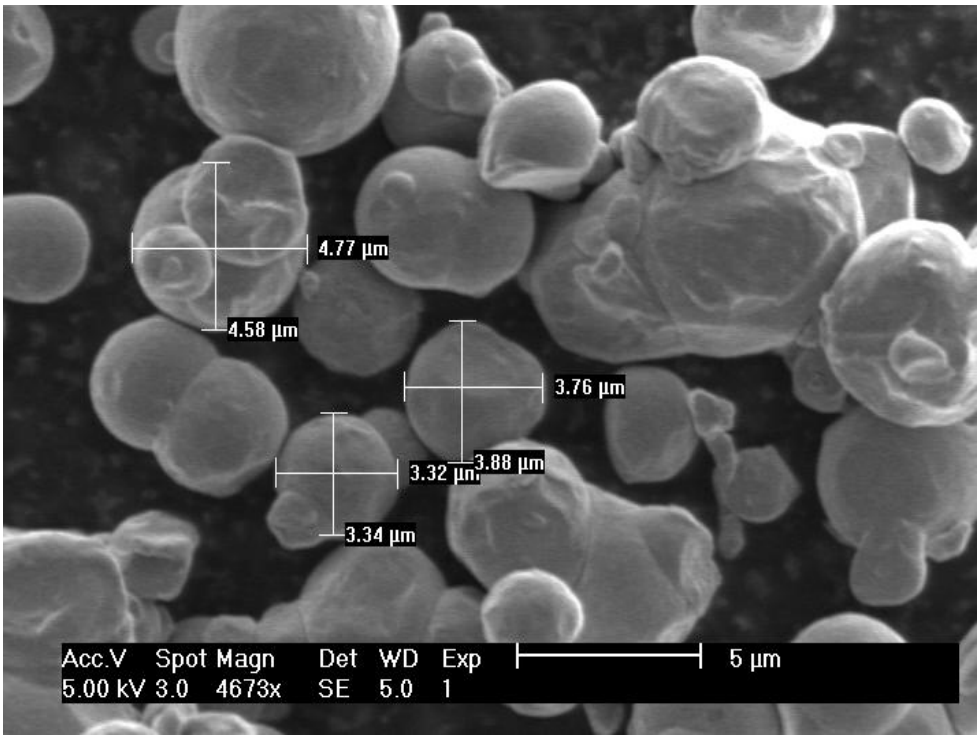
4.77 µm
4.58 µm
3.76 µm
3.88 µm
3.32 µm
3.34 µm
Acc.V Spot Magn Det WD Exp
5.00 kV 3.0 4673x SE 5.0 1
5 µm

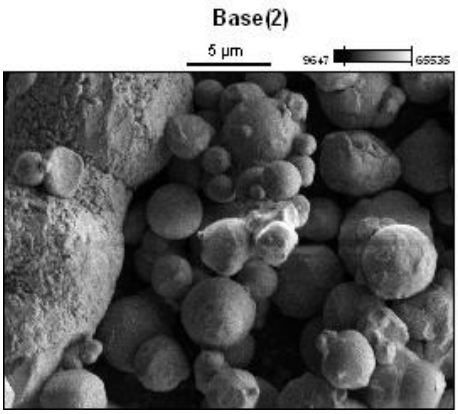
Base(2)
5 µm

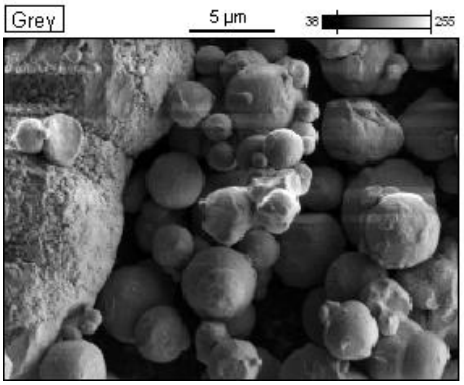
Grey
5 µm

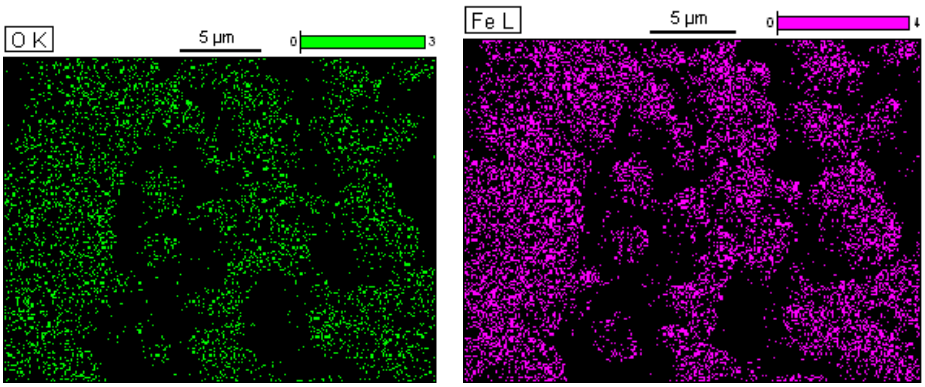

Data Type: Counts Mag: 4673 Acc. Voltage: 5.0 kV

Figure 10: The SEM images above show iron particles at a scale of 5 µm. The purple scattered dots indicate the atomic presence of the element iron.

The operation of SEM is relatively easier than that of TEMs, however, the SPIONs are quite small and even SEM can only produce images at a nanometer scale. Thus, SEM is only used to produce images of larger iron oxide particles whereas TEM is employed to produce images of SPIONs.

3.2.2 TEM

TEM (transmission electron micrographs) **(Fig. 11)** can obtain ultra-high-resolution images and atomic-scale information about nanoparticles. Single atom sensitivity allows TEM to perform acquisitions of real space images, reciprocal space diffraction patterns and the spectra of elements, electronic and chemical states. Samples are loaded in a vacuum chamber and exposed under an electron beam which passes through the condenser lens.

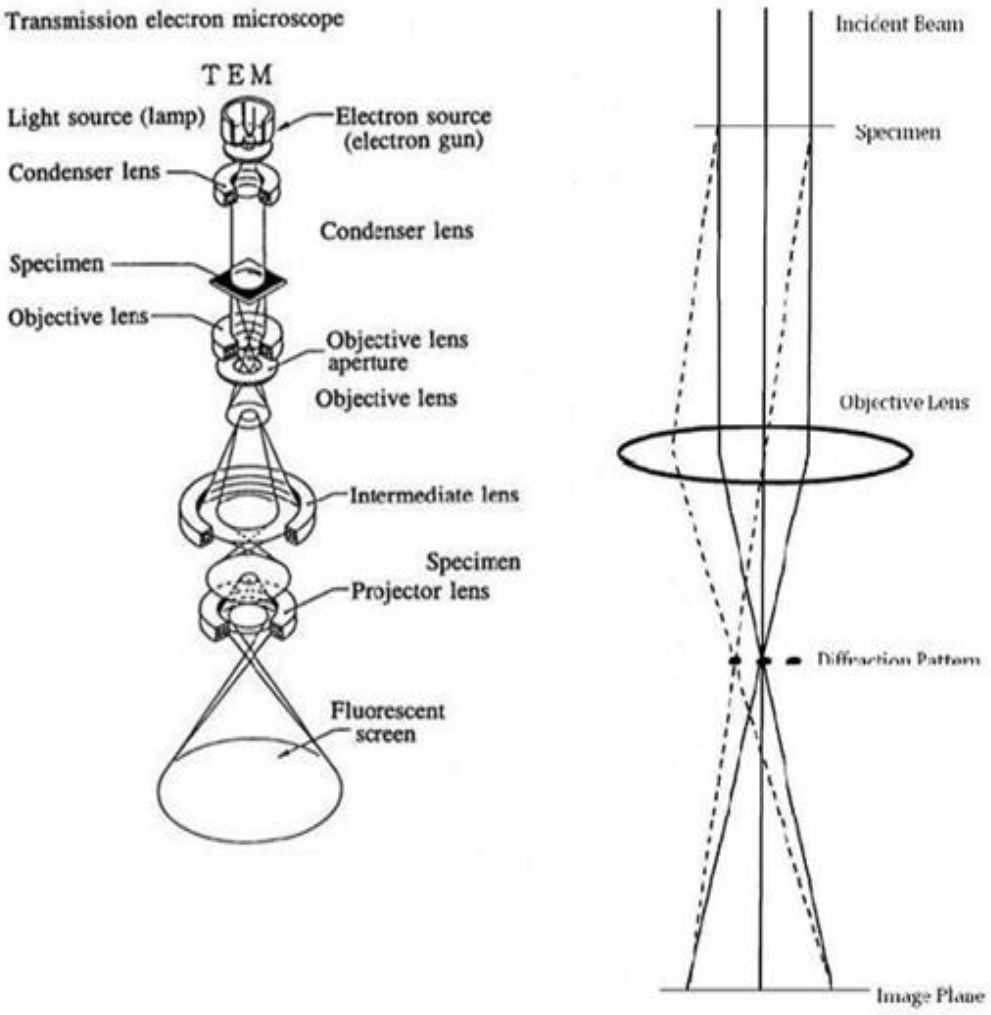

Figure 11: General layout of a TEM describing the path of the electron beam (Taken from JEOL 2000FX Handbook). [Source:URL:http://www2.warwick.ac.uk/fac/sci/physics/current/postgraduate/regs/mpags/ex5/techniques/structural/tem/]

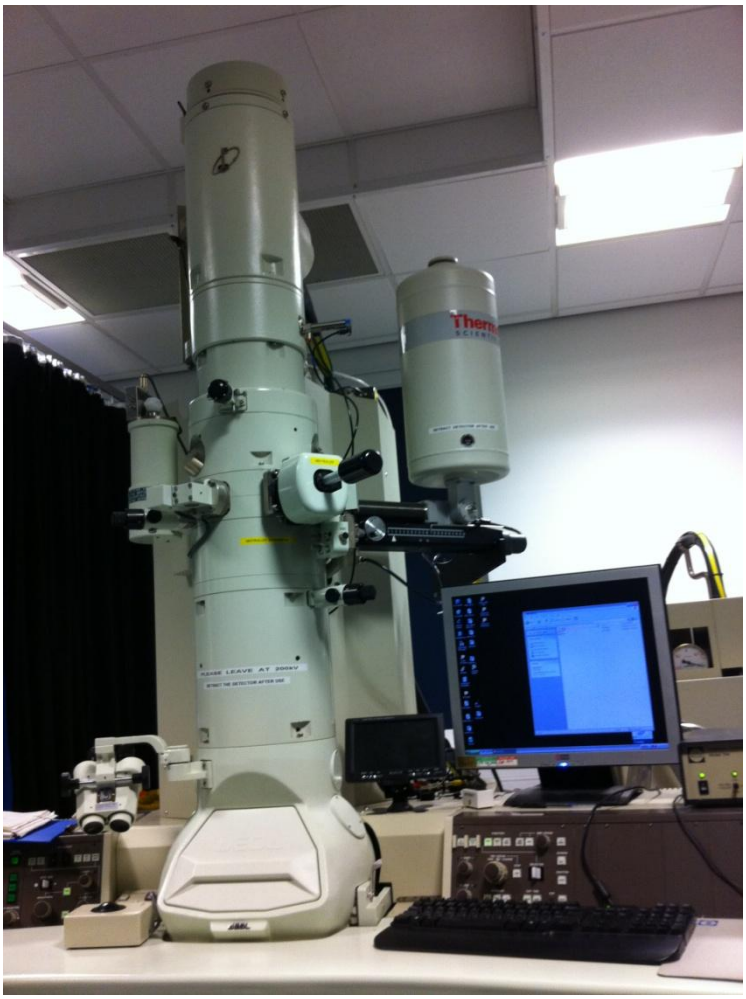

Figure 12: TEM at York JEOL Nanocentre.

Based on the extraordinary performance of TEM, images of SPIONs can be obtained and presenting particle morphologies.

3.2.3 VSM

A **vibrating sample magnetometer** or VSM is a scientific instrument that measures magnetic properties, invented in 1955 by Simon Foner at Lincoln Laboratory MIT. [22]**(S.FONER, 1959)** The VSM technique involves sinusoidal oscillation of the sample material within a uniform magnetic field and measuring the induced electromagnetic

field (EMF) created. Two immense electromagnets generate a uniform magnetic field which induces a dipole moment in the sample; the sample is then physically oscillated within this via a piezoelectric oscillating material (early VSMs used modified loudspeakers to create this oscillation). Pick-up coils are located close to the oscillated sample; EMF is induced in these pick-up coils according to Faraday's law of induction. The signal (induced voltage generated), which is proportional to the magnetization of the sample, is thus collected by the locking amplifier and transferred into computer interface (software) to form a hysteresis loop of the magnetic samples. An illustration of the VSM setup is shown in the following (**Fig.13**)

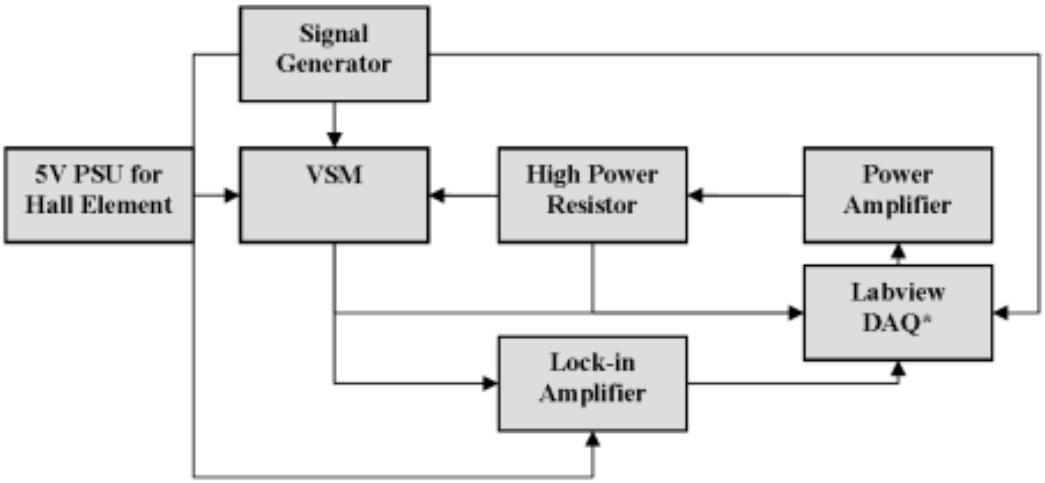

Figure 13: VSM general setup [source: [23] **(mullens, n.d.)]**

Content:

- Water cooled electromagnet and power supply
- Vibration exciter and sample holder

- Sensor coils (pick-up coils)
- Hall probe
- Amplifier
- Control chassis
- Lock in amplifier
- Meter
- Computer interface (software)

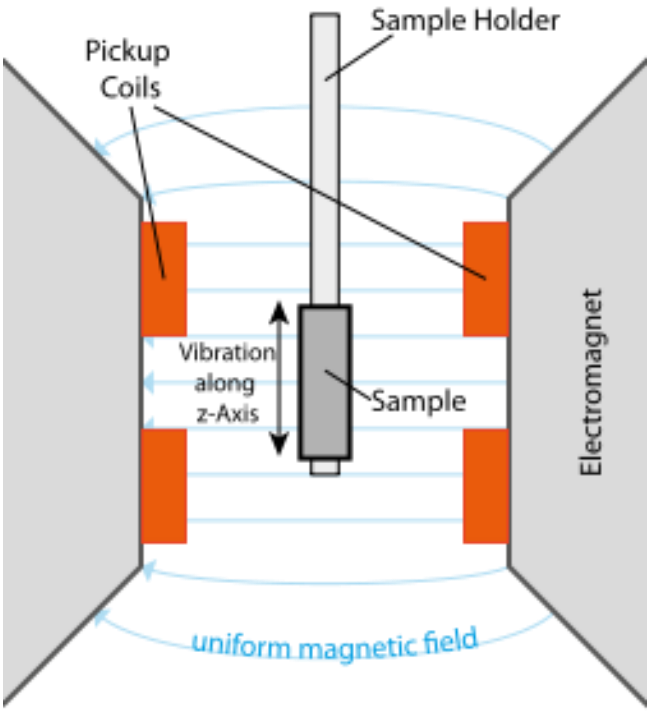

Figure 14: basic composition of VSM and principles of working. [source: http://en.wikipedia.org/wiki/File:VSM_en.svg]

By interpreting the hysteresis loop plotted by the labview software, many magnetic properties of the samples can be obtained, for example: remnant magnetisation, saturation magnetization, coercivity field etc. These properties provide extremely useful information which allows further analysis and discussion of samples.

4.1 Introduction

Wet chemistry synthesis is widely used to fabricate nanoparticles. Under particular circumstances, well-structured crystalline clusters of nanoparticles with extremely small size (less than 10 nm) can be fabricated easily by using wet chemistry synthesis. For example, the co-precipitation technique can be used; a detailed description of the experimental setup and procedure of the co-precipitation technique will be carried out in the following sections.

Ferrous sulphate and ferric sulphate, both in aqueous solution, are mixed in a particular molar ratio. Alkaline solution is slowly dropped into the mixture until the pH approaches 10 with mechanical or magnetic stirring. Black slurry precipitation is produced immediately when alkaline is added. After a long period of vigorous stirring, hydrochloric acid added to stabilize the nanoparticles. The precipitation is rinsed with acetone and D.I. (de-ionised) water after fabrication.

It is quite common to take at least 4 hours to finish one synthesis in order to give sufficient time for the dispersal of the SPIONs.

4.2 Production of SPIONP

As mentioned in the introduction, the production of SPIONP involves two major steps. The most essential one is to obtain superparamagnetic iron particles by using the co-precipitation technique, a method in which the production does not involve complicated instrument setup or great expense. The size of the SPIONs (Superparamagnetic Iron Oxide Nanoparticles) produced in this experiment should be less than 10 nanometers in diameter to achieve the superparamagnetic properties required.

4.2.1 Co-Precipitation Technique and the Experimental Setup

Chemicals: ferrous sulphate (Fe 2+); ferric sulphate (Fe 3+); ammonia (NH4OH); hydrochloric acid (HCl); acetone (C3H6O);

Aqueous solution ferrous sulphate (Fe 2+) and aqueous solution ferric sulphate (Fe 3+) are mixed in a molar ratio of 1: 1.8 at 40℃. Ammonia solution is slowly dropped into the mixture until the pH is approaching 10 with mechanical or magnetic stirring. Black slurry precipitation is produced immediately when ammonia is added. After half an hour of vigorous stirring, hydrochloric acid with a concentration of 35% is added to a pH of 3. The precipitation is rinsed with acetone and D.I. (de-ionised) water after the production and dried at 60℃ in the heating cabinet. (**Fig. 15**)

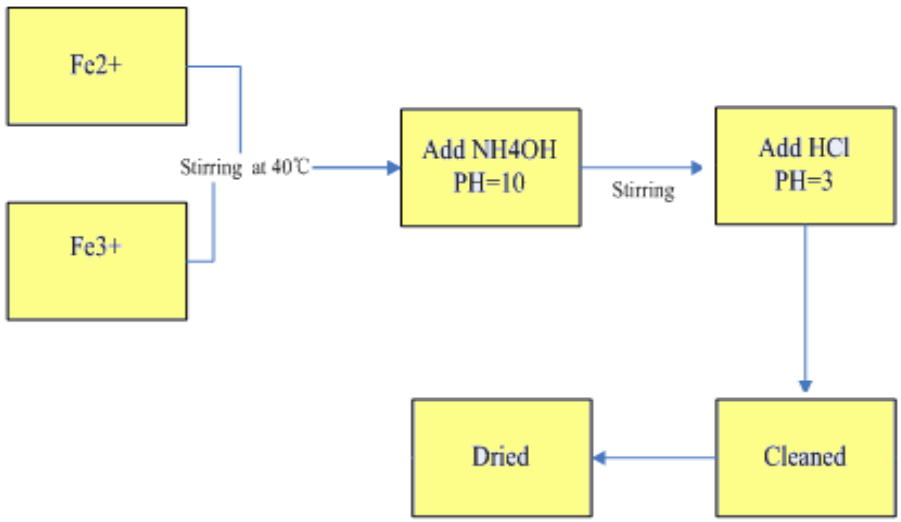

Figure 15: Co-precipitation technique of producing SPION

Due to the different type of stirrer used (magnetic or mechanical), the SPIONs obtained has slightly different properties. A detailed analysis of the results will be carried out later on.

Experimental Setup:

First of all, an aqueous solution of ferric sulphate $Fe_2 (SO_4)_3$ and an aqueous solution of ferrous sulphate heptahydrate, $FeSO_4.7H_2O$, both with concentration of 1mol/l, are prepared in separate beakers. In order to obtain 1mol/l solution, the molecular weight of each substance should be determined and weighed out. 1 litre (1000ml) of D.I. (de-ionised) water is then added to obtain the required concentration.

For Ferric sulphate $Fe_2(SO_4)_3$:

$\{(2X55.85)+3x[(1x32.07)+(4x16]\}g.mol^{-1} = 399.91\ g.mol^{-1}$

Whereas for ferrous sulphate heptahydrate $FeSO_4.7H_2O$:

$[(1x55.85) + (1x32.07) + (4x16.00) + 7x (2x1+1x16.00)]g.mol^{-1} = 277.93\ g.mol^{-1}$

However, when adding D.I. water, a proportionately lower amount is added to the ferrous sulphate heptahydrate due to the fact that each $FeSO_4$ molecule is hydrated with 7 H_2O molecules. The extra weight of water is:

7H2O = 7x (2x1+ax16.00)g =126 g or 126 ml

Therefore, to compensate, 1000 ml - 126 ml = 874 ml of water is added into 277.93 g of ferrous sulphate heptahydrate to obtain the required concentration of 1mol/l.

D.I. water is used to avoid mineral salt contamination of the solution. Both beakers are settled in a hot bath with a temperature of 40 ℃. This temperature parameter is changed several times in the later experiment to find out whether it has an impact on the manufacture of nanoparticles. After mixing up the two solutions, ammonium hydroxide solution (also termed: ammonia), NH_4OH, is added to the mixture to create a pH 10 solution while stirring vigorously with a magnetic or mechanical stirrer (**Fig.16**). By using different stirrers, the shapes of the particles are highly influenced, resulting in totally different morphologies. A detailed analysis will be carried out in the next section.

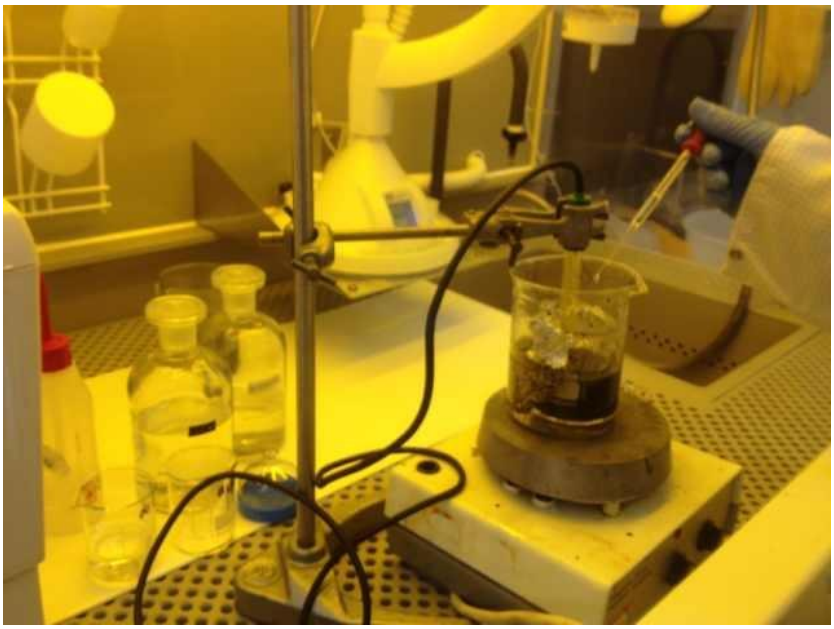

Figure 16: The experimental set up using magnetic stirrer underneath. To keep the reacting temperature at 40 ℃, the hot plate is turned on. The yellow tube shaped instrument is a PH meter which is used to monitor the reacting temperate and the PH value.

$$Fe^{2+}, Fe^{3+} + OH^- \longrightarrow Fe(OH)_2, Fe(OH)_3$$

The ammonia solution is denoted by NH_3 (aq). According to the results of 7 repeated manufacturing experiments, the speed and amount of dropping ammonia by pipette strongly affects the size of the iron particles obtained. Slow, constant and small drops result in more uniform and smaller particles. This is due to the fact that smaller drops have a relatively smaller contact/reacting surface and contain less reactant so that the molecules are more evenly dispersed through the solution. The spaces between the molecules are increased. Thus, the collisions between the molecules are slower.

While dropping ammonia, a pH meter is used to monitor the pH value and the reacting temperature. When pH 10 is reached, aqueous HCl is then added to produce a pH 3 solution. Almost instantly, slurry of nanoparticles is produced at the bottom of the beaker **(Fig. 17).** Rinsing the nanoparticles with acetone and D.I. water and drying them in the cabinet is the last step of this experiment.

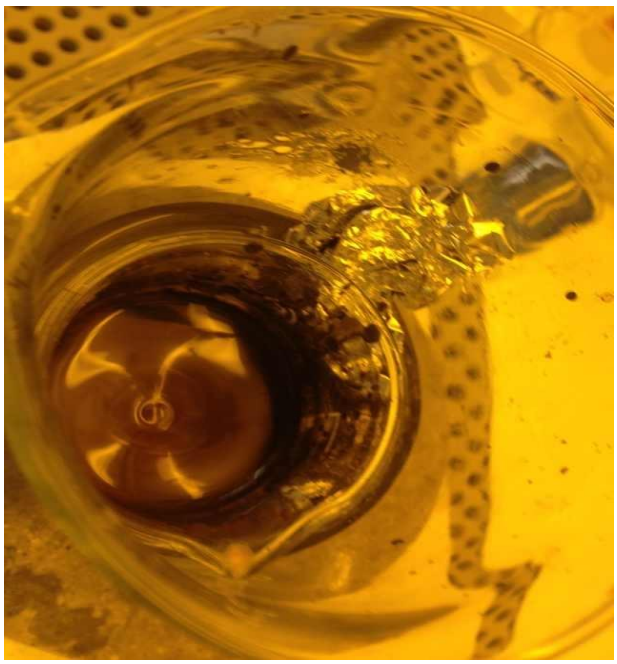

Figure 17: slurry of nanoparticles produced immediately when ammonia added.

4.3 Characterisation of Iron Oxide Nanoparticles

4.3.1 Size Distribution

As mentioned in the previous section, 7 repeated experiments were carried out, changing different parameters to explore the best pattern of manufacturing suitable SPIONs. The overview chart is given below (Tab.1);

Sample	Reaction Temp.	Ratio(Fe2+:Fe3+)	Stirrer	PH(HCL)	Drying Temp
S1	50	MASS 1:1.8	magnetic	2.7	20
S2	40	MASS 1:1.8	magnetic	3	20
S3	60	Mole 1:1.8	magnetic	no acid added	50
S4	40	Mole 1:1.8	mechanical	3.05	60
S5	50	Mole 1:1.8	mechanical	3	75
S6	60	Mole 1:1.8	mechanical	2.75	75
S7	70	Mole 1:1.8	mechanical	2.22	75

Sample	Rinse	Particle Size	Particle Shape	Colour	Drying PH
S1	ActoneX3 & D.I waterX3	<10 nm	Sphere and Rod	black	4.4
S2	ActoneX3 & D.I waterX3	around 10 nm	sphere	black	4.2
S3	ActoneX3 & D.I waterX4	<10 nm	sphere	brown	4.5
S4	D.I. water	<10 nm	sphere and rod	black	4.4
S5	D.I. water	<10 nm	sphere	black	4
S6	D.I. water	<10 nm	sphere	black	4.86
S7	D.I. water	<10 nm	sphere	black	3.58

Table 1: S1-S7 represent a different serious number of samples. Parameters such as reaction temperature, mixing ratio, type of stirrers, OH- pH, drying temperatures, particle morphologies and drying PH value are varied.

An SEM test was applied to my S1 sample but the result was very blurred and unsatisfactory. Figure 18 shows the SEM image of a piece of pure clumped SPIONs followed by EDX (Energy-dispersive X-ray) analysis. (Composition information)

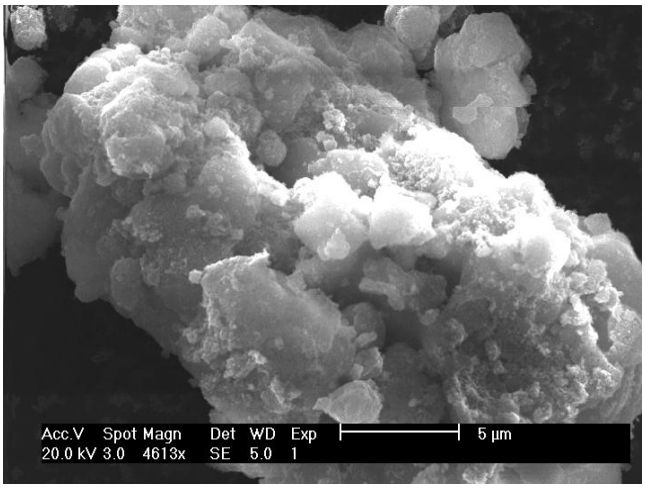
Acc.V Spot Magn Det WD Exp
20.0 kV 3.0 4613x SE 5.0 1
5 µm

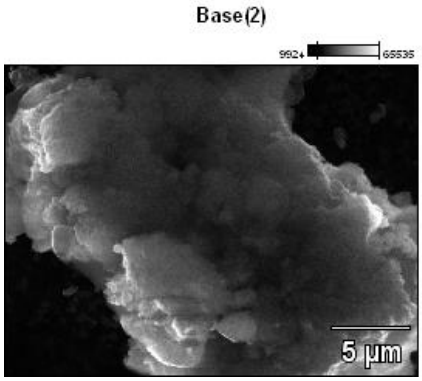
Base(2)
5 µm

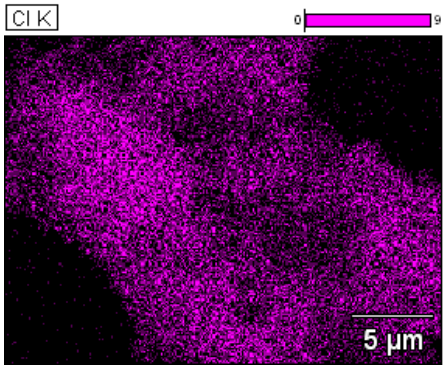
Cl K
5 µm

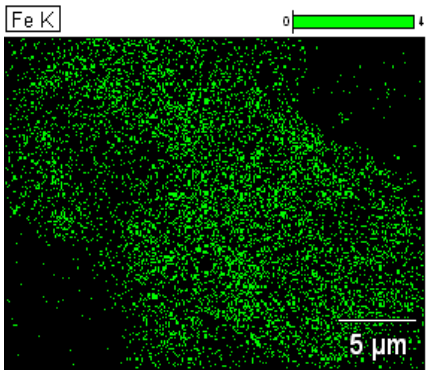
Fe K
5 µm

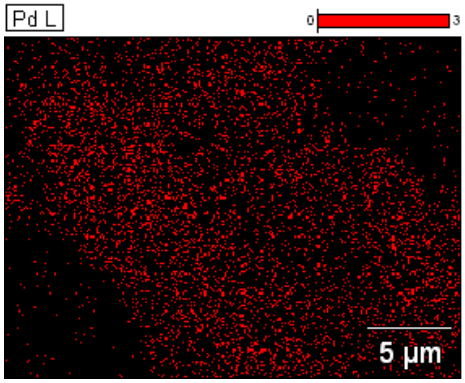
Pd L
5 µm

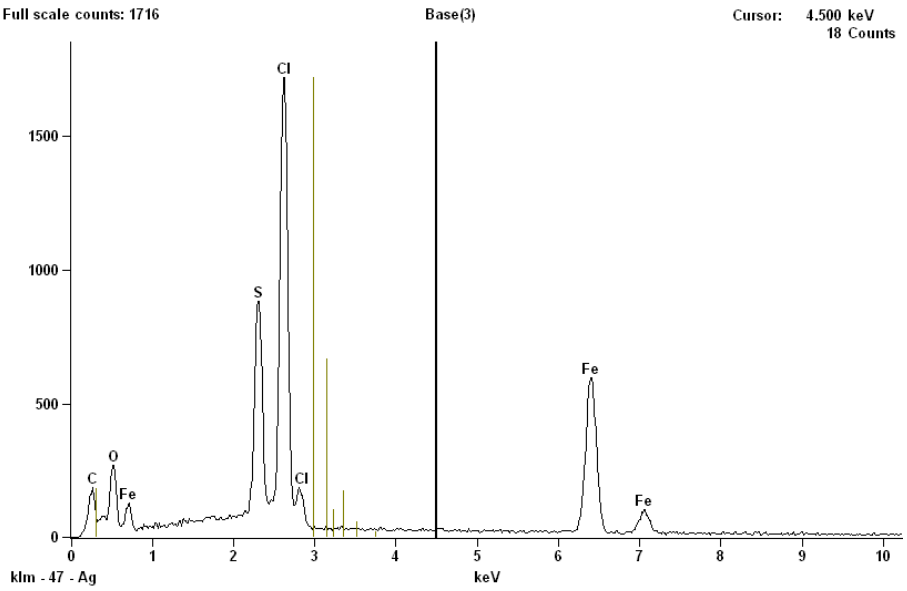

Figure 18: large peak of chloride indicates the excessive amount of chloride. Probably need more rinsing. Iron and oxygen peak show the composition of the SPION.

In order to get more accurate images to procure more information about the SPIONs manufactured, a TEM test should be applied.

S1: Particles are aligned in one direction when a magnetic field is applied. Crystallized structures **(Fig. 19)** are observed due to the excessive chloride and sulphate. More rinsing is required. Water is vaporized rapidly, which produces a turbulence force. Particles on the edge of the crystal structures are repelling each other to the opposite sides of the edges.

Figure 19: Crystal structure observed under the microscope. Dark spots concentrated on the edges are SPIONs.

TEM images of S1 show an impressive discovery. The presence of a nano-rod is observed. [**Fig. 20(a)(b)(c)**]

(a) 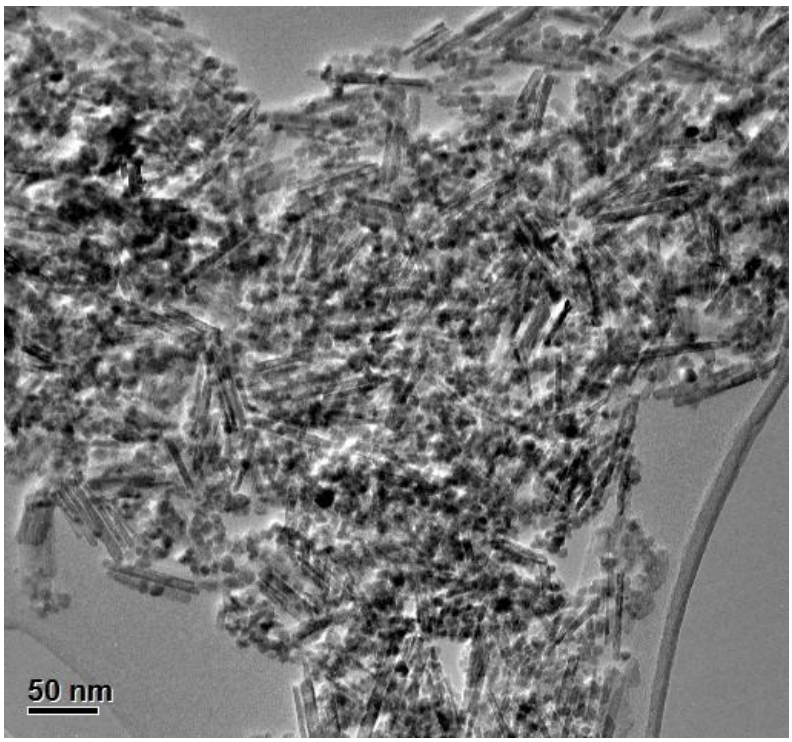

(b)

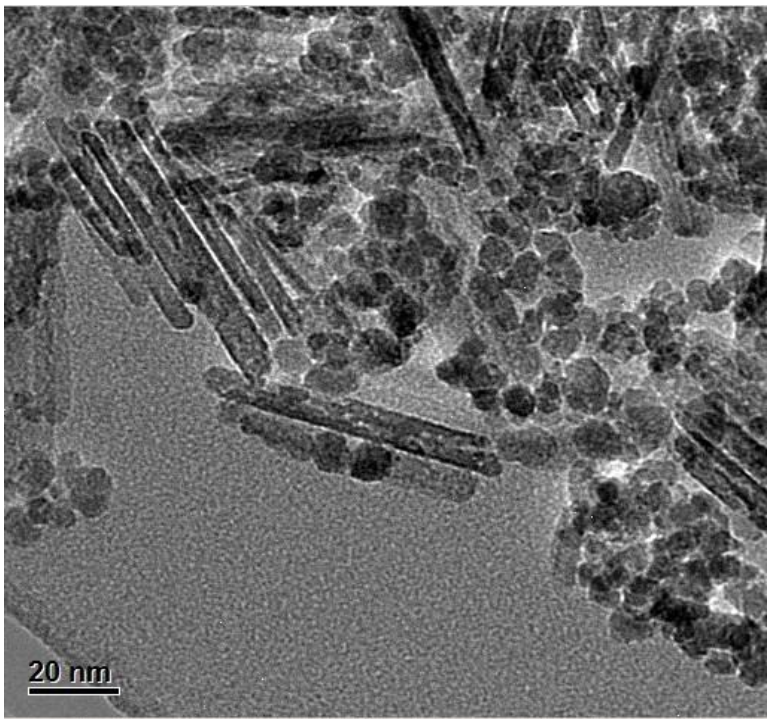

(c)

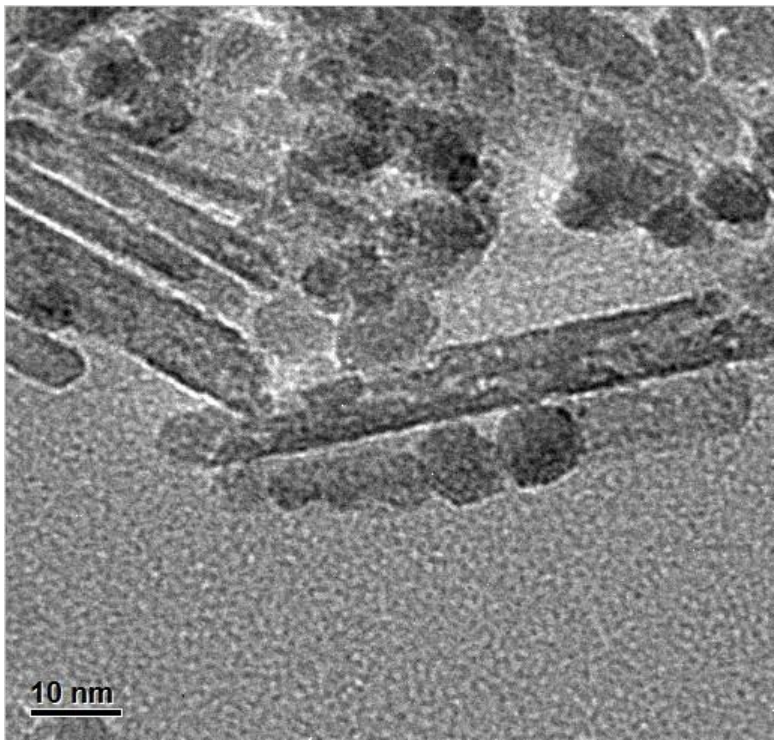

Figure 20: (a) At a scale of 50 nm. Numerous rod-shaped nano structures are observed along with massive nanoparticles aside. (b) At a scale of 20nm. Clear nano-rod structures are presented. Most of them are clumped with each other. Single rods are hard

to observe. (c) At a scale of 10 nm. SPIONs are distinctly observed. Most of them are under the size of 10nm according to the scale, which definitely could be superparamagnetic.

S1 obviously has a reasonable size to be superparamagnetic. The presence of unexpected nano-rod structures could be generated by the applied magnetic field of the magnetic stirrer when manufacturing. However, the sample obviously needs to be rinsed more with acetone or D.I. water.

S2: This sample is produced by completely following the experimental setup. However, this time the solvent used to make the TEM sample is RBS. There is a surface layer of detergent which produced a large amount of bubble-shaped substance that was burned away under the beam (**Fig. 21**). Fortunately, no discharge issues were experienced.

(a) 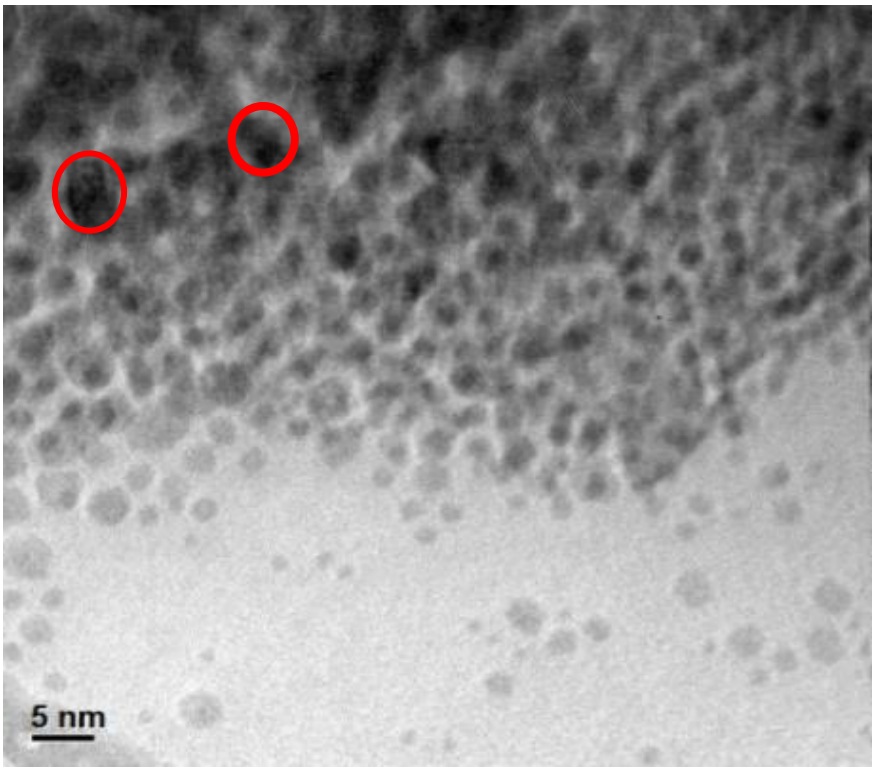

(b)

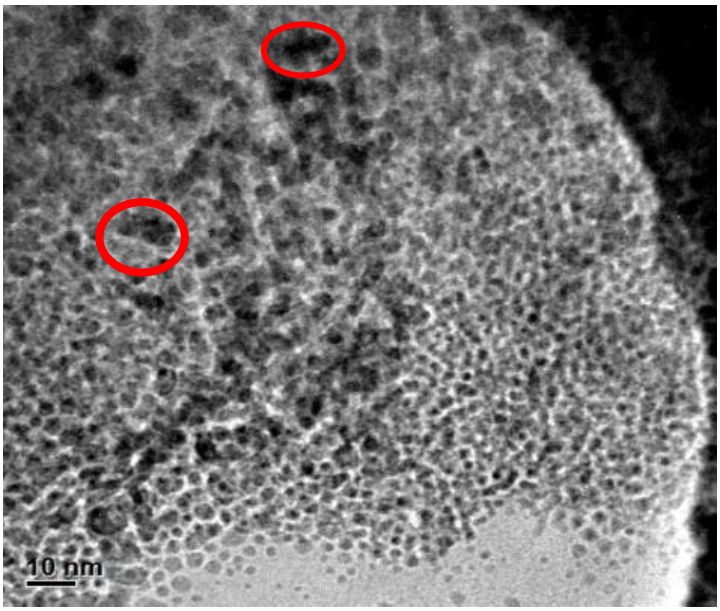

(c)

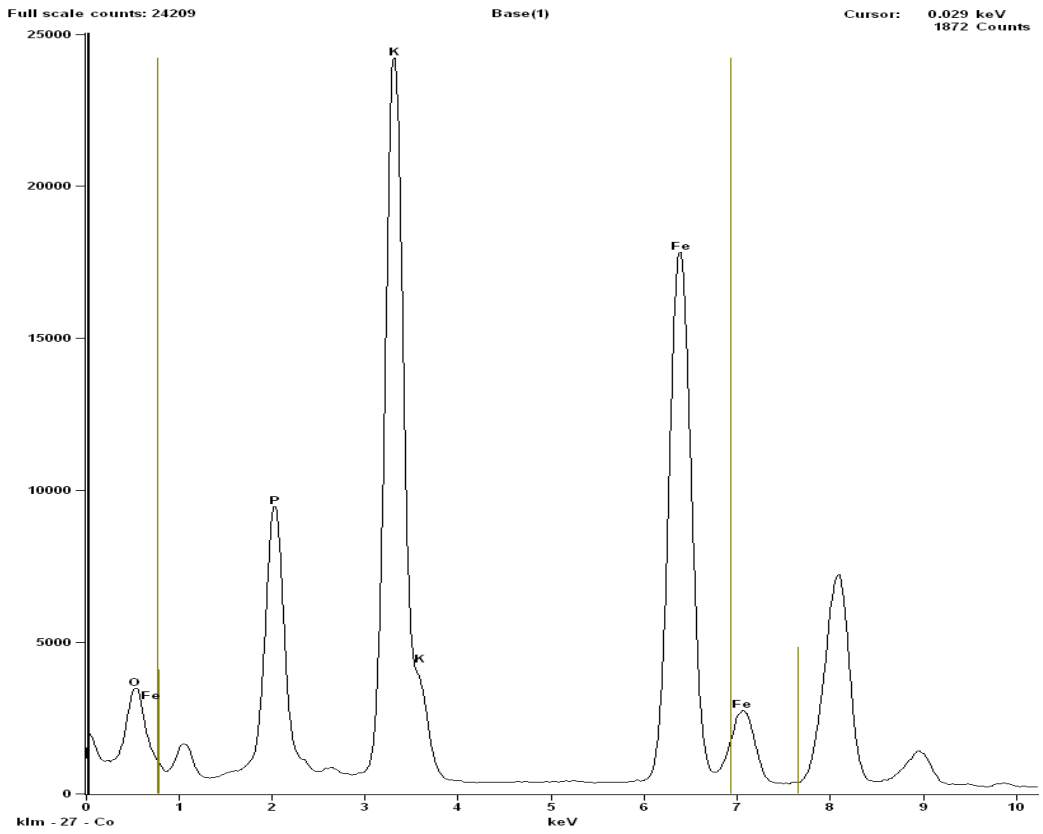

Figure 21: (a) and (b) show SPIONs at different scales. Massive detergent layers are overlaying the SPIONs yet it is still possible to discern them under the "bubble blanket". The red circle shows the image of possible SPIONs, which are also around 10 nm. (c) is

the EDX chart for S2. The exceptionally high peak of calcium indicates the presence of RBS. Iron peaks and an oxygen peak demonstrate the composition of the SPIONs.

S3: synthesized at the temperature of 60 ℃ with magnetic stirrer. No hydrochloric acid is added during the fabrication. Particles are brown and spherical. (**Fig. 22**)

(a) 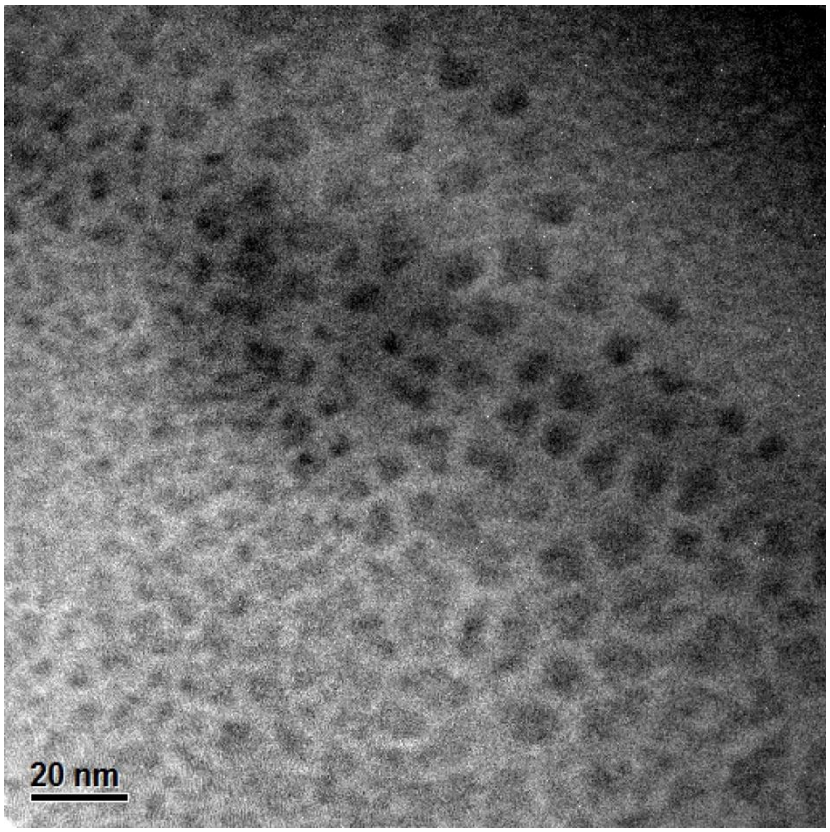

(b)

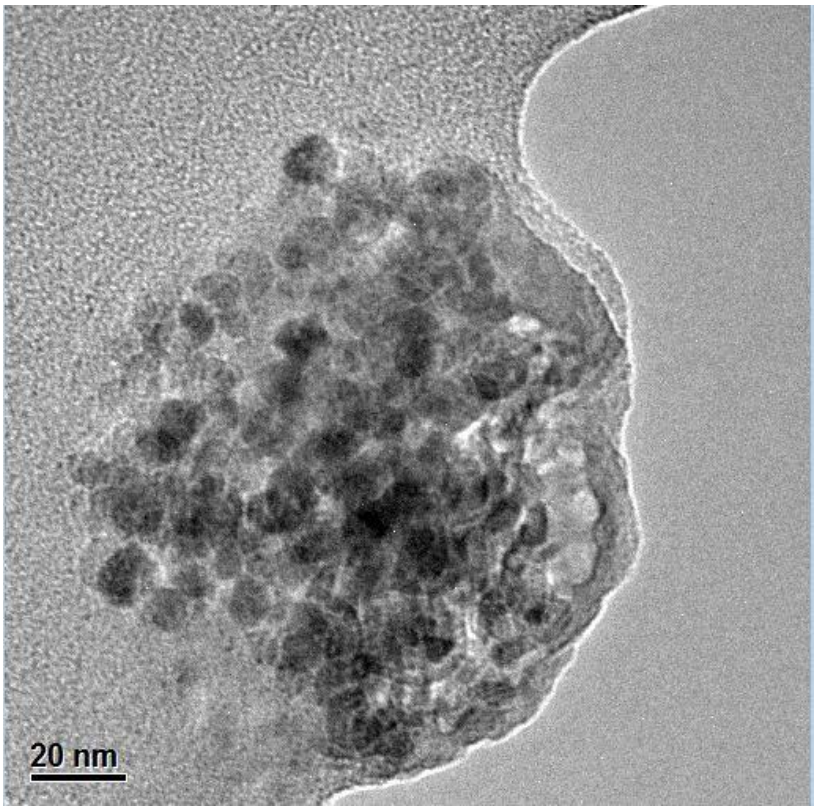

(c)

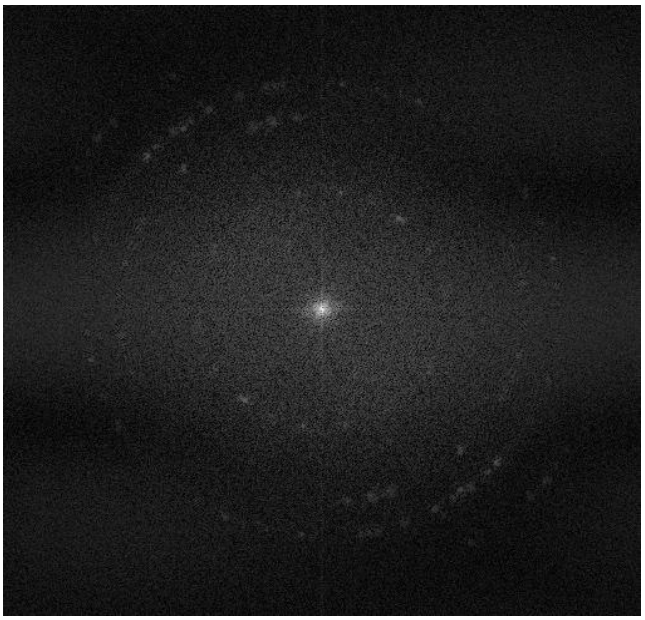

Figure 22: Particle clumps are easily defined. Synthesis without acid is strongly affecting the property of obtained particles. (a)(b) are two low resolution TEM images and (c) is the FFT image of the lattice orientation.

S4: Produced at a temperature of 40 ℃. This sample is quite unique as the other samples produced by using a mechanical stirrer tend to have a lot less evenly dispersed, and no presence of nano-rods, whereas in S4 there are massive nano-rods observed (**Fig.23**).

(a) 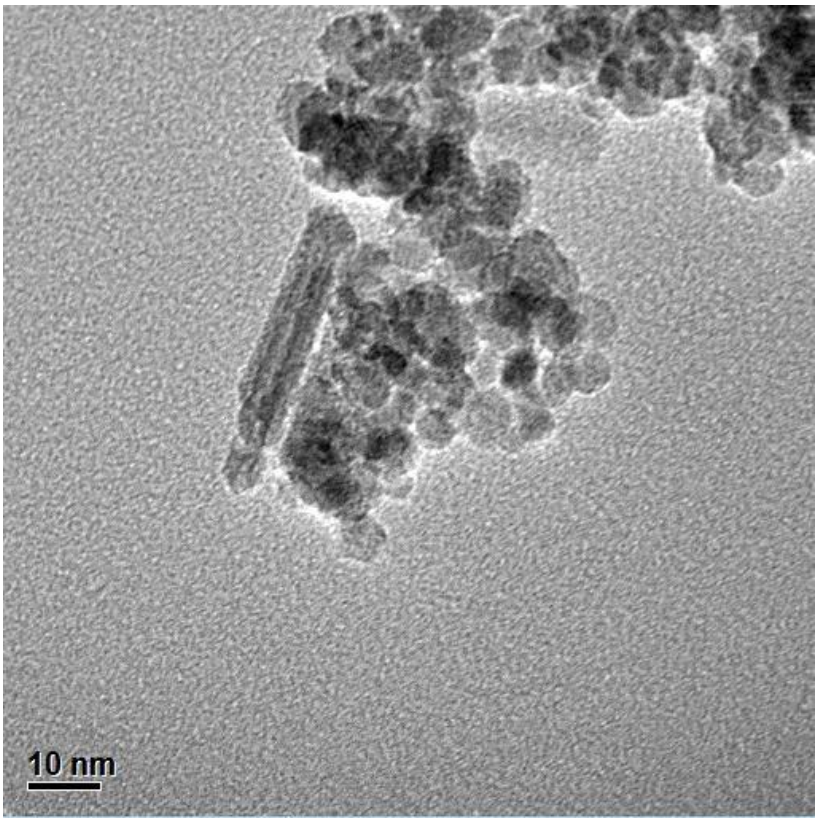

(b) 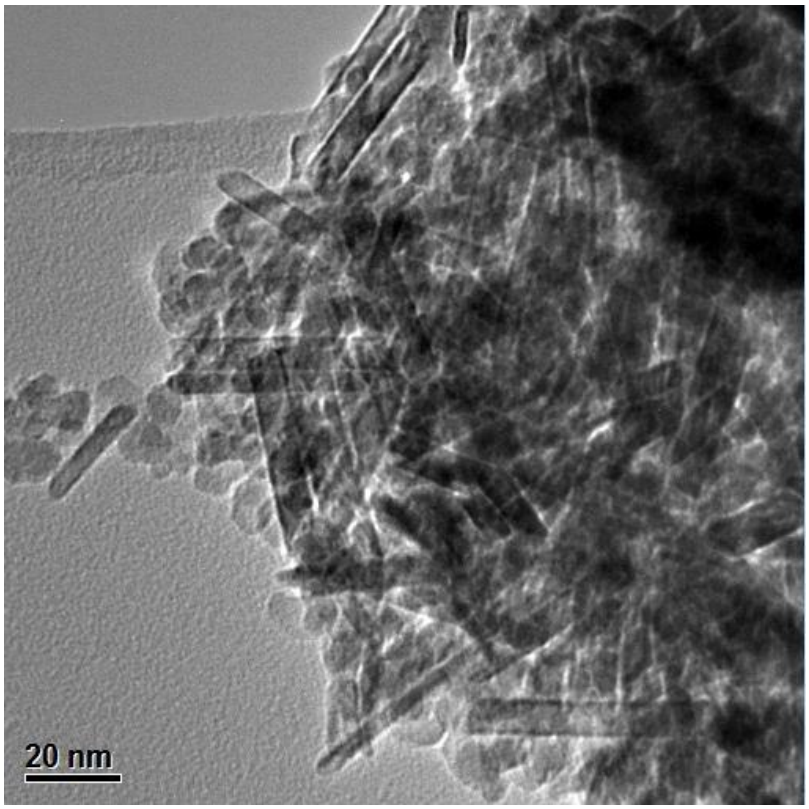

(c) 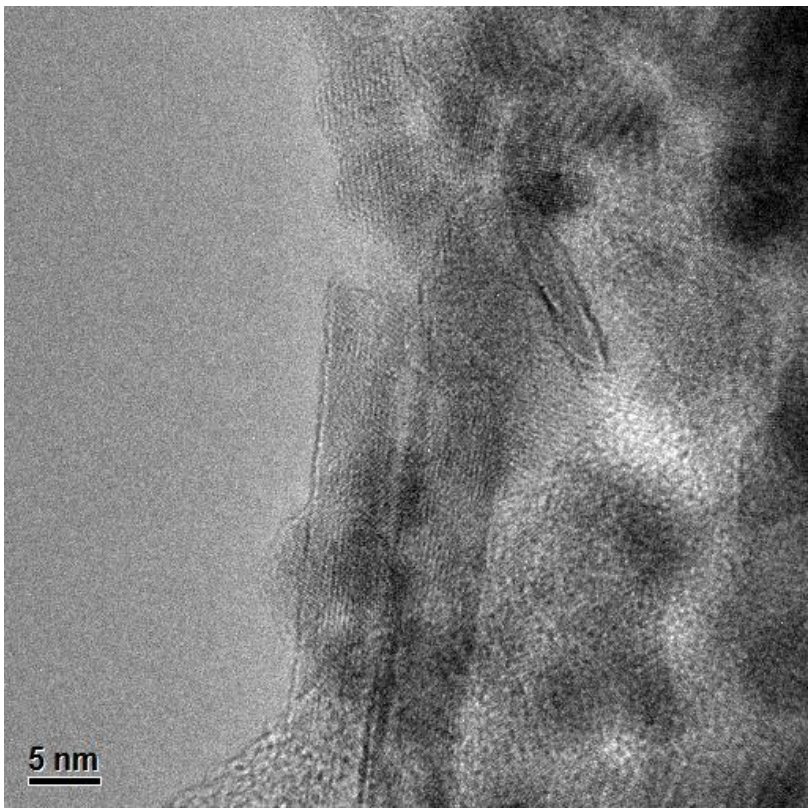

(d) 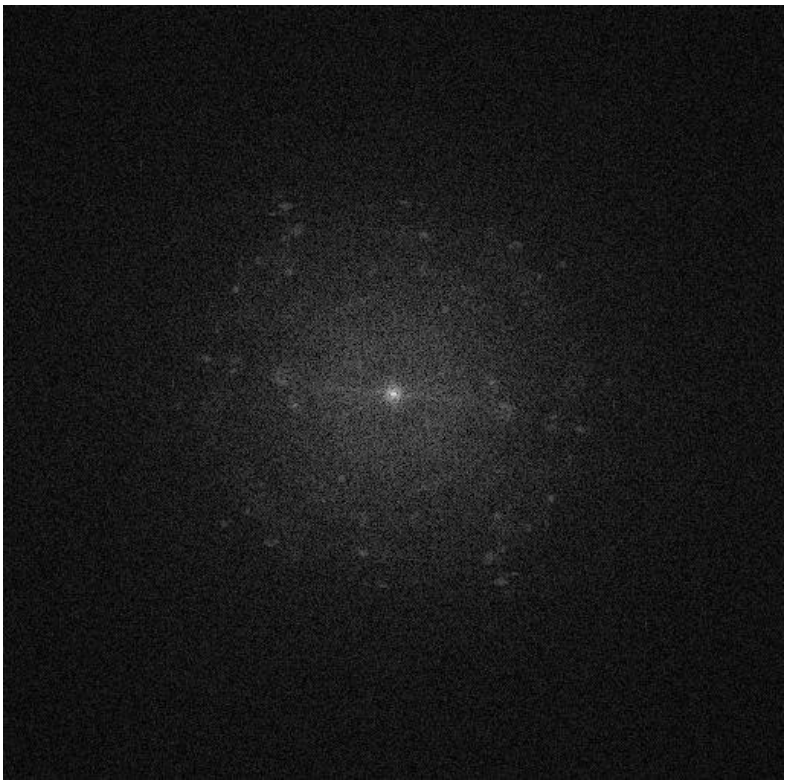

Figure 23: (a) The TEM images taken at a scale of 10nm. A clear rod shape is observed among the particles. (b) A massive number of nano-rods are observed. (c) The high resolution image of the nano-rod. (d) A live FFT image of (c). Diffraction analysis proved that the substance is Fe_3O_4, the detailed process will be described in the next section.

S5: This sample was produced at a temperature of 50 ℃ and dried at 70 ℃. The higher temperature results in a better reaction rate but a slightly higher chance of oxidation during the drying process. (**Fig. 24**)

(a) 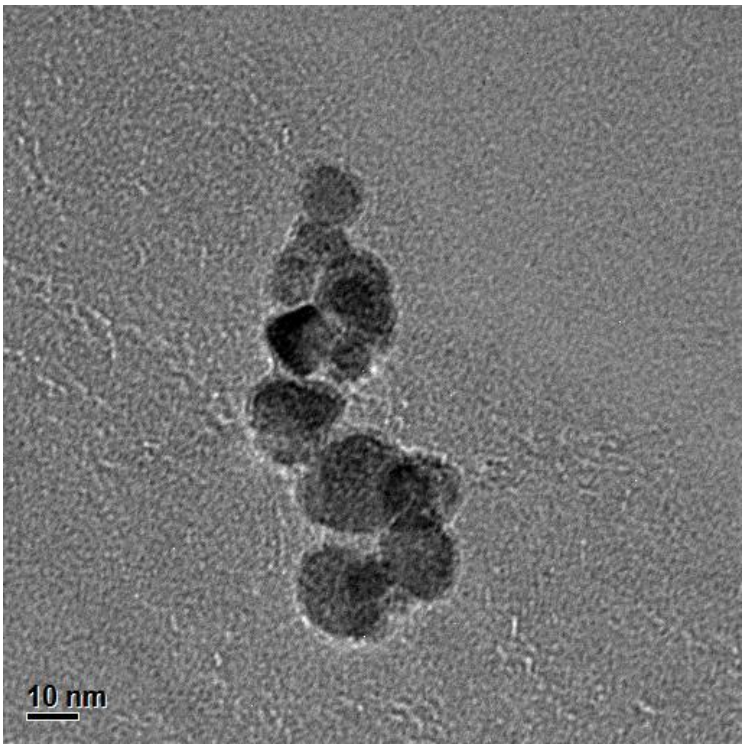

(b) 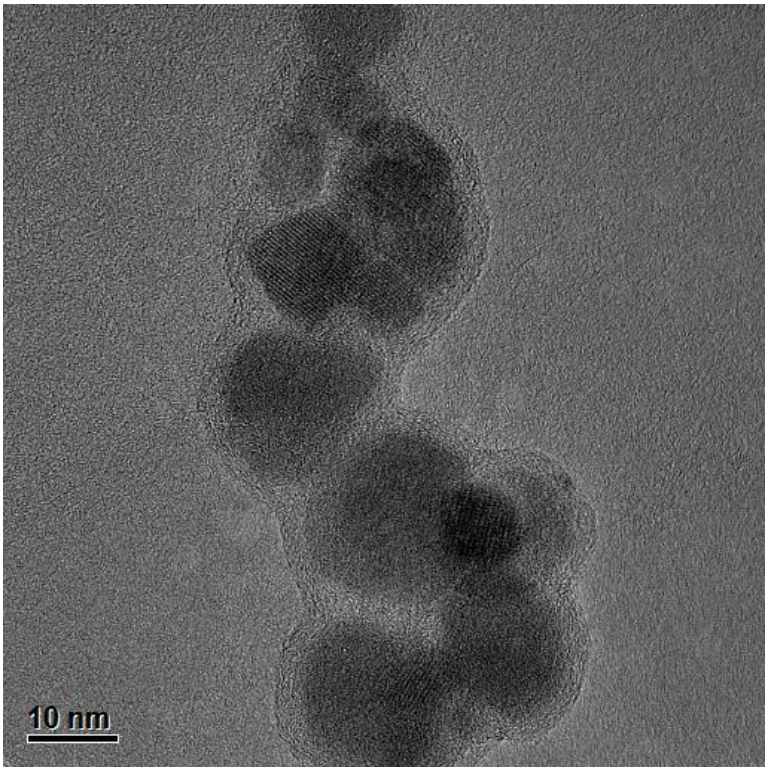

(c) 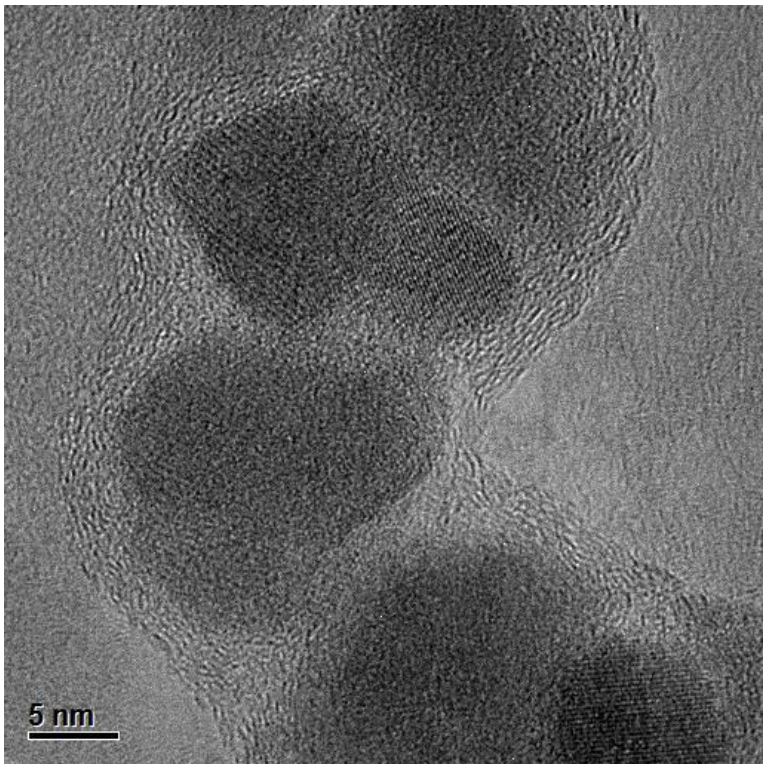

(d) 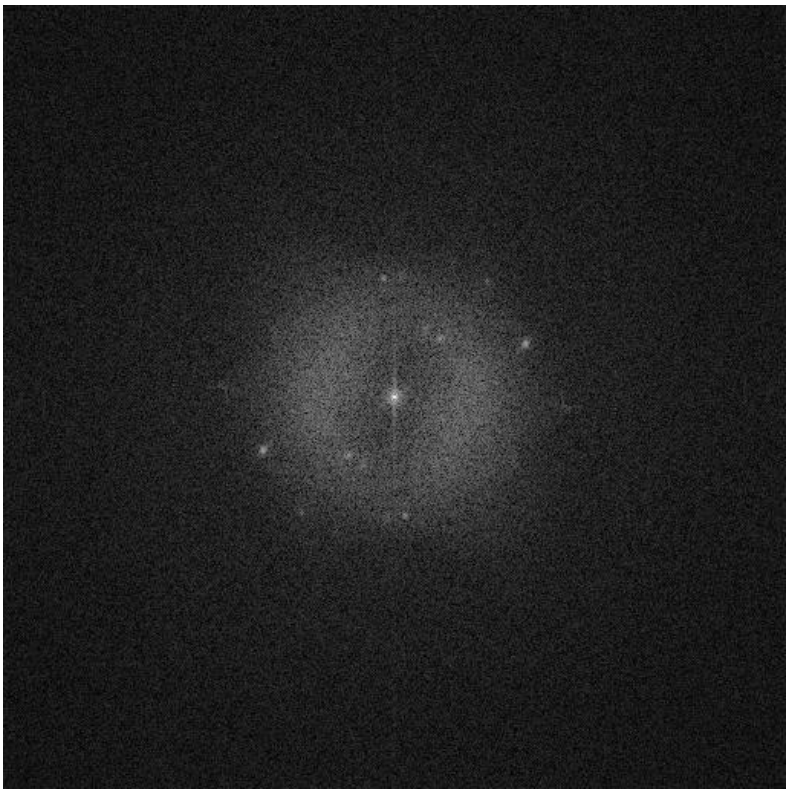

(e) 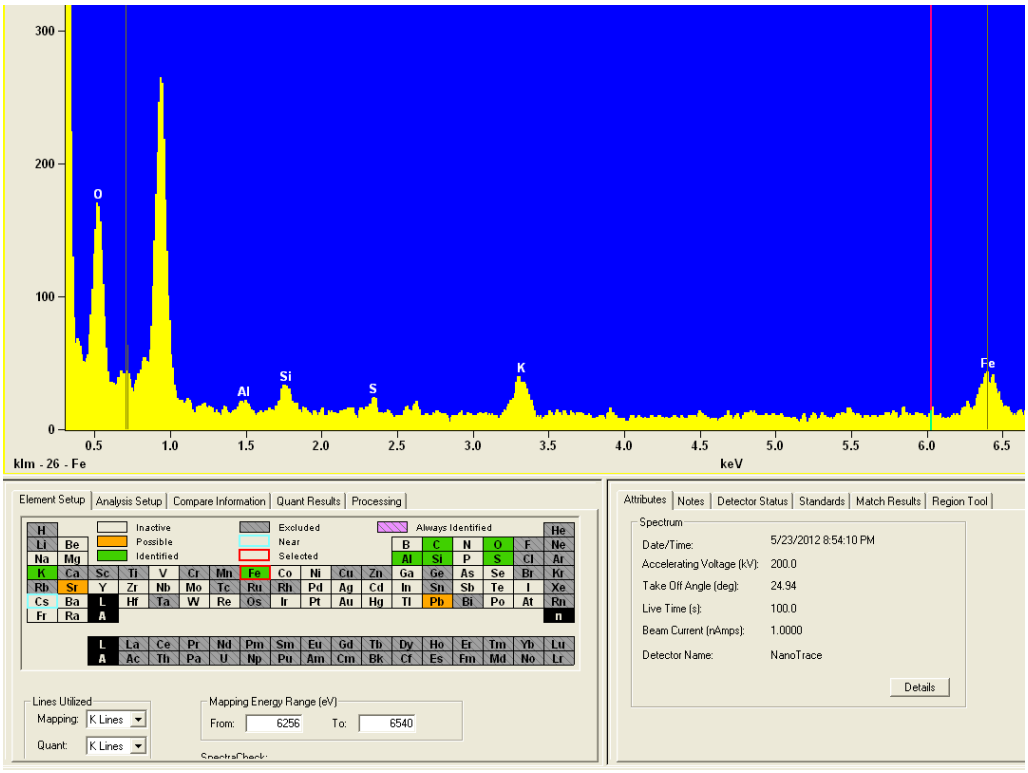

Figure 24: (a) and (b), low resolution images of S5 at a scale of 10 nm. The particles are clumped together without coating but the size is reasonably satisfying (< 10 nm). (c) A high resolution image of S5 at a scale of 5 nm. A light residue of acetone around the particles is observed and the shapes of the particles are significantly irregular. No presence of needle shapes/nano-rods. (d) A Fast Fourier Transform (FFT) image of (c). A clear lattice orientation is presented. Further detailed diffraction analysis is carried out hereafter. (e) The EDX (Energy Dispersive X-ray) analysis which shows the elemental composition of S5. Iron peaks and oxygen peaks are observed.

S6: This sample is made at 60 ℃ with more vigorous stirring and dried at 75 ℃. As it is sealed when drying, less oxidation occurs. Samples should retain strong magnetic properties as iron (III) oxide is one of the most important ferromagnets. **(Fig. 25)**

(a)

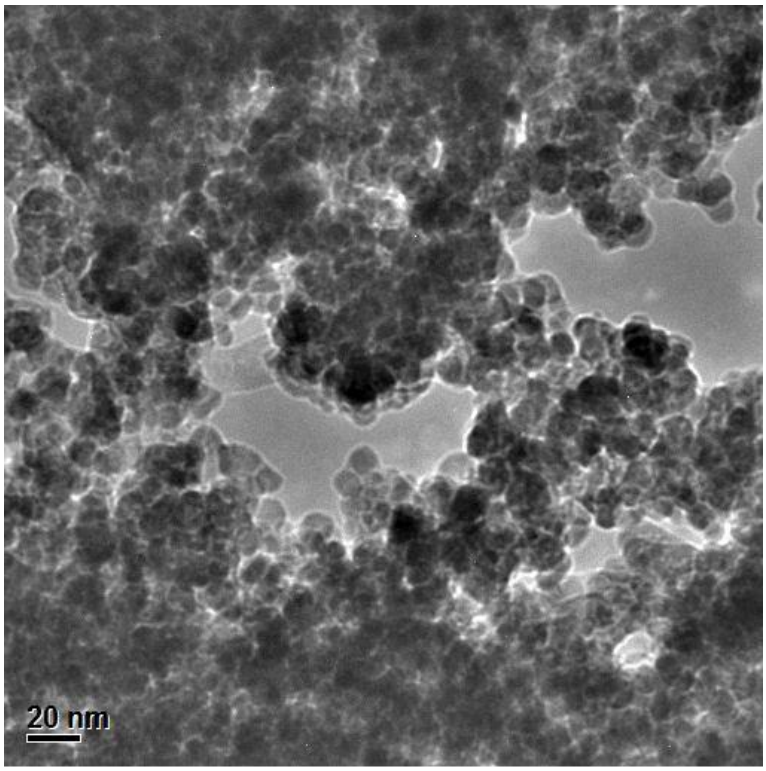

(b)

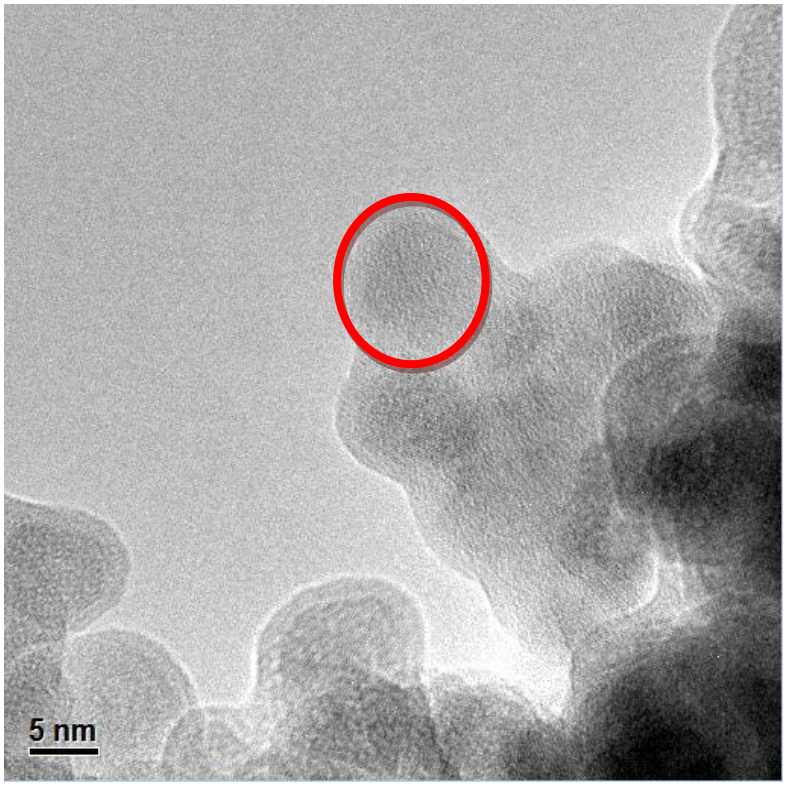

(c) 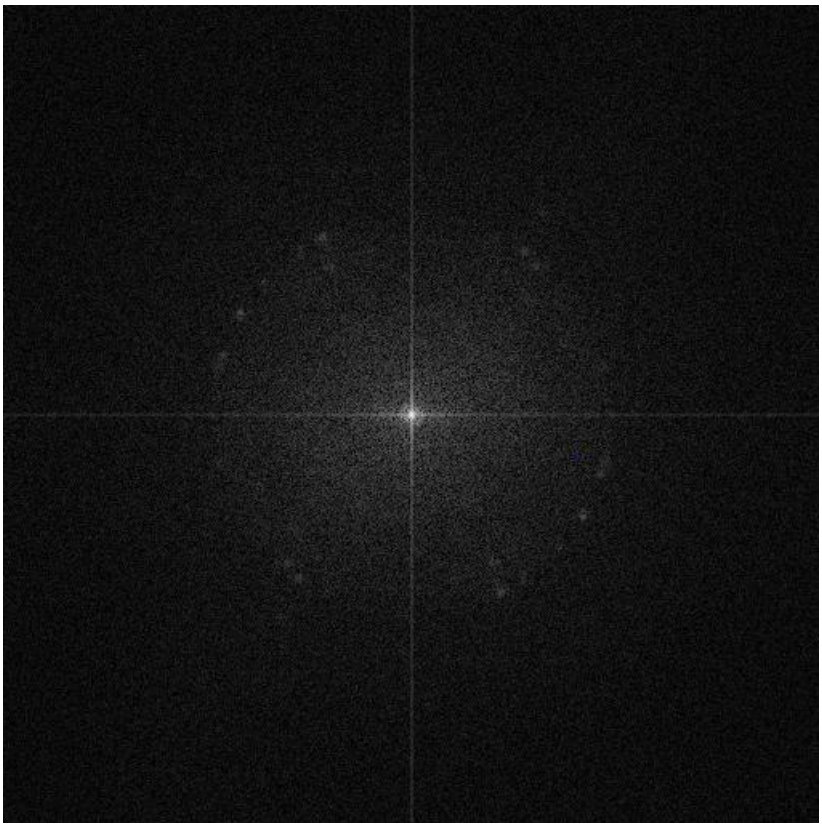

Figure 25: (a) shows a better dispersion of particles compared to the others due to the more vigorous stirring. (b) a high resolution TEM image of S6 which clearly proves the size of the SIONPs (<10 nm) with decent separation and dispersion. The red circle highlights a single particle. (c) Is an FFT image of the circled particle

S7: Synthesized at a temperature of 70 ℃ and stirred with a mechanical stirrer. The pH dropped to 2.22 due to an excess of hydrochloric acid added accidentally; but sustained at around 3.5 when ammonia was added. Dried at a temperature of 75 ℃

(a) 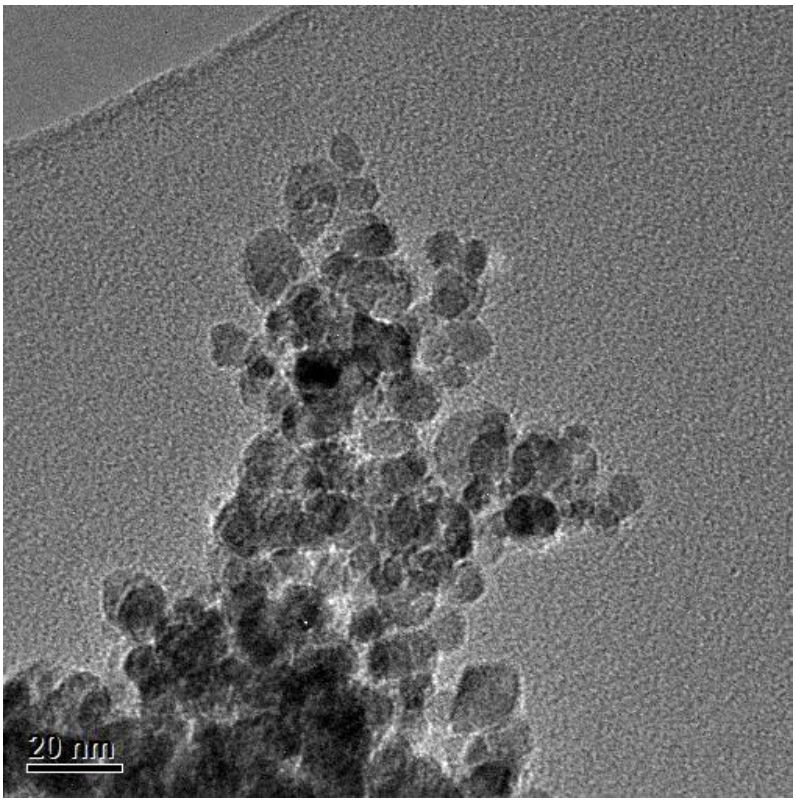

(b) 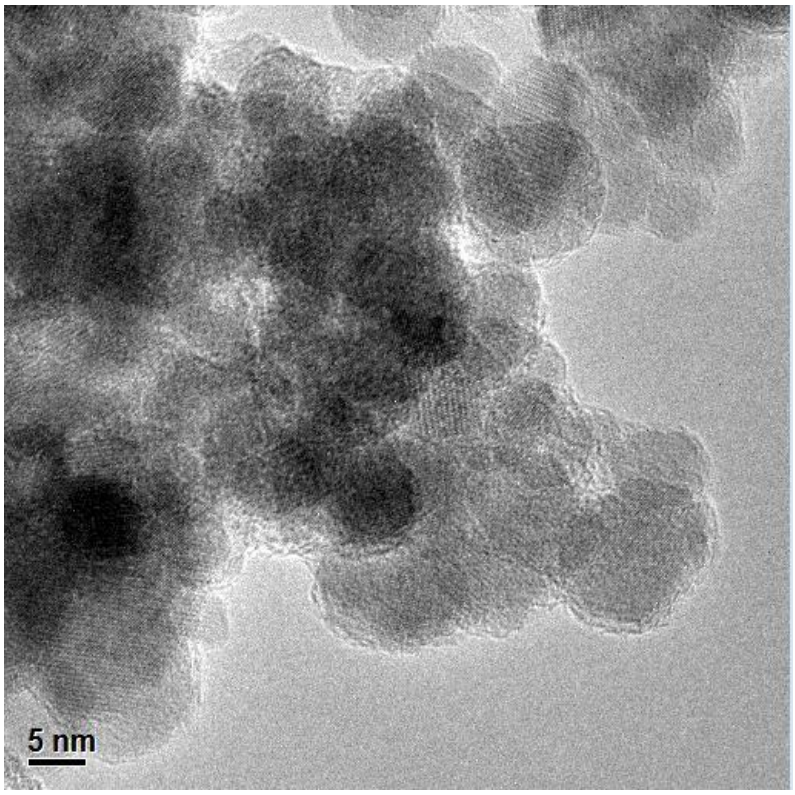

(c) 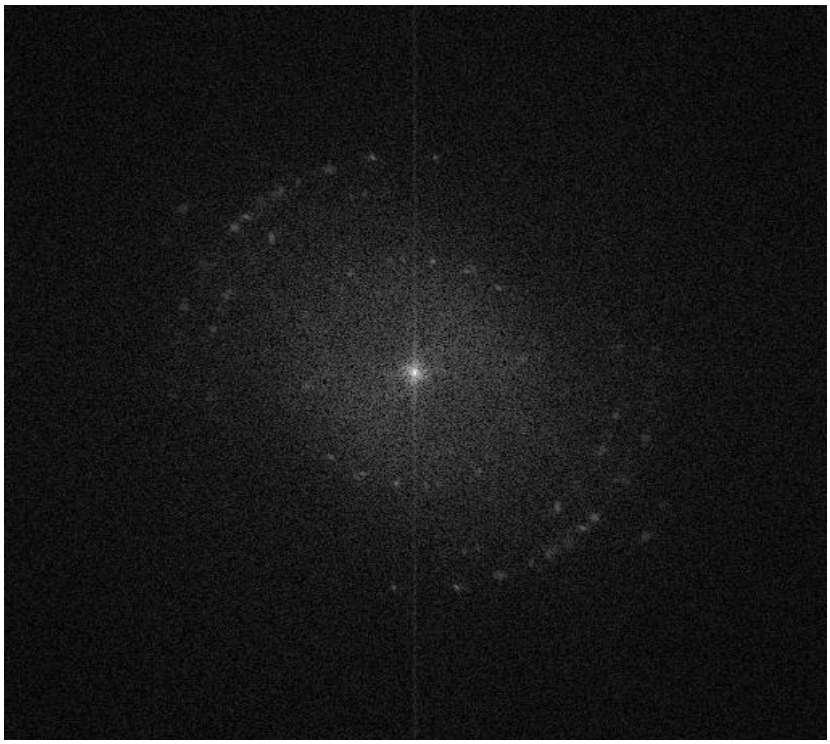

Figure 26: (a) is a lower resolution image at a scale of 20nm. (b) is a high resolution image showing the morphological characteristics of the particles, most of which are spherical. (c) is an FFT image of (b).

4.3.2 Composition of Particles

JEMS analysis of SPIONs

Although the EDX analysis of the SPIONs shows the right content of elements, it is still necessary to prove that the particles produced are exactly Fe_3O_4, rather than another member of the iron oxide group. The FFT images are extremely useful in determining different substances by proceeding with a diffraction analysis. JEMS, the software, is used during this process.

The basic methodology is that by halving the measurement of the distances between two bright dots (lattice orientations) on the ring of the image across the centre (**Fig. 27**), the radius of different rings can be obtained. The unit of the value of the radius is the inverse of nm, which apparently determines the inverse of the distances between the atoms. By comparing the values obtained to the powder line tables of known samples (single crystals) below (Tab. 2), the substance can be determined.

(a) 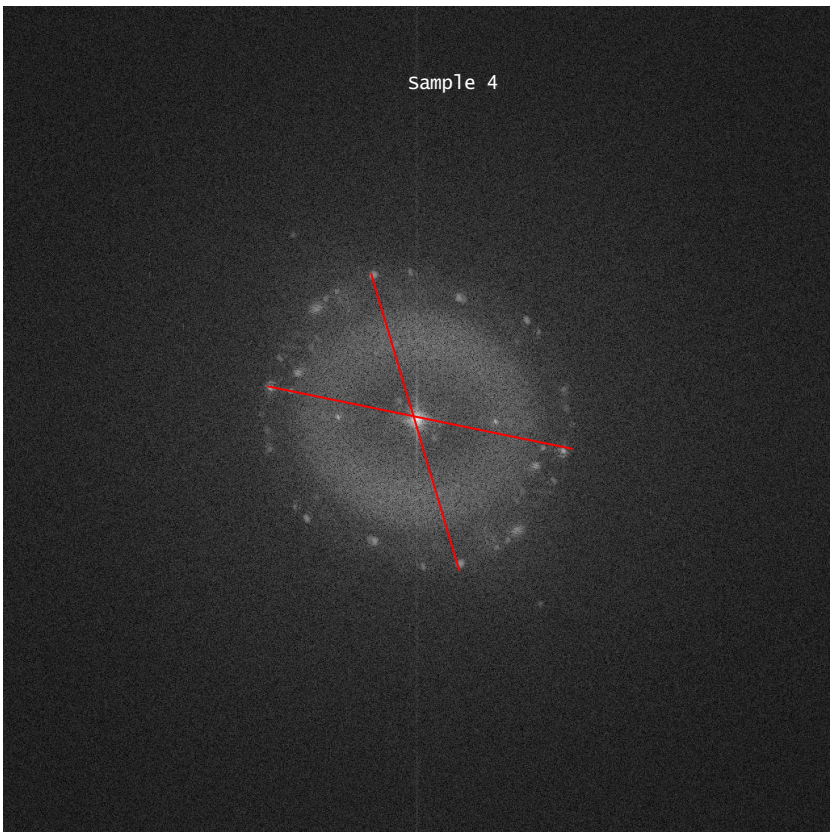

(b)

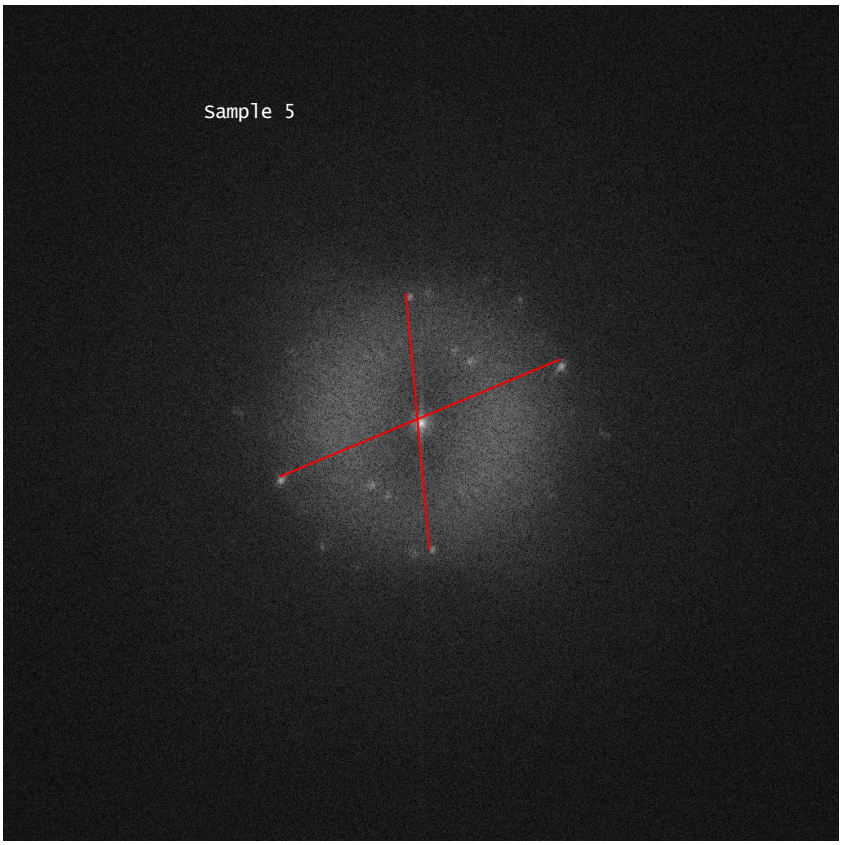

(c)

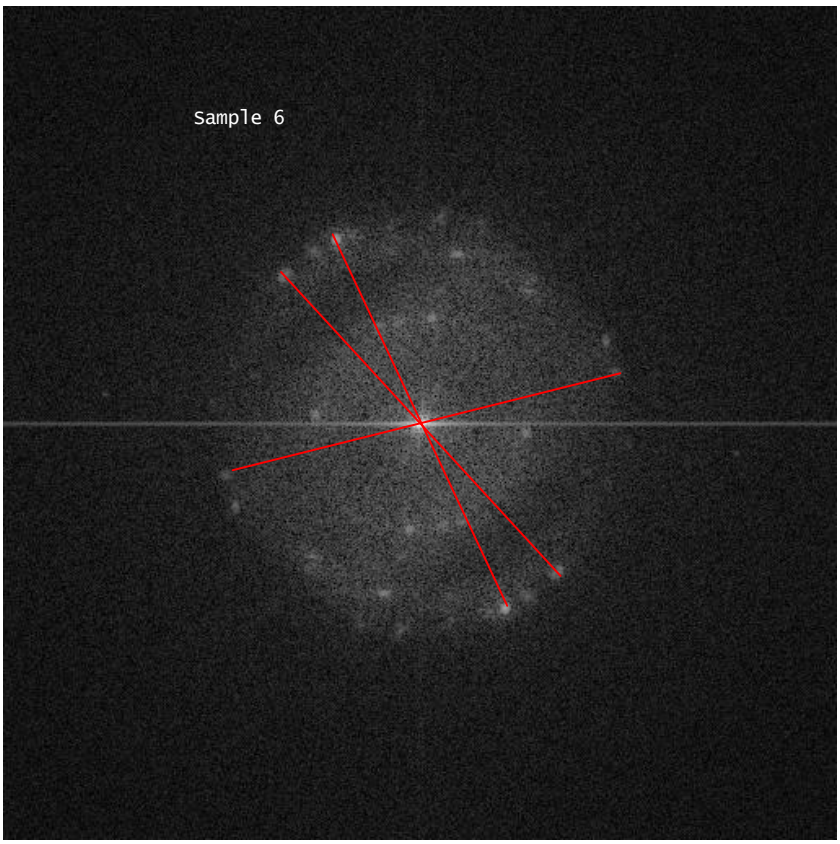

(d) 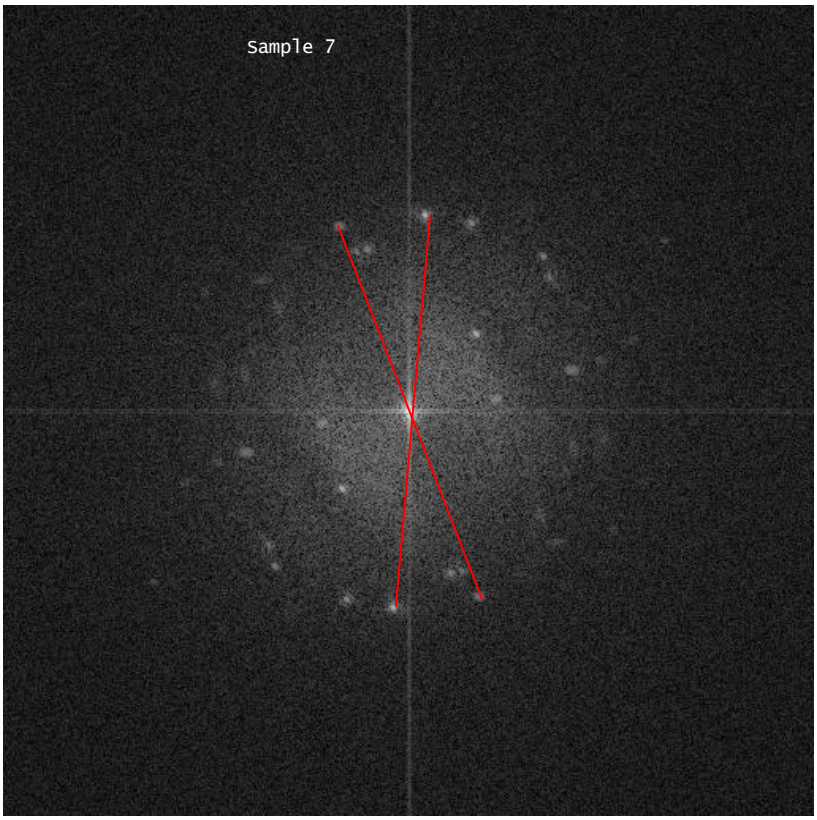

Figure 27: (a) (b) (c) (d) are FFT images taken by TEM. The redlines across the ring is the inverse of atomic distance between two atoms in the lattice.

Calibration from single crystal known sample:

Diameter (nm^{-1})	**radius**	**minus 15%**
10.922	5.461	4.64185
7.843	3.9215	3.333275
Sample1		
4.8562	2.4281	2.063885
9.2023	4.60115	3.9109775
7.7321	3.86605	3.2861425
14.1	7.05	5.9925
Sample2		

4.7593	2.37965	2.0227025
9.1476	4.5738	3.88773
10.6235	5.31175	4.5149875
Sample3		
4.0072	2.0036	1.70306
7.8241	3.91205	3.3252425
13.1565	6.57825	5.5915125
Sample 4		
4.816	2.408	2.0468
7.9	3.95	3.3575
9.13	4.565	3.88025
13.498	6.749	5.73665
Sample5		
4.751	2.3755	2.019175
9.091	4.5455	3.863675
9.657	4.8285	4.104225
10.97	5.485	4.66225
Sample 6		
4.91	2.455	2.08675
7.74	3.87	3.2895
9.275	4.6375	3.941875
Sample 7		
4.709	2.3545	2.001325
4.09	2.045	1.73825
7.811	3.9055	3.319675
9.5	4.75	4.0375

Table 2: the measurements of the radius of the rings from FFT images of S1-S7

Fe_3O_4 Powder lines

Powder lines table

Multi.	(h,k,l)	d* / nm-1	2 Theta / Deg.	Intens.	Bragg / mRad	Vr [V||nm||e]	Vi [V||nm||e]	Ampli. [V||nm|
1	(0, 0, 0)	0.000	0.000	0	0.000	34.587	1.358	34.614
8	(1, 1, 1)	2.077	0.300	40	2.604	-0.991	-1.089	1.473
12	(0, 2, 2)	3.391	0.490	233	4.253	3.729	0.175	3.733
24	(1, 1, 3)	3.977	0.580	903	4.987	4.158	-3.785	5.623
8	(2, 2, 2)	4.154	0.600	44	5.209	-0.051	-2.197	2.197
6	(0, 0, 4)	4.796	0.690	624	6.014	-10.263	-0.348	10.269
24	(1, 3, 3)	5.226	0.760	12	6.554	-0.510	-0.561	0.758
24	(2, 2, 4)	5.874	0.850	103	7.366	2.309	0.109	2.312
8	(3, 3, 3)	6.230	0.900	84	7.813	2.751	-2.504	3.719
24	(1, 1, 5)	6.230	0.900	252	7.813	2.504	2.751	3.719
12	(0, 4, 4)	6.783	0.980	1000	8.506	10.921	0.424	10.929
48	(1, 3, 5)	7.094	1.020	10	8.895	-0.412	0.375	0.558
24	(0, 2, 6)	7.583	1.090	47	9.510	1.770	0.083	1.772
24	(3, 3, 5)	7.863	1.130	122	9.860	1.956	2.149	2.907
24	(2, 2, 6)	7.954	1.150	4	9.974	0.044	0.557	0.559
8	(4, 4, 4)	8.307	1.200	126	10.417	-5.258	-0.181	5.261
24	(1, 1, 7)	8.563	1.240	3	10.738	-0.335	0.305	0.453
24	(1, 5, 5)	8.563	1.240	3	10.738	-0.305	-0.335	0.453

(a)

Fe_2O_3 alpha Powder lines

Powder lines table

Multi.	(h,k,l)	d* / nm-1	2 Theta / Deg.	Intens.	Bragg / mRad	Vr [V||nm||e]	Vi [V||nm||e]
1	(0, 0, 0)	0.000	0.000	0	0.000	34.918	1.353
2	(0, 1, 2)	2.713	0.390	424	3.402	-4.334	-0.181
2	(-1, 0, 2)	2.713	0.390	424	3.402	-4.334	-0.181
2	(1, -1, 2)	2.713	0.390	424	3.402	-4.334	-0.181
2	(0, -1, 4)	3.700	0.540	1000	4.640	-7.769	-0.384
2	(1, 0, 4)	3.700	0.540	1000	4.640	-7.769	-0.384
2	(-1, 1, 4)	3.700	0.540	1000	4.640	-7.769	-0.384
2	(1, 1, 0)	3.970	0.580	363	4.978	4.842	0.311
2	(-1, 2, 0)	3.970	0.580	363	4.978	4.842	0.311
2	(-2, 1, 0)	3.970	0.580	363	4.978	4.842	0.311
2	(0, 0, 6)	4.357	0.630	118	5.463	-2.903	0.022
2	(1, 1, 3)	4.528	0.660	693	5.678	7.162	0.208
2	(-1, -1, 3)	4.528	0.660	693	5.678	-7.162	-0.208
2	(-2, 1, 3)	4.528	0.660	693	5.678	7.162	0.208
2	(2, -1, 3)	4.528	0.660	693	5.678	-7.162	-0.208
2	(-1, 2, 3)	4.528	0.660	693	5.678	-7.162	-0.208
2	(1, -2, 3)	4.528	0.660	693	5.678	7.162	0.208
2	(2, 0, 2)	4.809	0.700	4	6.030	-0.559	-0.052

(b)

Fe_2O_3 beta Powder lines

Powder lines table

Multi.	(h,k,l)	d* / nm-1	2 Theta / Deg.	Intens.	Bragg / mRad	Vr [V||nm||e]	Vi [V||nm||e]
1	(0, 0, 0)	0.000	0.000	0	0.000	34.013	1.318
6	(0, 0, 2)	2.129	0.310	19	2.670	1.096	0.038
24	(1, 1, 2)	2.608	0.380	209	3.270	2.035	0.083
12	(0, 2, 2)	3.011	0.440	7	3.776	-0.554	-0.016
8	(2, 2, 2)	3.688	0.530	1000	4.625	9.158	0.429
48	(1, 2, 3)	3.983	0.580	287	4.995	-2.084	-0.043
6	(0, 0, 4)	4.258	0.620	9	5.340	1.038	0.172
24	(1, 1, 4)	4.517	0.650	9	5.664	0.552	-0.013
24	(0, 2, 4)	4.761	0.690	0	5.970	0.073	0.018
24	(2, 3, 3)	4.994	0.720	367	6.262	-3.729	-0.123
24	(2, 2, 4)	5.216	0.750	26	6.540	1.015	0.041
48	(1, 3, 4)	5.429	0.790	275	6.807	2.378	0.093
48	(1, 2, 5)	5.831	0.840	43	7.312	0.976	0.041
12	(0, 4, 4)	6.022	0.870	839	7.552	8.752	0.347
24	(3, 3, 4)	6.208	0.900	17	7.784	0.896	0.047
24	(2, 4, 4)	6.388	0.920	8	8.010	0.635	0.021
6	(0, 0, 6)	6.388	0.920	4	8.010	0.905	0.046
48	(2, 3, 5)	6.563	0.950	37	8.230	0.960	0.039

(c)

Fe_2O_3 gamma Powder lines

Powder lines table

Multi.	(h,k,l)	d* / nm-1	2 Theta / Deg.	Intens.	Bragg / mRad	Vr [V||nm||e]	Vi [V||nm||e]
1	(0, 0, 0)	0.000	0.000	0	0.000	31.849	1.233
8	(1, 0, 1)	1.263	0.190	7	1.584	0.240	-0.217
8	(1, 0, 2)	1.440	0.210	15	1.806	0.505	0.026
2	(0, 0, 4)	1.598	0.230	6	2.004	0.668	0.033
4	(1, 1, 0)	1.694	0.250	29	2.125	-1.058	-0.044
8	(1, 0, 3)	1.695	0.250	32	2.125	0.531	0.583
8	(1, 1, 1)	1.741	0.260	4	2.183	0.016	-0.290
8	(1, 1, 2)	1.873	0.270	3	2.349	-0.236	-0.014
8	(1, 0, 4)	1.997	0.290	0	2.504	0.002	-0.100
8	(1, 1, 3)	2.075	0.300	56	2.603	0.044	-1.155
8	(1, 1, 4)	2.329	0.340	5	2.921	0.377	0.018
8	(1, 0, 5)	2.329	0.340	1	2.921	0.102	-0.089
4	(2, 0, 0)	2.396	0.350	0	3.005	-0.079	-0.002
8	(2, 0, 1)	2.429	0.350	6	3.046	-0.276	-0.304
8	(2, 0, 2)	2.526	0.370	0	3.168	-0.004	0.110
8	(1, 1, 5)	2.619	0.380	5	3.284	0.019	-0.368
8	(2, 1, 0)	2.679	0.390	30	3.360	0.960	0.043
8	(2, 0, 3)	2.679	0.390	31	3.360	-0.717	0.656

(d)

FeO Powder lines

(e)

Powder lines table

Multi.	(h,k,l)	d* / nm-1	2 Theta / Deg.	Intens.	Bragg / mRad	Vr [V|nm|e]	Vi [V|nm|e]	Ampli. [V|
1	(0, 0, 0)	0.000	0.000	0	0.000	30.863	1.330	30.891
8	(1, 1, 1)	4.037	0.590	357	5.063	7.165	0.423	7.177
6	(0, 0, 2)	4.662	0.670	1000	5.846	14.895	0.622	14.908
12	(0, 2, 2)	6.593	0.950	734	8.268	10.728	0.447	10.737
24	(1, 1, 3)	7.731	1.120	151	9.695	3.728	0.223	3.735
8	(2, 2, 2)	8.075	1.170	254	10.126	8.557	0.357	8.564
6	(0, 0, 4)	9.324	1.340	116	11.692	7.164	0.300	7.170
24	(1, 3, 3)	10.161	1.470	66	12.741	2.820	0.165	2.825
24	(0, 2, 4)	10.425	1.500	306	13.072	6.163	0.259	6.168
24	(2, 2, 4)	11.420	1.650	215	14.320	5.399	0.227	5.404
8	(3, 3, 3)	12.112	1.750	12	15.189	2.260	0.130	2.263
24	(1, 1, 5)	12.112	1.750	35	15.189	2.260	0.130	2.263
12	(0, 4, 4)	13.186	1.900	59	16.536	4.311	0.182	4.315
48	(1, 3, 5)	13.790	1.990	43	17.294	1.869	0.107	1.872
24	(2, 4, 4)	13.986	2.010	92	17.539	3.912	0.165	3.916
6	(0, 0, 6)	13.986	2.010	23	17.539	3.912	0.165	3.916
24	(0, 2, 6)	14.743	2.120	73	18.488	3.581	0.151	3.584
24	(3, 3, 5)	15.285	2.200	14	19.169	1.594	0.091	1.596

Table 3: (a) (b) (c) (d) and (e) are the powder line tables of different iron oxide groups. By comparing the calibrated value of the radius of the ring (**see Tab 2**) respectively to the value circled in red in the table, it is obvious that the only matching table would be (a). Thus, the particles manufactured from the co-precipitating technique are definitely Fe3O4.

Once the composition of the SPIONs was confirmed, further work could be carried out. Sample 6 was selected to synthesize SPIONP pellets as it has the best morphology, dispersion and magnetic properties (detailed interpretation see the VSM results in Chapter 5.1.4)

4.4 SPIONP Synthesis

The polymer carrier used to produce SPIONP is as shown below:

Product information: DOW CORNING(R) 785 SANITARY ACETOXY SILICONEE WHITE (see Tab 4 below)

Oxidizing properties: No

COMPOSITION / INFORMATION ON INGREDIENTS

Chemical characterization: Silicone elastomer

Hazardous Ingredients:

Name	CAS-No.	EINECS/ ELINCS No.	Conc. (% w/w)	Classification	
Triacetoxy(ethyl)silane	17689-77-9	241-677-4	1.9		R14
				C	R34
				Xn	R22
Methyltriacetoxysilane	4253-34-3	224-221-9	1.7		R14
				C	R34
				Xn	R22

Table 4: Composition/information on ingredients of DOW CORNING(R) 785 SANITARY ACETOXY SILICONEE WHITE, rubber silicone

The main composition, as shown, is Triacetoxy(ethyl)silane and Methyltriacetoxysilane. It is essential to know their chemical and physical properties since the preparation of SPIONP involves mixing them with coated superparamagnetic iron particles. If there were chemical reactions between the siliconee matrix and the coating material of the iron particles during the mixing process, the properties of SPIONP would be impacted.

Physical properties:

Triacetoxy(ethyl)silane	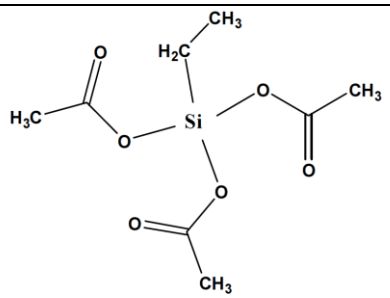	Molecular Formula: $C_8H_{14}O_6Si$ Melting point: 8.4 ℃ Boiling point 227 ℃ at 1013 hPa Relative density 1.1437 at 20 ℃
Methyltriacetoxysilane	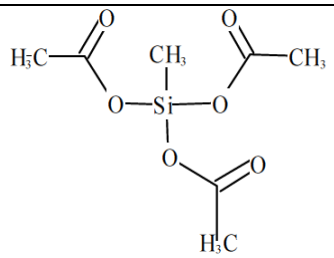	Molecular Formula: $C_7H_{12}O_6Si$ Melting point : 40.5 ℃ Boiling point: 220 ℃ at 1013 hPa Relative density 1.1697 at 20 ℃

Three samples with different concentrations of magnetic particles, 15%, 25% and 30%, respectively, are produced and made into pellets by the ejector shown below. (**Fig.28**)

(a) 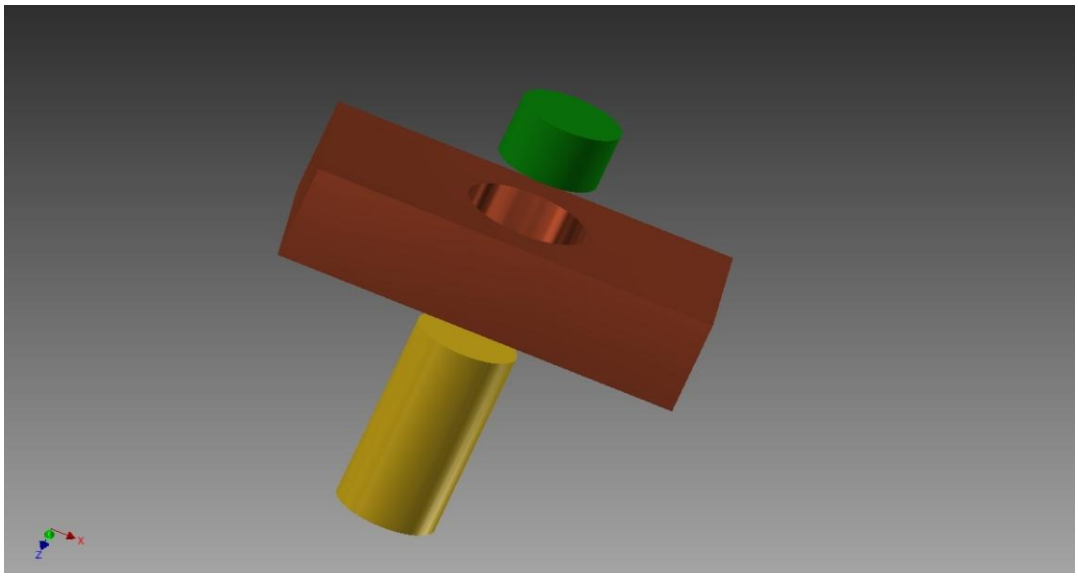

(b) 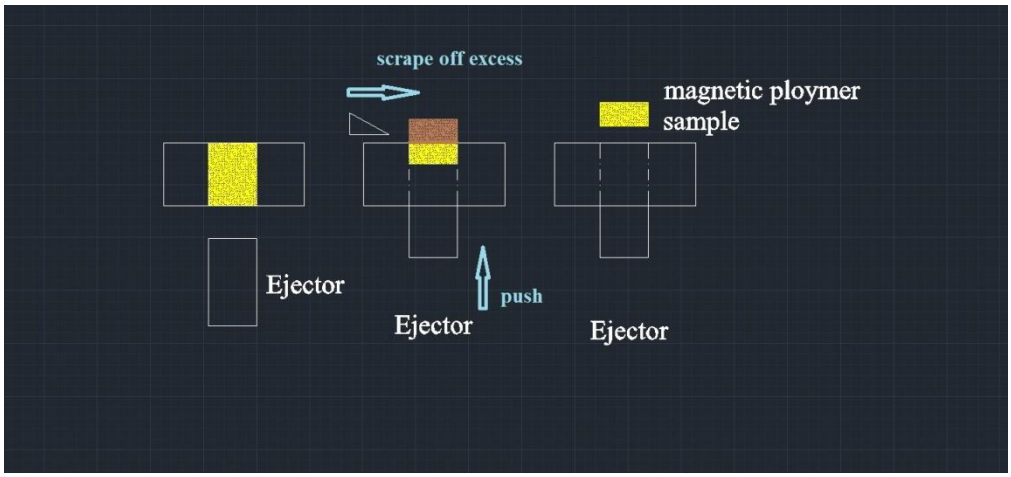

Figure 28: (a) 3-dimensional illustration of the structure of the ejector (b) The mixtures of SPIONP in different concentrations are injected into the ejector separately. Scrape off the excess if any. Eject out the SPIONP sample pellets after the mixtures are entirely dried out.

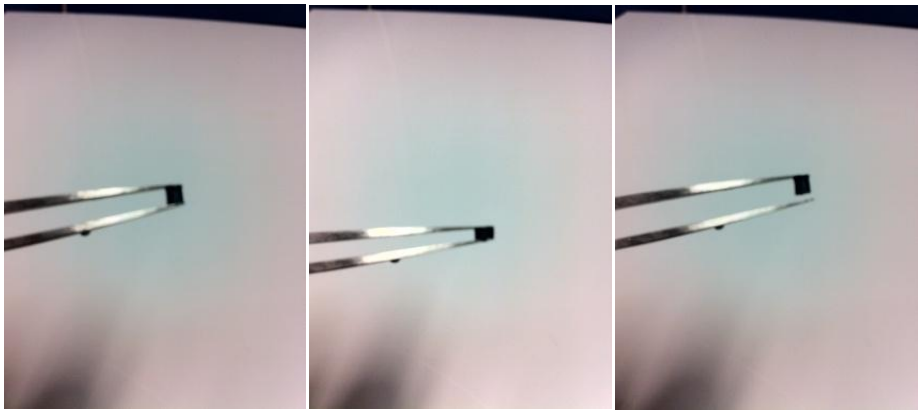

Figure 29: The picture shows the finished pellets of SPIONP. After squeezing, it tends to bounce back to the original shape, which is typical behaviour for silicone rubber.

The particle concentration of the pellet sample is significantly influencing their magnetic properties. In order to find the connection between strain change and magnetic properties. A critical concentration has to be found to make the most eligible test sample.

According the hysteresis loop from the VSM result (see details in the following chapter), before the particle concentration of 30%, the samples stay superparamagnetic with relatively low magnetization, however, when the concentration is approaching 30 %, the samples abruptly behave as ferromagnetic.

Therefore, 30% concentration is a critical. In order to acquire some data to compare with the tested sample, further samples with concentrations of 25% and 15% are also subjected to VSM measurement.

Chapter 5: Magnetic Properties

5.1 Principles and Instrumentation

To discover whether changing the distance between SPIONs in the silicone matrix by applying a compressing strength could orientate or change the magnetization, a measurement with the VSM is performed. A test of the relationship between the distance between SPIONs and the enhancement of their interaction (by direct exchange interaction or dipole interaction) is carried out. A brand new VSM is assembled specifically for this research and a unique sample holder attached to the end of the VSM probe is designed particularly for this experiment.

5.1.1 VSM Assemble and Working Principles

As this experiment involves compressing SPIONP pellet samples, a particular sample holder and a corresponding VSM which has a demountable probe to let different sample holders fit into it has to be designed and assembled.

The author, Dr. Iain Will, Mr Charan Panesar, Mr Nicholas Maltby and Mr Cong Lu have teamed up as a group, each with a different division of specialization (hardware, computer assembly, labview software and calibration) to work on this VSM project.

First of all, the VSM is assembled piece by piece with different hardware parts including a water-cooled electromagnet and power supply, a vibration exciter and samples rod, sensor coils (pick-up coils), Hall sensor amplifier and control chassis, lock-in amplifier and computer interface (software).

The following series of photos shows the flow path of assembly; (Fig. 30)

(a)

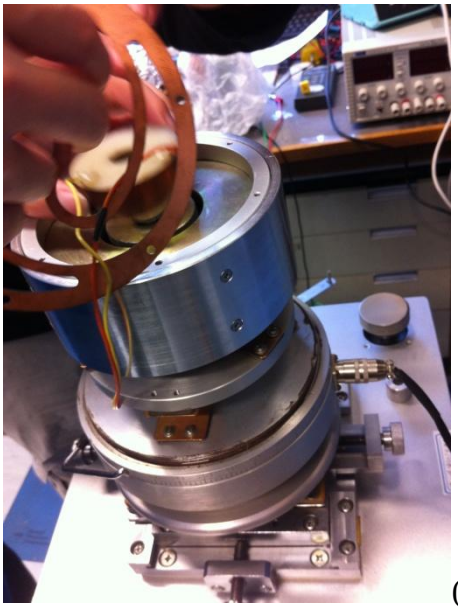

(b)

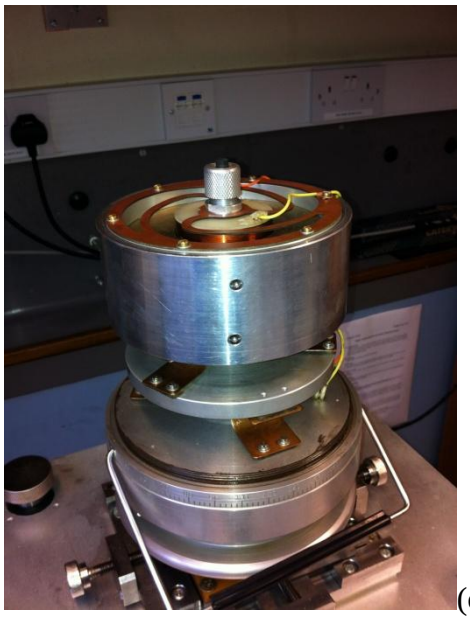

(c)

(d)

(e) 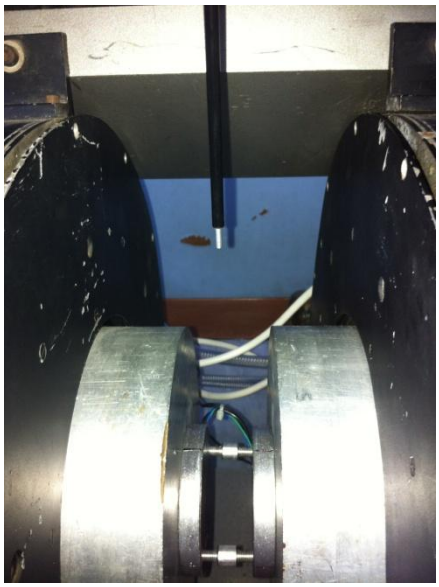 (f) 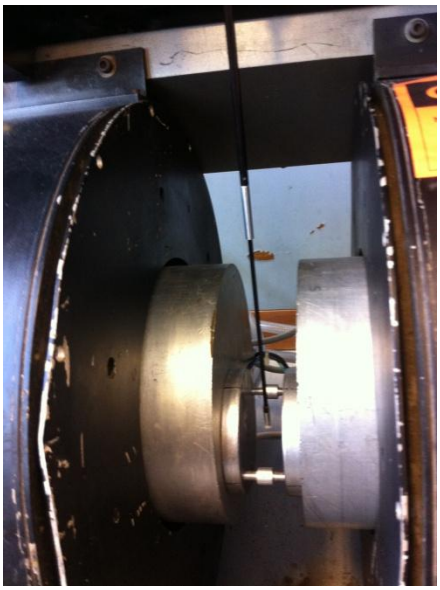

(g) 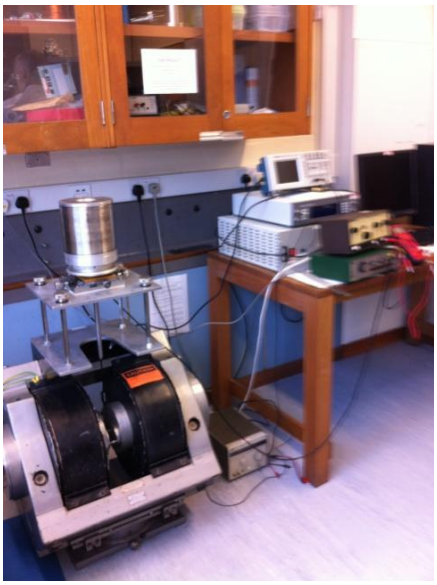 (h) 

Figure 30: (a) The head-core part (vibration exciter and sample rod), which includes a small ring-shaped magnet in the central part trapped with an internal steel sleeve, was designed by the team and crafted by Mr Charan Panesar. (b) A copper spring coil attached to the internal sleeve is welded with wires connecting to the amplifier. (c) Completed vibration exciter with sample rod in the middle. (d) Design of outer sleeve to protect the whole setup of the head-core part. (e) The large black chunks on the outside are the water cooled electromagnet connected to the main power supply. The inmost pair of coils is the sensor coil (Hall sensor) which is used to pick up signals of induced

voltage and connect to the locking amplifier. (f) Self-designed demountable sample rod. (g) (h) Whole VSM system completed.

Mr Nicholas Maltby started to work on the computer interface as soon as the VSM was assembled. Labview software designing took about another two months before our VSM could actually be used.

Mr Cong Lu and the author began to grow samples such as SPIONs and thin films to calibrate the whole VSM system.

A schematic chart (fig) shows the working principle of this particular VSM.

The sample is inserted into the sample holder and plugged into the end of the probe in the middle of the sensor coil. The two water-cooled electromagnets, one on each side of the sample, are powered by a DAC output and start to generate a magnetic field. The audio amplifier supplies power to the vibrating head (vibrating exciter) and hence the sample starts to vibrate vertically. Since it is passing through the magnetic field, an induced voltage is generated according to Faraday's law in the form of signals that are gathered by the pick-up coil. All the signals are transferred to the locking amplifier and hence brought to a computer interface.

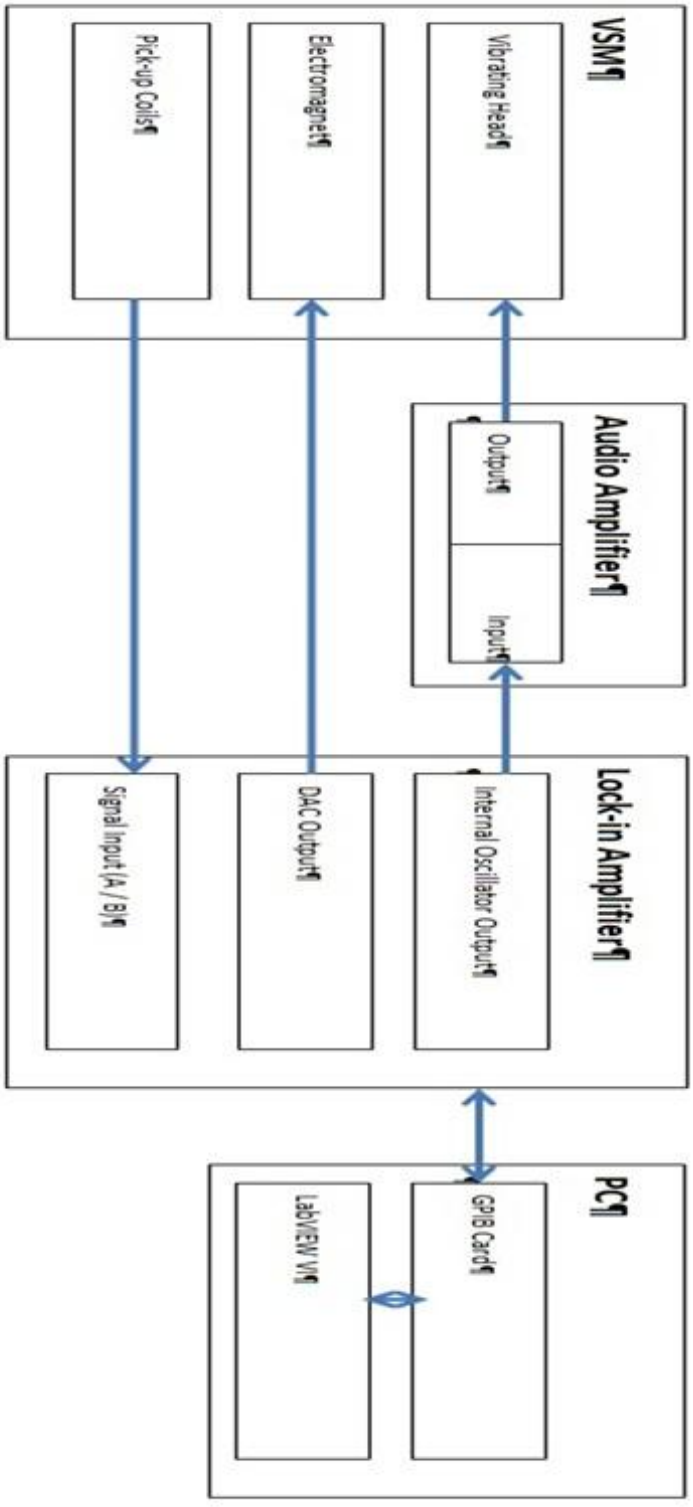

Figure 31: Schematic chart of this VSM

5.1.2 Sample Holder Design

The sample holder attached to the end of the VSM probe is designed to be made from acrylics and brass to minimize the impact on the result due to the magnetization of metal parts.

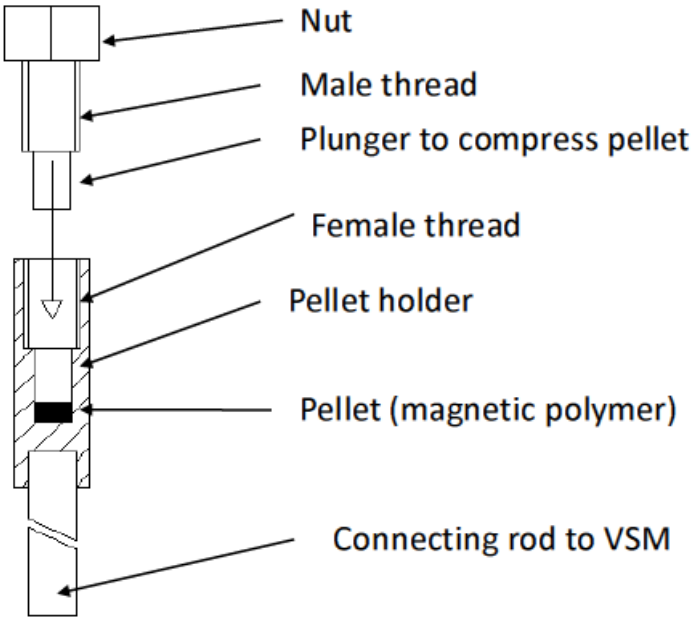

Basic Principle

The plunger screws into the pellet holder until the plunger end hits the pellet and compresses it. Spacers between the Nut head and pellet holder determines the amount of pellet compression

Figure 32: Schematic of Proposed Sample Holder and Compressor (Cooperative Design with Dr. Iain Will, crafted by Mr Charan Panesar, Electronics Department, University of York)

Figure 33: The photos above show the finished product of the sample holder. The transparent pellet holder is made of non-magnetic acrylics and the golden thread part is made of brass. These two parts comprise the SPIONP pellet holder. The black rod is made of carbon fishing rod, which is also non-magnetic. The silver thread part connects directly with the VSM probe and holds the sample between two pick-up coils.

5.1.3 Large Iron Oxide Particles Measurements from Physics Department

In Chapter 3, to get more familiar with the properties of Iron Oxide Particles; large Iron Oxide particles with size 1-7μm are used to obtain SEM images. They are made into polymer pellets as well to be put into the pre-test. Three samples with different concentrations of magnetic particles, 15%, 25% and 30%

The VSM result is as follows (for detailed result data, see Appendix I):

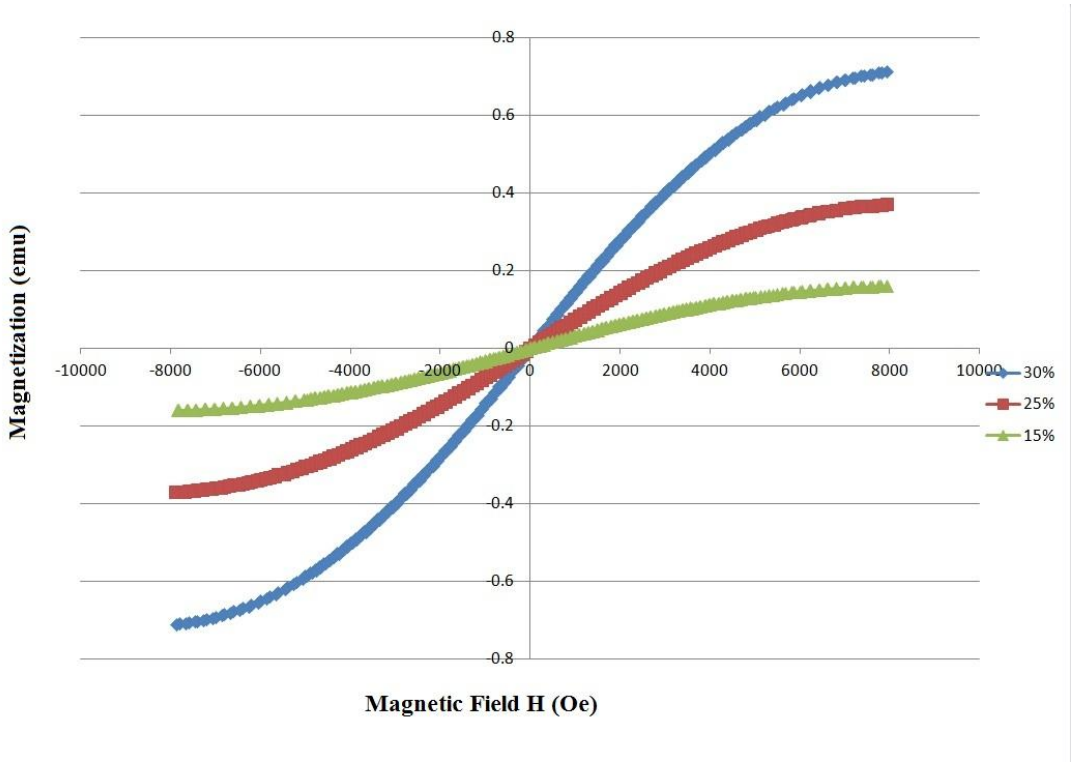

Figure 34: an apparent increasing trend with the increase in particle concentration presented in hysteresis curves.

The result is reasonably satisfying, as expected. These particles are too large to behave as superparamagnetic nanoparticles. However, knowing that magnetic moment is proportional to the concentration of particles, even in a non-conductive silicone rubber matrix, allows further research on SPIONPs.

5.1.4 SPION VSM Measurements from the Physics Department

Before starting to synthesize SPIONPs, the magnetic properties of SPIONs should be determined. As there were seven different SPIONs fabricated (see Chapter 4) under

various conditions, the one with the best dispersion and highest magnetic moment should be selected to synthesize SPIONP pellets in order to get the most reliable result. Various sources of data acquisition should be taken from the pre-test of the VSM system we built to get a more accurate calibration. Therefore, SPIONs are ground into clear films, mixed with resin and made into thin films to be taken to the other VSM in the physics department. The results are shown below (for detailed data see Appendix II):

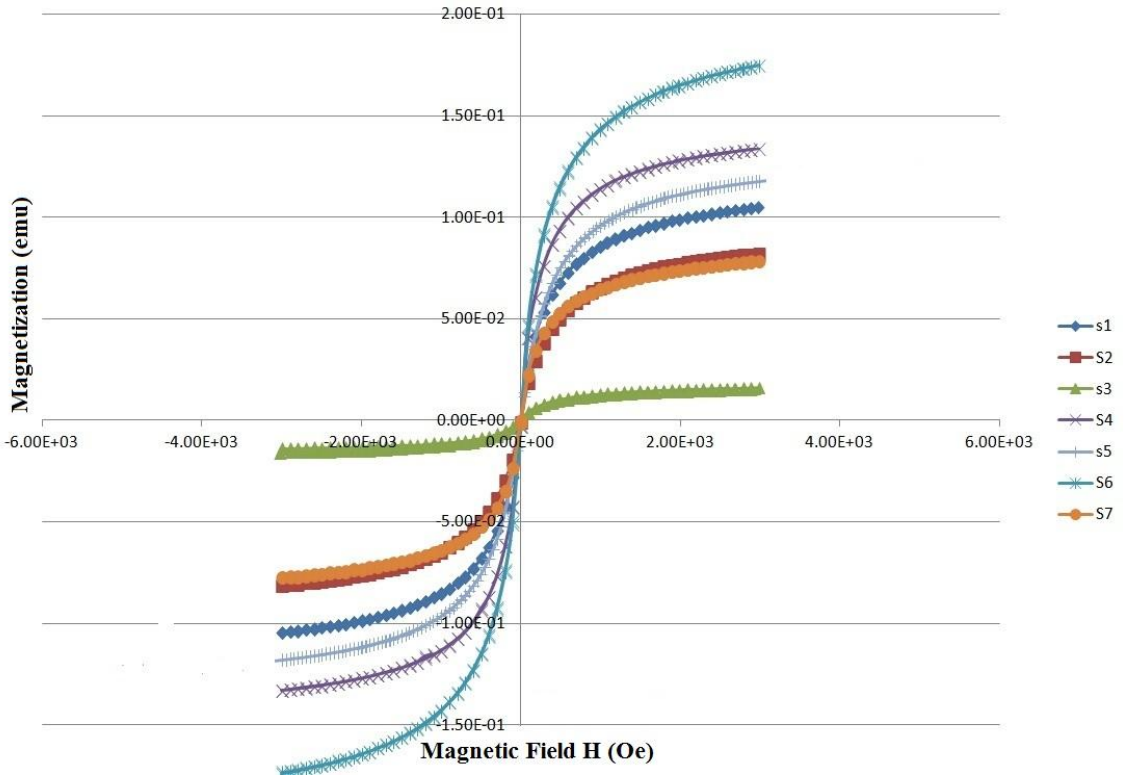

Figure 35: The hysteresis curve clearly shows the magnetic moments of S1-S7. S6 and S4 have the highest and 2nd highest magnetic moments, respectively, whereas S3 has the lowest. S2 and S7 have similar figures.

It is quite obvious that S6 has the highest magnetic moment as well as the best dispersion distribution under TEM. The factors which influence the magnetic and morphological properties of SPIONs are indicated according to this result.

- Reaction Temperature: around 60℃. A lower temperature results in a slower reaction rate during the chemical synthesis; however, if the temperature is too high, Fe^{2+} is more likely to be oxidized before the precipitation of SPIONs happens.
- Drying: When drying the SPIONs, the container should be hermetically sealed or at least relatively hermetically sealed so that there is less chance of them becoming contaminated.
- Acid: S3, with the lowest magnetic moment, is the only SPION sample that was fabricated without involving hydrochloric acid. The particles therefore, are not properly stabilized.

5.2 Measurements and Analysis

After several measurements taken from the VSM in the physics department, it is time to use the newly assembled VSM to achieve the main objective of this research; to investigate whether the distance between the particles can be changed to enhance their interaction (by direct exchange interaction or dipole interaction), so that they become ferromagnetic or ferrimagnetic or vice versa. SPIONP pellets are measured in our VSM both before compressing and after so that a comparable result can be obtained.

5.2.1 SPIONP VSM Measurement

Three samples with different concentrations of magnetic particles of 15%, 25% and 30% respectively are produced and made into pellets by the ejector shown below. The most

ideal concentration is found to be 30% through the Hall sensor test; this concentration is a critical locus of just being magnetic after and non-magnetic before pressing the SPIONP pellet sample. In order to acquire some data to compare with the tested sample, further samples with concentrations of 25% and 15% were also measured with the VSM.

In contrast to the VSM used in Sections 5.1.3 and 5.1.4, the new VSM assembled by the team can only present the hysteresis loop with field versus induced voltage instead of field versus magnetic moment. Noise is another issue that has yet to be solved. The following graph shows the hysteresis loops for concentrations of 15%, 25% and 30% SPIONP pellets both before and after compression. The red dots (P15, P25 and P30) in the hysteresis loops represent the data after compression whereas the blue dots (P15_S, P25_S and P30-S) represent the data before compression. (**Fig.36, Fig.37, Fig.38**)

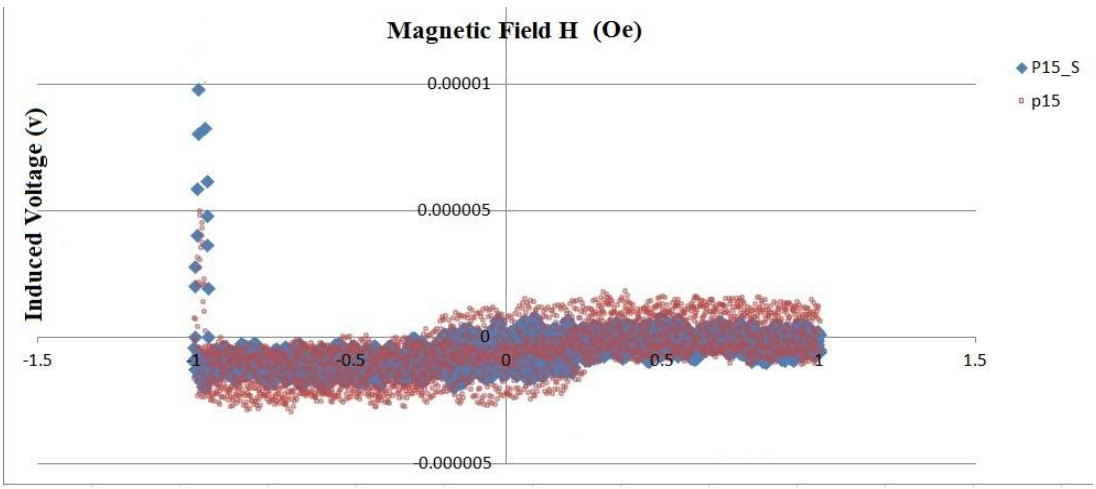

Figure 36: Hysteresis loop of SPIONP pellet with 15% concentration

Noise is detected when a negative field is applied, the magnetic moment of P15_S shows a slight decrease compared to that of P15. However, no major changes are detected.

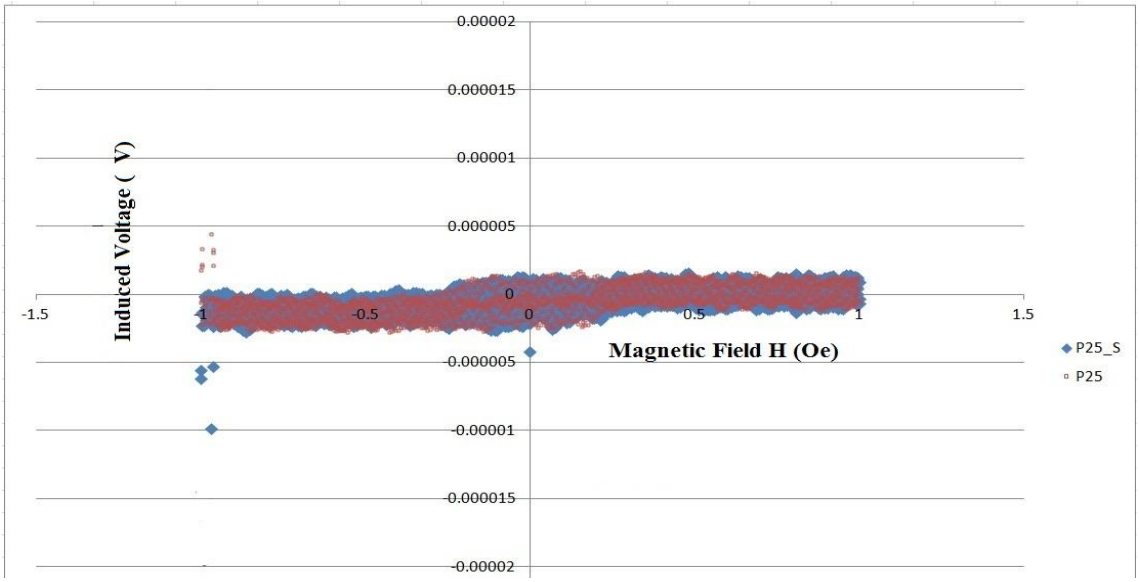

Figure 37: Hysteresis loop of SPIONP pellet with 25% concentration

Still, noise is detected when a negative field is applied. No major change in magnetic moment is noticed before and after the compression.

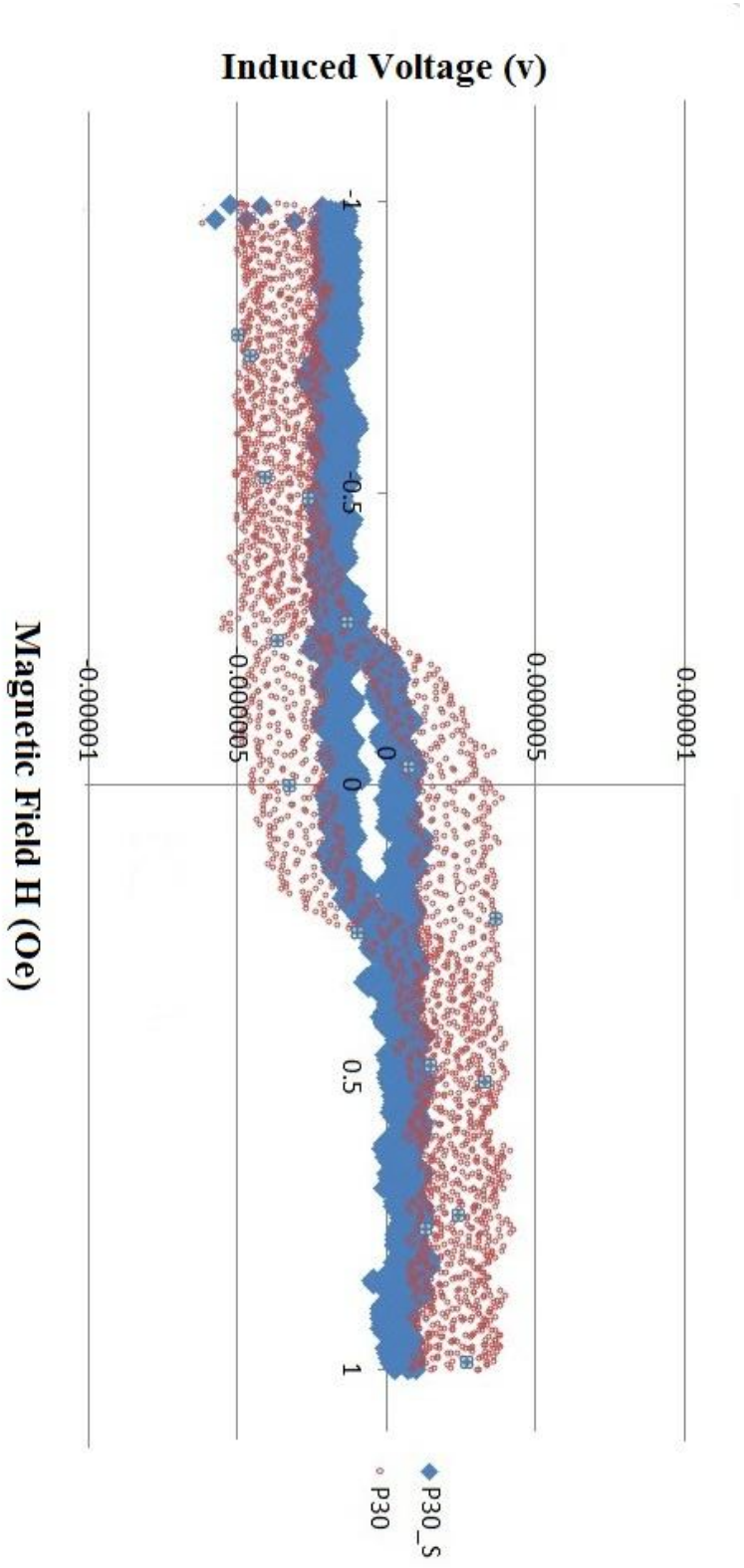

Figure 38: Hysteresis loop of SPIONP pellet with 30% concentration

A significant decrease in magnetic moment between P30 and P30_S is noticed. The deformation of the pellets results in a change of distance between the SPIONs in the silicone matrix, which strongly influences the dipole interaction. Decreased distance leads to a reduction in magnetization. Further analysis and research will be carried out in the next section.

.

5.2.2 Analysis of VSM Measurements

Theoretically, when the distance between two SPIONs is decreased, hence bringing them close enough to interact with each other, their magnetic properties should be changed to behave as ferromagnetic particles due to the dipole interaction. The magnetization should be increased to generate a signal. However, this does not happen in the SPIONP pellets in the way we expected. Apparently, the magnetic moment is reduced after the compression. Why is this happening?

Concepts of the Poisson Effect and Magnetic Anisotropy are now introduced to this research, which could be used to explain the result.

Poisson effect (**Fig.39)**: In a 3-dimensional phase, materials tend to expand along two perpendicular axes when a longitudinal compression force is applied. *Poisson's ratio (ν), named after Siméon Poisson, is the ratio, when a sample object is stretched, of the contraction or transverse strain (perpendicular to the applied load), to the extension or axial strain (in the direction of the applied load).*[24] (GERCEK, January 2007) Different materials have different Poisson ratios.

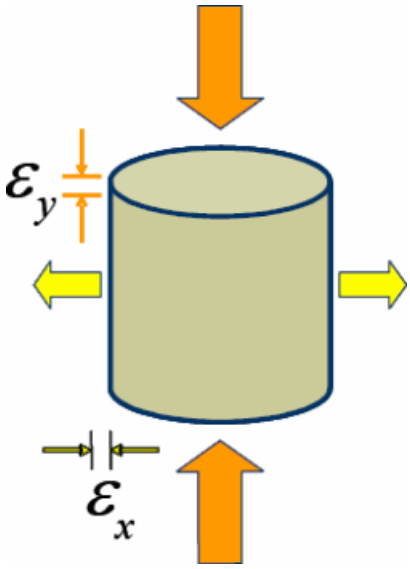

Figure 39: Poisson effect [Source: http://www.mechanicalengineeringblog.com/wp-content/uploads/2011/04/01-poissons-ratio-strain-changes_thumb.gif]

In this case, when SPIONP pellets are compressed in the sample holder (**Fig.40**) i.e., applying strain (ε) = ΔY/Y along the longitudinal axis, this results in a Poisson Strain in the perpendicular direction, which is equal to:

$$\boldsymbol{\varepsilon_{perp} = \upsilon \varepsilon_{long}}$$

Where $\boldsymbol{\varepsilon_{perp}}$ is the perpendicular strain and $\boldsymbol{\varepsilon_{long}}$ is the longitudinal strain, $\boldsymbol{\upsilon}$ is Poisson's ratio for this material.

Since $\boldsymbol{\varepsilon_{long}}$ = ΔY/Y, thus, $\boldsymbol{\varepsilon_{long} Y = \Delta Y}$

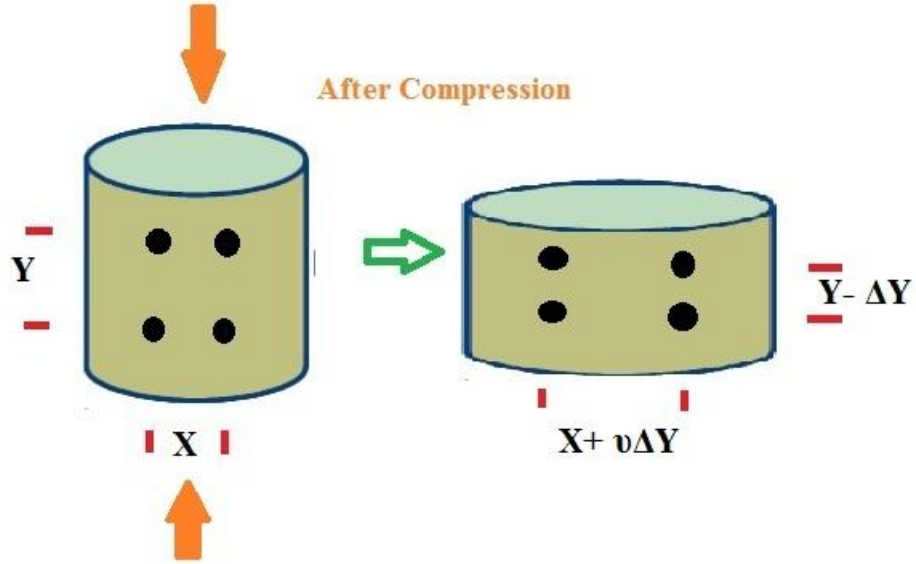

Figure 40: SPIONP pellet compressed longitudinally in the sample holder. Black dots symbolize the SPIONs in the silicone matrix.

Therefore, although the distance between SPIONs along the longitudinal axis is decreased, along the perpendicular axis, this distance is actually increasing due to the expanding volume.

Magnetic Anisotropy: The magnetic properties of materials are direction dependent. *In the absence of an applied magnetic field, a magnetically isotropic material has no preferential direction for its magnetic moment while a magnetically anisotropic material will align its moment with one of the easy axes.* **(Direct quote from Wikipedia, the free encyclopaedia)** That is to say, directional change is also one of the most important factors which could influence the magnetization.

In this case, imagine that the SPIONP pellet is a small magnet compressed vertically in the sample holder. Along the longitudinal axis, the distances between the SPIONs are shortened; therefore the magnetization is increased in this direction. However, according to Poisson's Effect, the distance between particles along the perpendicular axis is increased, i.e., the magnetization is decreased in this direction. Based on the theory of Faraday's Law, shown in the following illustration, if there is a magnetization change in (a), the voltage induced is not affected whereas in (b), significant changes would be identified. (**Fig.41**)

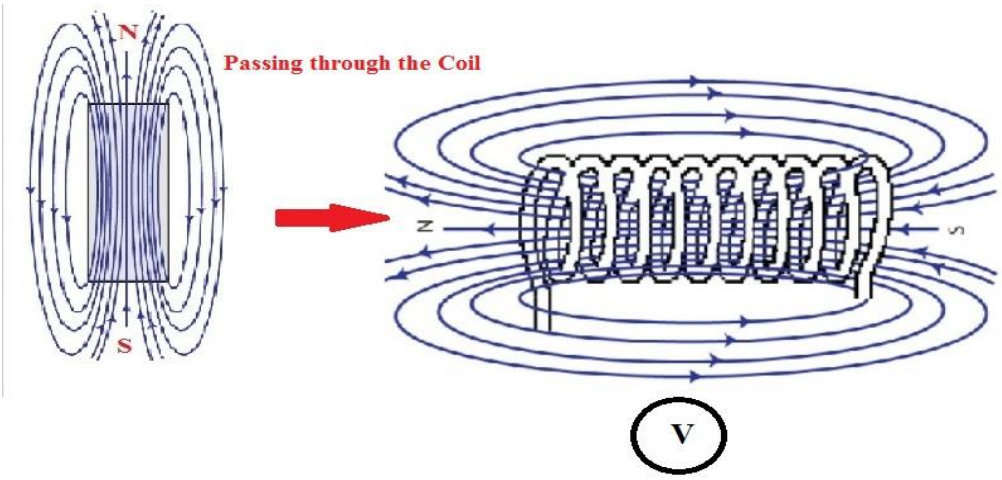

(a)

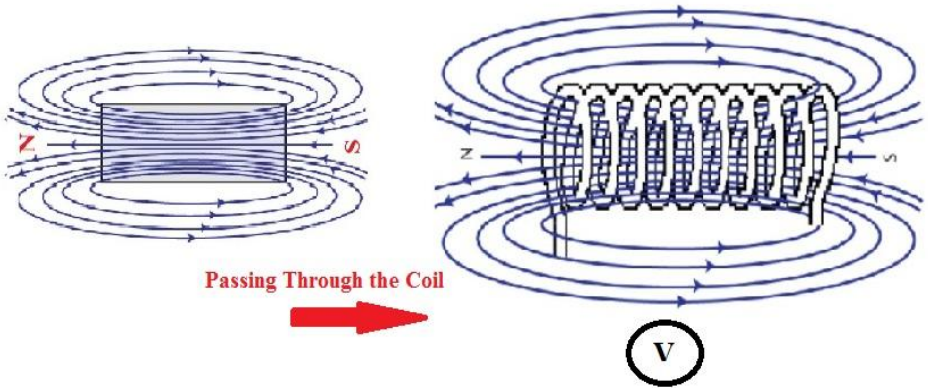

(b)

Figure 41: (a) the voltage induced is not affected whereas in (b) significant changes would be identified.

Overall, the magnetic anisotropy of the SPIONP pellet prevents our VSM from picking up signals horizontally where the magnetization is changed after compression. Fortunately, it is still proved that the changes in strain of SPIONP strongly influence the magnetisation or magnetic anisotropic.

Chapter 6: Conclusion

Due to the hugely increasing demand for SPION applications, this research was proposed to discover more characteristics of SPIONs and motivated by the possibility of finding ways to synthesize new materials (SPIONP) based on the corresponding discovery. Although the experimental result was not exactly what was expected, it still demonstrated that the interaction between SPIONs caused by a change in distance could have a severe impact on its magnetic properties. Six main sections of work have been carried out during this research:

- the background research and literature review;
- the wet chemistry fabrication of SPIONs;
- TEM, SEM AND JEMS measurement of SPIONs,
- the synthesis of SPIONP,
- design and assembly of new sample holder and VSM
- The VSM measurement of both SPIONs and SPIONP.

Background research provides the essential and fundamental ideas in my subject. Basic theories and information about magnetic nanoparticles are comprehended by reading the previous work of others in this field.

The wet chemistry fabrication of SPIONs produced seven different samples (S1-S7) under various conditions. During the fabrication process, the greatest difficulty experienced was finding a proper mechanical stirrer with tiny size which fits into small beakers but has strong power so that the SPIONs are sufficiently separated. At last, we

had to design and craft our own mechanical stirrer and the problem was solved. From all the samples, S6 with the highest magnetic moment as well as the best dispersion distribution was chosen to synthesize SPIONP.

TEM and SEM measurement is massively time consuming, yet it shows a clear morphology and distribution for each SPION sample. Not only spherical nanoparticles are fabricated but also nanorods are unexpectedly fabricated. JEMS diffraction analysis based on the high resolution FFT images from TEM allowed the author to confirm the lattice structure of the SPION samples, and hence be able to determine the composition of the SPIONs as iron (III) oxide.

The synthesis of SPIONP pellets is relatively easier than the fabrication of SPIONs. Unfortunately, neither TEM nor SEM measurement could determine the particle distribution in the SPIONP pellets since it is too difficult to prepare them into samples that fit into the TEM, and also the silicone rubber matrix is non-conductive.

Design and assembly of the sample holder and VSM was an excellent piece of team work. The VSM was assembled piece by piece. Although there were still problems with the new VSM, such as the noise issue, software crash issues and minor calibration problems etc, it was still working properly most of the time and provided sensibly reliable measurements. Further work could be carried out to improve the current VSM system.

The VSM measurements of SPIONs presented a clear result showing the magnetization of SPIONs. For SPIONP pellets, three different concentrations (15%, 25%, 30%) of pellets are prepared into samples, which were tested both before and after compression

in the sample holder. The result was rather disappointing at first but usefully revealing after further research and analysis were carried out. According to the Poisson Effect, the distance between particles along the perpendicular axis is increased, i.e., the magnetization is decreased in this direction. The magnetic anisotropy of the SPIONP pellets prevented our VSM from picking up signals horizontally where the magnetization is changed after compression. Fortunately, it is still proved that the changes in strain of SPIONP strongly influence the magnetisation or magnetic anisotropic, i.e., the magnetic properties could be altered by stain change of SPIONP.

Due to the time limitation, further work in this research has not been carried through. Therefore, there are still problems to be clarified and investigated in the research topic. New sample holders need to be designed, which will allow the SPIONP pellets to be tested both vertically and horizontally after compression along the longitudinal axis. Once this is accomplished, new measurements could be taken to determine whether the SPIONP pellets are generating signals after compression. This would be a great step forward in material science, and hence industrial applications of SPIONP could be discovered.

Appendices I:

Large particles VSM DATASHEET:

XYB1:

Field(G)	Moment(emu)
7929.24	0.712109
7743.91	0.709363
7554.27	0.705858
7364.94	0.701935
7176.23	0.697426
6989.91	0.692231
6799.38	0.686158
6611.28	0.679461
6423.5	0.672157
6235.65	0.663961
6050.19	0.654501
5860.2	0.644946
5672.84	0.634436
5485.12	0.623046
5297.53	0.610843
5109.95	0.597937
4976.71	0.587697
4879.14	0.580432
4779.07	0.57271
4679.11	0.564779
4579.12	0.556624
4479.39	0.548319
4380.14	0.539838
4279	0.53099
4179.06	0.521976
4079.04	0.512862
3979.05	0.503536
3880.26	0.49411
3779.06	0.484313
3678.99	0.474433
3578.96	0.464337
3479.03	0.454065
3379.97	0.443706

3279.23	0.433023
3178.9	0.422238
3078.94	0.411312
2978.86	0.40021
2878.79	0.388942
2780.12	0.377641
2678.83	0.365838
2578.92	0.354051
2478.97	0.342021
2378.88	0.329887
2279.64	0.3177
2179.41	0.305201
2078.81	0.292545
1982.74	0.280247
1884.51	0.26764
1784.4	0.25467
1685.72	0.241739
1584.43	0.22826
1484.4	0.214828
1384.44	0.201317
1284.42	0.187681
1184.93	0.173955
1085.24	0.160111
984.434	0.145986
884.387	0.131887
784.524	0.117711
684.464	0.103408
585.726	0.089204
488.538	0.075091
390.05	0.060838
290.09	0.046201
190.127	0.031564
90.7128	0.016933
-9.20352	0.002091
-109.908	-0.01283
-209.821	-0.02761
-309.891	-0.04233
-409.873	-0.05692
-503.252	-0.07056
-601.615	-0.08464
-701.587	-0.09905
-801.65	-0.11332
-901.609	-0.12749
-1001.39	-0.14157

-1100.58	-0.15542
-1201.58	-0.16944
-1301.59	-0.1832
-1401.61	-0.19689
-1501.62	-0.21046
-1600.33	-0.22365
-1701.67	-0.23717
-1801.63	-0.25035
-1901.6	-0.26338
-1995.2	-0.27555
-2091.8	-0.28779
-2193.1	-0.3006
-2293.13	-0.31312
-2393.03	-0.32548
-2493.07	-0.33766
-2593.02	-0.34967
-2691.82	-0.36141
-2793.08	-0.37327
-2893.1	-0.38478
-2993.02	-0.39609
-3093.03	-0.40725
-3192.17	-0.41824
-3292.76	-0.42916
-3392.99	-0.43989
-3493.05	-0.45045
-3593.01	-0.4608
-3692.95	-0.47098
-3791.72	-0.4809
-3892.95	-0.49083
-3992.96	-0.50047
-4093.01	-0.50989
-4192.85	-0.51914
-4291.92	-0.5281
-4392.66	-0.537
-4492.89	-0.54564
-4592.91	-0.55408
-4692.89	-0.56233
-4792.92	-0.57037
-4891.63	-0.57805
-5014.85	-0.58719
-5207.66	-0.60101
-5407.62	-0.61468
-5607.65	-0.62755
-5805.42	-0.63932

-6006.81	-0.65034
-6207.12	-0.66046
-6407.07	-0.6696
-6606.83	-0.67789
-6806.33	-0.68521
-7003.64	-0.69164
-7205.62	-0.69735
-7405	-0.70224
-7604.12	-0.70644
-7803.49	-0.71004
-7867.88	-0.7115
-7670.6	-0.70843
-7466.86	-0.70455
-7264.84	-0.70004
-7063.46	-0.69474
-6862.49	-0.68864
-6664.25	-0.68179
-6461.15	-0.67386
-6260.9	-0.66521
-6060.46	-0.65564
-5860.49	-0.64521
-5661.82	-0.63392
-5461.09	-0.6216
-5259.86	-0.60838
-5064.07	-0.59451
-4963.66	-0.58661
-4864.72	-0.57923
-4765.93	-0.57152
-4664.63	-0.56347
-4564.7	-0.55532
-4464.58	-0.54694
-4364.66	-0.5384
-4264.84	-0.52961
-4165.57	-0.5207
-4064.54	-0.51135
-3964.67	-0.50206
-3864.48	-0.49254
-3764.54	-0.48274
-3665.79	-0.47291
-3564.54	-0.4626
-3464.48	-0.45226
-3364.49	-0.44171
-3264.39	-0.43104
-3164.72	-0.42024

-3065.33	-0.40932
-2964.43	-0.39806
-2864.43	-0.38675
-2764.45	-0.37529
-2664.46	-0.36363
-2565.55	-0.35187
-2464.47	-0.3397
-2364.42	-0.32749
-2264.32	-0.31515
-2164.39	-0.30264
-2065.35	-0.29011
-1970.66	-0.2779
-1872.43	-0.26533
-1772.42	-0.25225
-1672.41	-0.2391
-1572.46	-0.22578
-1473.7	-0.21251
-1372.39	-0.19874
-1272.45	-0.18509
-1172.42	-0.17127
-1072.33	-0.1574
-973.1	-0.14339
-872.654	-0.1292
-772.447	-0.11499
-672.355	-0.10061
-572.393	-0.08619
-478.188	-0.0725
-382.234	-0.05865
-280.925	-0.04381
-180.969	-0.02911
-81.0207	-0.01433
19.0556	0.000453
118.289	0.01521
218.488	0.030004
319.024	0.044787
419.041	0.059371
512.781	0.073085
610.744	0.087167
709.48	0.10142
810.724	0.115878
910.753	0.13004
1010.69	0.144123
1110.73	0.158109
1210.2	0.171946

1309.95	0.185658
1410.63	0.199381
1510.72	0.212947
1610.68	0.226307
1710.74	0.239564
1809.37	0.252532
1910.65	0.265675
2004.66	0.277854
2102.54	0.290273
2202.59	0.302899
2302.31	0.315329
2401.58	0.32754
2502.63	0.339821
2602.56	0.35184
2702.53	0.36366
2802.63	0.375333
2901.32	0.386657
3002.53	0.398075
3102.59	0.409189
3202.57	0.420167
3302.51	0.430965
3401.29	0.441472
3502.58	0.452151
3602.45	0.462483
3702.58	0.47262
3802.44	0.482563
3902.44	0.492339
4001.24	0.501825
4102.37	0.511333
4202.39	0.520566
4302.4	0.529603
4402.43	0.538412
4501.43	0.546941
4602.12	0.555427
4702.35	0.563673
4802.35	0.571687
4902.38	0.579457
5026.34	0.588573
5217.6	0.602246
5420	0.615984
5620.07	0.628726
5819.79	0.640502
6019.84	0.651385
6218.36	0.6612

6418.39	0.670228
6619.24	0.678339
6818.86	0.685597
7018.24	0.691938
7217.84	0.697584
7414.66	0.702398
7616.3	0.706603
7815.28	0.710178

XYB2:

Field(G)	Moment(emu)
7925.14	0.370536
7739.34	0.369111
7549.46	0.367382
7360.27	0.365369
7171.36	0.362917
6985.08	0.360179
6794.6	0.356995
6606.65	0.353458
6418.74	0.349465
6230.85	0.345071
6044.6	0.340311
5856.61	0.335088
5668.02	0.32938
5480.44	0.323305
5292.94	0.316836
5105.19	0.309963
4976.2	0.304694
4878.96	0.300866
4779.05	0.296816
4678.91	0.292625
4578.95	0.288356
4479.73	0.283973
4379.43	0.279486
4278.9	0.274883
4178.92	0.270183
4078.83	0.26539

3978.9	0.260478
3880.09	0.255563
3778.84	0.2504
3678.75	0.245229
3578.85	0.239979
3478.74	0.234653
3379.27	0.229222
3279.45	0.223689
3178.68	0.218076
3078.66	0.212403
2978.7	0.206617
2878.65	0.200784
2779.93	0.194911
2678.71	0.188835
2578.65	0.182672
2478.76	0.176474
2378.65	0.170172
2279.2	0.16384
2179.48	0.157424
2078.68	0.150838
1983.36	0.14453
1886.15	0.138109
1786.11	0.131376
1687.37	0.124665
1586.13	0.117763
1486.18	0.110859
1386.06	0.10387
1286.19	0.096794
1187.32	0.089805
1086.11	0.082565
986.03	0.075328
886.146	0.068045
786.14	0.060736
686.125	0.053369
587.382	0.046041
491.188	0.038812
393.905	0.031602
294.05	0.024074
194.01	0.016506
94.767	0.009011
-5.89064	0.001331
-106.018	-0.00633
-206.093	-0.01395
-306.057	-0.02152

-406.058	-0.02904
-498.52	-0.03603
-597.764	-0.04331
-697.743	-0.05076
-797.711	-0.05815
-897.771	-0.06541
-997.206	-0.0727
-1097.23	-0.07991
-1197.66	-0.08711
-1297.74	-0.09424
-1397.75	-0.10127
-1497.74	-0.10828
-1596.45	-0.11513
-1697.71	-0.1221
-1797.71	-0.12889
-1897.66	-0.13562
-1990.89	-0.14191
-2088.81	-0.14833
-2188.13	-0.15485
-2289.17	-0.16137
-2389.13	-0.16776
-2489.09	-0.17406
-2589.07	-0.1803
-2687.86	-0.18643
-2789.23	-0.19253
-2889.16	-0.19851
-2989.04	-0.20436
-3089.2	-0.21021
-3187.83	-0.21587
-3289.1	-0.22158
-3389.05	-0.22716
-3489.04	-0.23269
-3589.05	-0.23809
-3689.05	-0.2434
-3787.62	-0.24855
-3889.02	-0.25374
-3988.98	-0.25878
-4089.03	-0.2637
-4188.92	-0.26853
-4287.99	-0.27323
-4388.71	-0.27791
-4488.88	-0.28244
-4588.98	-0.28688
-4688.97	-0.29124

-4788.85	-0.29545
-4887.64	-0.29953
-5010.75	-0.30434
-5203.58	-0.31165
-5403.58	-0.31891
-5603.35	-0.32572
-5801.84	-0.33202
-6002.2	-0.33791
-6203.1	-0.34331
-6402.81	-0.34817
-6602.69	-0.35262
-6802.32	-0.3565
-6999.4	-0.35996
-7201.43	-0.36294
-7401	-0.36551
-7600.16	-0.36765
-7799.23	-0.3695
-7886.19	-0.37038
-7696.32	-0.36893
-7492.26	-0.36699
-7290.08	-0.3647
-7088.67	-0.362
-6887.68	-0.35885
-6689.37	-0.35524
-6486.35	-0.35109
-6286.03	-0.34654
-6085.72	-0.34152
-5885.68	-0.33597
-5685.84	-0.32994
-5487.19	-0.3235
-5285.21	-0.31655
-5085.64	-0.30915
-4969.95	-0.30433
-4872.42	-0.30051
-4773.63	-0.29648
-4672.35	-0.29226
-4572.41	-0.28794
-4472.37	-0.28357
-4372.4	-0.27908
-4273.33	-0.27451
-4172.36	-0.26977
-4072.27	-0.26497
-3972.39	-0.26008
-3872.29	-0.25509

-3772.27	-0.24998
-3673.3	-0.24481
-3572.24	-0.23948
-3472.29	-0.23412
-3372.26	-0.22867
-3272.25	-0.22311
-3173.22	-0.21755
-3072.38	-0.21178
-2972.12	-0.20596
-2872.12	-0.20009
-2772.18	-0.19415
-2672.11	-0.1881
-2573.44	-0.18204
-2472.14	-0.17572
-2372.19	-0.16943
-2272.12	-0.16305
-2172.15	-0.15657
-2072.89	-0.15007
-1978.11	-0.14378
-1880.2	-0.13728
-1780.16	-0.13055
-1680.22	-0.12375
-1580.11	-0.11687
-1481.41	-0.11003
-1380.25	-0.10293
-1280.2	-0.09588
-1180.2	-0.08875
-1080.13	-0.08157
-980.867	-0.07442
-880.709	-0.06716
-780.248	-0.05975
-680.244	-0.05238
-580.157	-0.04492
-483.796	-0.03776
-386.76	-0.03053
-285.538	-0.02293
-185.5	-0.01532
-85.58	-0.00769
14.3992	-0.0001
114.27	0.007503
213.408	0.01508
314.474	0.022719
414.513	0.03023
509.002	0.037355

606.07	0.044516
704.744	0.051862
806.078	0.059365
906.047	0.066678
1006.02	0.073935
1106.09	0.08118
1204.72	0.088237
1306.12	0.09541
1406.12	0.102483
1505.98	0.109509
1606.08	0.116403
1706.05	0.123268
1804.75	0.129971
1905.93	0.136725
2000.66	0.143094
2097.51	0.149415
2197.51	0.155963
2296.7	0.162365
2397.07	0.168801
2497.43	0.175126
2597.45	0.181329
2697.59	0.187522
2797.53	0.193548
2896.25	0.199443
2997.49	0.205363
3097.56	0.211152
3197.52	0.216853
3297.45	0.222439
3397.15	0.227992
3496.71	0.233444
3597.41	0.23886
3697.45	0.244181
3797.39	0.249325
3897.38	0.254452
3996.15	0.259401
4097.35	0.264369
4197.3	0.269196
4297.28	0.273951
4397.35	0.278563
4496.03	0.283038
4597.23	0.287516
4697.31	0.291818
4797.25	0.296051
4897.27	0.300151

5021.08	0.304963
5212.16	0.312178
5414.64	0.319465
5614.75	0.326234
5814.57	0.332537
6014.52	0.338371
6212.95	0.343602
6413.76	0.348438
6613.92	0.352779
6813.71	0.356642
7013.03	0.360037
7212.47	0.363015
7409.47	0.365496
7610.99	0.367655
7810.04	0.369446

xyb3:

Field(G)	Moment(emu)
7929.36	0.160326
7744.08	0.159751
7554.47	0.15903
7365.03	0.158155
7176.39	0.157163
6990.2	0.155994
6799.46	0.154625
6611.4	0.15309
6423.71	0.151363
6235.72	0.14947
6048.62	0.14741
5862.01	0.145159
5672.82	0.142669
5485.5	0.140078
5297.69	0.137245
5110.29	0.134268
4965.73	0.131773
4866.35	0.130054
4766.26	0.128292

4666.26	0.12646
4566.31	0.124609
4467.5	0.122745
4366.31	0.120772
4266.19	0.11877
4166.27	0.116758
4066.12	0.11467
3966.29	0.112572
3867.45	0.110438
3766.09	0.10821
3666.19	0.105979
3566.15	0.10366
3466.05	0.101363
3367.1	0.099027
3266.36	0.096616
3165.98	0.094191
3066.04	0.09174
2966	0.08927
2865.98	0.086737
2767.24	0.084194
2666.04	0.081553
2566.03	0.078881
2466.06	0.076233
2366.05	0.073487
2266.8	0.070772
2166.54	0.067931
2066.03	0.065141
1972	0.062439
1874.18	0.059619
1774.06	0.056685
1675.36	0.053834
1574.12	0.050807
1474.12	0.047803
1374.12	0.044791
1274.07	0.041717
1174.88	0.038654
1074.65	0.03554
974.168	0.032373
874.088	0.029247
774.104	0.026068
674.133	0.022879
575.319	0.019664
480.729	0.016618
382.546	0.013419

282.592	0.010155
182.528	0.006848
83.0924	0.003548
-16.6144	0.000232
-117.458	-0.00309
-217.518	-0.00643
-317.379	-0.00968
-417.355	-0.01296
-512.956	-0.01608
-612.435	-0.01929
-712.244	-0.0225
-812.415	-0.02571
-912.312	-0.02891
-1012.11	-0.03204
-1111.36	-0.03511
-1212.36	-0.03828
-1312.31	-0.04136
-1412.3	-0.04443
-1512.3	-0.04746
-1611.13	-0.0504
-1712.32	-0.05341
-1812.39	-0.05635
-1912.23	-0.05927
-2006.09	-0.06201
-2102.79	-0.06475
-2204.03	-0.06757
-2304.04	-0.07037
-2404.02	-0.07312
-2503.96	-0.07585
-2603.93	-0.07856
-2702.82	-0.0812
-2804.03	-0.08383
-2904.01	-0.08642
-3003.95	-0.08894
-3104.01	-0.09148
-3202.94	-0.09389
-3303.75	-0.09635
-3403.92	-0.09874
-3503.9	-0.10112
-3603.94	-0.10344
-3703.92	-0.10574
-3802.7	-0.10795
-3903.94	-0.11019
-4003.83	-0.1124

-4103.81	-0.11449
-4203.83	-0.11658
-4303.2	-0.1186
-4403.26	-0.1206
-4503.84	-0.12253
-4603.78	-0.12441
-4703.81	-0.12631
-4803.82	-0.12813
-4902.54	-0.1299
-5036.48	-0.13211
-5233.65	-0.13534
-5433.57	-0.13844
-5633.37	-0.14138
-5832.88	-0.14406
-6031.38	-0.1466
-6233.22	-0.14891
-6432.81	-0.151
-6632.47	-0.15291
-6832.21	-0.15453
-7029.38	-0.15598
-7231.31	-0.15723
-7430.83	-0.15831
-7629.87	-0.15916
-7829.16	-0.1599
-7854.46	-0.1601
-7649.98	-0.15942
-7447.51	-0.15857
-7245.41	-0.15755
-7044.06	-0.15635
-6843.18	-0.15495
-6645.01	-0.15333
-6441.95	-0.15151
-6241.54	-0.14945
-6041.3	-0.14721
-5841.17	-0.14478
-5643.71	-0.14215
-5440.87	-0.13932
-5240.76	-0.13625
-5049.58	-0.1331
-4973.71	-0.13169
-4877.43	-0.13009
-4778.67	-0.12835
-4677.44	-0.12651
-4577.4	-0.12468

-4477.4	-0.12278
-4377.32	-0.12083
-4278.09	-0.11887
-4177.88	-0.11685
-4077.24	-0.11474
-3977.31	-0.11263
-3877.31	-0.11046
-3777.29	-0.10826
-3678.52	-0.10606
-3577.28	-0.10376
-3477.25	-0.10145
-3377.26	-0.09907
-3277.22	-0.09669
-3177.58	-0.09429
-3077.93	-0.09181
-2977.23	-0.08929
-2877.07	-0.08676
-2777.21	-0.0842
-2677.13	-0.0816
-2578.47	-0.07898
-2477.2	-0.07625
-2377.14	-0.07353
-2277.14	-0.07075
-2177.15	-0.06794
-2077.61	-0.06519
-1982.83	-0.06245
-1885.14	-0.05967
-1785.19	-0.05674
-1685.13	-0.05378
-1585.16	-0.05083
-1486.34	-0.04786
-1385.18	-0.0448
-1285.1	-0.04176
-1185.12	-0.03867
-1085.15	-0.03556
-986.349	-0.03249
-885.173	-0.02929
-785.16	-0.02613
-685.152	-0.02291
-585.113	-0.01966
-490.404	-0.0166
-394.45	-0.01351
-293.243	-0.01021
-193.255	-0.00693

-93.2291	-0.0036
6.67817	-0.00028
105.499	0.002981
206.745	0.006339
306.807	0.00964
406.784	0.01294
501.705	0.016032
598.444	0.019132
697.165	0.02235
798.409	0.025609
898.397	0.028739
998.432	0.031909
1098.46	0.035075
1197.66	0.038147
1297.91	0.041213
1398.43	0.04429
1498.4	0.047326
1598.35	0.050316
1698.36	0.053289
1797.08	0.056165
1898.43	0.059119
1993.73	0.061888
2090.18	0.064611
2190.34	0.067466
2289.72	0.07021
2389.49	0.073009
2490.21	0.075721
2590.22	0.078412
2690.2	0.081071
2790.28	0.083701
2889	0.086237
2990.25	0.088762
3090.18	0.091295
3190.31	0.093764
3290.22	0.09619
3389.91	0.098585
3489.17	0.100918
3590.18	0.103255
3690.18	0.105543
3790.19	0.107785
3890.19	0.109994
3988.84	0.112136
4090.04	0.114289
4190.06	0.116374

4290.11	0.118395
4390.03	0.120425
4488.82	0.122348
4590	0.124293
4690.07	0.126137
4789.96	0.127966
4890.04	0.129743
5012	0.131803
5202.47	0.134905
5404.73	0.138089
5604.84	0.141033
5804.6	0.143751
6004.5	0.146263
6203.08	0.148571
6403.3	0.15068
6604.07	0.152584
6803.63	0.15427
7003.27	0.155708
7202.61	0.156982
7399.31	0.158052
7601.23	0.158951
7800.22	0.159708

Appendices II:

The VSM value of SPIONs,

S1:

-3.00E+03	-1.05E-01
-2.90E+03	-1.04E-01
-2.81E+03	-1.04E-01
-2.70E+03	-1.03E-01
-2.60E+03	-1.02E-01
-2.51E+03	-1.02E-01
-2.40E+03	-1.01E-01
-2.30E+03	-1.01E-01
-2.21E+03	-1.00E-01
-2.10E+03	-9.96E-02
-2.00E+03	-9.87E-02
-1.91E+03	-9.78E-02
-1.80E+03	-9.68E-02
-1.70E+03	-9.56E-02
-1.61E+03	-9.48E-02
-1.50E+03	-9.35E-02
-1.40E+03	-9.22E-02
-1.31E+03	-9.07E-02
-1.20E+03	-8.92E-02
-1.10E+03	-8.72E-02
-1.01E+03	-8.56E-02
-9.00E+02	-8.28E-02
-7.95E+02	-8.01E-02
-7.05E+02	-7.71E-02
-6.00E+02	-7.33E-02
-4.95E+02	-6.77E-02
-4.05E+02	-6.26E-02
-3.00E+02	-5.42E-02
-1.95E+02	-4.27E-02
-1.05E+02	-2.80E-02
0.00E+00	-1.76E-03
9.00E+01	2.60E-02
1.80E+02	4.11E-02
2.85E+02	5.33E-02
3.90E+02	6.18E-02
4.80E+02	6.75E-02

5.85E+02	7.28E-02
6.90E+02	7.70E-02
7.80E+02	7.99E-02
8.85E+02	8.29E-02
9.90E+02	8.55E-02
1.07E+03	8.73E-02
1.19E+03	8.92E-02
1.29E+03	9.12E-02
1.38E+03	9.22E-02
1.49E+03	9.36E-02
1.59E+03	9.51E-02
1.68E+03	9.59E-02
1.79E+03	9.72E-02
1.89E+03	9.81E-02
1.98E+03	9.89E-02
2.09E+03	9.96E-02
2.19E+03	1.00E-01
2.28E+03	1.01E-01
2.39E+03	1.02E-01
2.49E+03	1.02E-01
2.58E+03	1.03E-01
2.69E+03	1.04E-01
2.79E+03	1.04E-01
2.88E+03	1.04E-01
2.97E+03	1.05E-01
2.88E+03	1.05E-01
2.79E+03	1.04E-01
2.69E+03	1.03E-01
2.58E+03	1.03E-01
2.49E+03	1.02E-01
2.39E+03	1.02E-01
2.28E+03	1.01E-01
2.19E+03	1.00E-01
2.09E+03	9.97E-02
1.98E+03	9.88E-02
1.89E+03	9.81E-02
1.79E+03	9.70E-02
1.68E+03	9.61E-02
1.59E+03	9.51E-02
1.49E+03	9.37E-02
1.38E+03	9.23E-02
1.28E+03	9.10E-02
1.17E+03	8.94E-02
1.08E+03	8.74E-02

9.90E+02	8.56E-02
8.85E+02	8.31E-02
7.80E+02	8.00E-02
6.90E+02	7.71E-02
5.85E+02	7.28E-02
4.80E+02	6.75E-02
3.90E+02	6.20E-02
2.85E+02	5.33E-02
1.80E+02	4.13E-02
9.00E+01	2.58E-02
0.00E+00	-1.32E-03
-1.05E+02	-2.84E-02
-1.95E+02	-4.27E-02
-3.00E+02	-5.44E-02
-4.05E+02	-6.25E-02
-4.95E+02	-6.81E-02
-6.00E+02	-7.29E-02
-7.05E+02	-7.73E-02
-7.95E+02	-8.01E-02
-9.00E+02	-8.30E-02
-1.01E+03	-8.54E-02
-1.10E+03	-8.74E-02
-1.20E+03	-8.93E-02
-1.31E+03	-9.08E-02
-1.40E+03	-9.23E-02
-1.50E+03	-9.37E-02
-1.61E+03	-9.50E-02
-1.70E+03	-9.57E-02
-1.80E+03	-9.69E-02
-1.91E+03	-9.78E-02
-2.00E+03	-9.87E-02
-2.10E+03	-9.94E-02
-2.21E+03	-1.00E-01
-2.30E+03	-1.01E-01
-2.40E+03	-1.02E-01
-2.51E+03	-1.02E-01
-2.60E+03	-1.03E-01
-2.70E+03	-1.03E-01
-2.81E+03	-1.04E-01
-2.90E+03	-1.04E-01
-3.00E+03	-1.05E-01

S2:

-3.00E+03	-8.13E-02
-2.90E+03	-8.10E-02
-2.81E+03	-8.08E-02
-2.70E+03	-8.02E-02
-2.60E+03	-7.99E-02
-2.51E+03	-7.93E-02
-2.40E+03	-7.88E-02
-2.30E+03	-7.81E-02
-2.21E+03	-7.78E-02
-2.10E+03	-7.69E-02
-2.00E+03	-7.64E-02
-1.91E+03	-7.57E-02
-1.80E+03	-7.47E-02
-1.70E+03	-7.39E-02
-1.61E+03	-7.32E-02
-1.50E+03	-7.21E-02
-1.40E+03	-7.09E-02
-1.31E+03	-6.97E-02
-1.20E+03	-6.82E-02
-1.10E+03	-6.65E-02
-1.01E+03	-6.49E-02
-9.00E+02	-6.28E-02
-7.95E+02	-6.01E-02
-7.05E+02	-5.76E-02
-6.00E+02	-5.41E-02
-4.95E+02	-4.97E-02
-4.05E+02	-4.53E-02
-3.00E+02	-3.86E-02
-1.95E+02	-2.96E-02
-1.05E+02	-1.95E-02
0.00E+00	-8.77E-04
9.00E+01	1.83E-02
1.80E+02	2.92E-02
2.85E+02	3.80E-02
3.90E+02	4.52E-02
4.80E+02	4.97E-02
5.85E+02	5.44E-02
6.90E+02	5.78E-02
7.80E+02	6.03E-02
8.85E+02	6.29E-02
9.90E+02	6.52E-02
1.08E+03	6.70E-02
1.19E+03	6.86E-02

1.29E+03	7.02E-02
1.38E+03	7.13E-02
1.49E+03	7.27E-02
1.59E+03	7.36E-02
1.68E+03	7.46E-02
1.79E+03	7.52E-02
1.89E+03	7.61E-02
1.98E+03	7.67E-02
2.09E+03	7.76E-02
2.19E+03	7.82E-02
2.28E+03	7.89E-02
2.39E+03	7.94E-02
2.49E+03	7.99E-02
2.58E+03	8.03E-02
2.69E+03	8.08E-02
2.79E+03	8.12E-02
2.88E+03	8.16E-02
2.99E+03	8.21E-02
2.88E+03	8.15E-02
2.79E+03	8.13E-02
2.69E+03	8.08E-02
2.58E+03	8.03E-02
2.48E+03	7.98E-02
2.39E+03	7.95E-02
2.27E+03	7.87E-02
2.19E+03	7.82E-02
2.09E+03	7.75E-02
1.98E+03	7.68E-02
1.89E+03	7.62E-02
1.79E+03	7.56E-02
1.68E+03	7.45E-02
1.59E+03	7.39E-02
1.49E+03	7.26E-02
1.38E+03	7.14E-02
1.29E+03	7.02E-02
1.19E+03	6.86E-02
1.08E+03	6.71E-02
9.90E+02	6.52E-02
8.85E+02	6.32E-02
7.80E+02	6.04E-02
6.90E+02	5.78E-02
5.85E+02	5.42E-02
4.80E+02	4.99E-02
3.90E+02	4.52E-02

2.85E+02	3.84E-02
1.80E+02	2.92E-02
9.00E+01	1.83E-02
0.00E+00	-8.75E-04
-1.05E+02	-1.94E-02
-1.95E+02	-2.99E-02
-3.00E+02	-3.87E-02
-4.05E+02	-4.55E-02
-4.95E+02	-4.98E-02
-6.00E+02	-5.40E-02
-7.05E+02	-5.76E-02
-7.95E+02	-6.03E-02
-9.00E+02	-6.27E-02
-1.01E+03	-6.49E-02
-1.10E+03	-6.66E-02
-1.20E+03	-6.82E-02
-1.31E+03	-6.96E-02
-1.40E+03	-7.10E-02
-1.50E+03	-7.21E-02
-1.61E+03	-7.31E-02
-1.70E+03	-7.40E-02
-1.80E+03	-7.49E-02
-1.91E+03	-7.57E-02
-2.00E+03	-7.62E-02
-2.10E+03	-7.71E-02
-2.21E+03	-7.77E-02
-2.30E+03	-7.83E-02
-2.40E+03	-7.88E-02
-2.51E+03	-7.95E-02
-2.60E+03	-7.96E-02
-2.70E+03	-8.02E-02
-2.81E+03	-8.06E-02
-2.90E+03	-8.10E-02
-3.00E+03	-8.14E-02

S3:

-3.02E+03	-1.61E-02
-2.90E+03	-1.55E-02
-2.81E+03	-1.56E-02
-2.70E+03	-1.54E-02

-2.60E+03	-1.56E-02
-2.51E+03	-1.53E-02
-2.40E+03	-1.53E-02
-2.30E+03	-1.51E-02
-2.21E+03	-1.50E-02
-2.10E+03	-1.49E-02
-2.00E+03	-1.48E-02
-1.91E+03	-1.48E-02
-1.80E+03	-1.44E-02
-1.70E+03	-1.42E-02
-1.61E+03	-1.41E-02
-1.50E+03	-1.39E-02
-1.40E+03	-1.36E-02
-1.31E+03	-1.34E-02
-1.20E+03	-1.29E-02
-1.10E+03	-1.27E-02
-1.01E+03	-1.24E-02
-9.00E+02	-1.22E-02
-7.95E+02	-1.14E-02
-7.05E+02	-1.11E-02
-6.00E+02	-1.07E-02
-4.95E+02	-9.75E-03
-4.05E+02	-8.90E-03
-3.00E+02	-7.54E-03
-1.95E+02	-6.01E-03
-1.05E+02	-3.74E-03
0.00E+00	-2.49E-04
9.00E+01	3.78E-03
1.80E+02	5.94E-03
2.85E+02	7.86E-03
3.90E+02	9.11E-03
4.80E+02	9.95E-03
5.85E+02	1.07E-02
6.90E+02	1.15E-02
7.80E+02	1.18E-02
8.85E+02	1.24E-02
9.90E+02	1.26E-02
1.08E+03	1.31E-02
1.19E+03	1.32E-02
1.29E+03	1.36E-02
1.38E+03	1.37E-02
1.49E+03	1.40E-02
1.59E+03	1.40E-02
1.68E+03	1.44E-02

1.79E+03	1.44E-02
1.89E+03	1.47E-02
1.98E+03	1.47E-02
2.09E+03	1.51E-02
2.19E+03	1.50E-02
2.28E+03	1.51E-02
2.39E+03	1.53E-02
2.49E+03	1.54E-02
2.58E+03	1.54E-02
2.67E+03	1.54E-02
2.79E+03	1.55E-02
2.88E+03	1.56E-02
2.99E+03	1.59E-02
2.88E+03	1.54E-02
2.79E+03	1.56E-02
2.69E+03	1.51E-02
2.58E+03	1.53E-02
2.49E+03	1.50E-02
2.39E+03	1.50E-02
2.28E+03	1.47E-02
2.19E+03	1.47E-02
2.09E+03	1.44E-02
1.98E+03	1.45E-02
1.89E+03	1.41E-02
1.79E+03	1.44E-02
1.68E+03	1.40E-02
1.58E+03	1.38E-02
1.49E+03	1.36E-02
1.38E+03	1.35E-02
1.29E+03	1.31E-02
1.19E+03	1.27E-02
1.08E+03	1.26E-02
9.90E+02	1.23E-02
8.85E+02	1.19E-02
7.80E+02	1.14E-02
6.90E+02	1.10E-02
5.85E+02	1.04E-02
4.65E+02	9.60E-03
3.90E+02	8.86E-03
2.85E+02	7.55E-03
1.80E+02	5.95E-03
9.00E+01	3.96E-03
0.00E+00	1.12E-04
-1.05E+02	-3.23E-03

-1.95E+02	-5.34E-03
-3.00E+02	-6.93E-03
-4.05E+02	-8.21E-03
-4.95E+02	-8.91E-03
-6.00E+02	-9.65E-03
-7.05E+02	-1.03E-02
-7.95E+02	-1.06E-02
-9.00E+02	-1.11E-02
-1.01E+03	-1.13E-02
-1.10E+03	-1.15E-02
-1.20E+03	-1.20E-02
-1.31E+03	-1.23E-02
-1.40E+03	-1.23E-02
-1.50E+03	-1.24E-02
-1.61E+03	-1.25E-02
-1.70E+03	-1.30E-02
-1.80E+03	-1.28E-02
-1.91E+03	-1.30E-02
-2.00E+03	-1.32E-02
-2.10E+03	-1.34E-02
-2.21E+03	-1.33E-02
-2.30E+03	-1.36E-02
-2.40E+03	-1.35E-02
-2.51E+03	-1.37E-02
-2.60E+03	-1.36E-02
-2.70E+03	-1.39E-02
-2.81E+03	-1.38E-02
-2.90E+03	-1.41E-02
-3.00E+03	-1.38E-02

S4:

-3.00E+03	-1.73E-01
-2.90E+03	-1.73E-01
-2.81E+03	-1.72E-01
-2.70E+03	-1.71E-01
-2.60E+03	-1.71E-01
-2.51E+03	-1.70E-01
-2.40E+03	-1.69E-01
-2.30E+03	-1.68E-01
-2.21E+03	-1.67E-01

-2.10E+03	-1.66E-01
-2.00E+03	-1.64E-01
-1.91E+03	-1.63E-01
-1.80E+03	-1.61E-01
-1.70E+03	-1.60E-01
-1.61E+03	-1.58E-01
-1.50E+03	-1.56E-01
-1.40E+03	-1.54E-01
-1.31E+03	-1.52E-01
-1.20E+03	-1.49E-01
-1.10E+03	-1.46E-01
-1.01E+03	-1.43E-01
-9.00E+02	-1.39E-01
-7.95E+02	-1.34E-01
-7.05E+02	-1.29E-01
-6.00E+02	-1.23E-01
-4.95E+02	-1.15E-01
-4.05E+02	-1.06E-01
-3.00E+02	-9.24E-02
-1.95E+02	-7.38E-02
-1.05E+02	-5.00E-02
0.00E+00	-2.93E-03
9.00E+01	4.62E-02
1.80E+02	7.11E-02
2.85E+02	9.08E-02
3.90E+02	1.04E-01
4.80E+02	1.14E-01
5.85E+02	1.22E-01
6.90E+02	1.29E-01
7.80E+02	1.34E-01
8.85E+02	1.39E-01
9.90E+02	1.43E-01
1.08E+03	1.46E-01
1.19E+03	1.49E-01
1.28E+03	1.52E-01
1.38E+03	1.54E-01
1.49E+03	1.57E-01
1.59E+03	1.58E-01
1.68E+03	1.60E-01
1.79E+03	1.62E-01
1.89E+03	1.64E-01
1.97E+03	1.65E-01
2.09E+03	1.66E-01
2.19E+03	1.67E-01

2.28E+03	1.68E-01
2.39E+03	1.70E-01
2.49E+03	1.71E-01
2.58E+03	1.71E-01
2.69E+03	1.72E-01
2.78E+03	1.73E-01
2.88E+03	1.74E-01
2.99E+03	1.75E-01
2.88E+03	1.74E-01
2.79E+03	1.73E-01
2.69E+03	1.72E-01
2.58E+03	1.71E-01
2.49E+03	1.70E-01
2.39E+03	1.70E-01
2.28E+03	1.68E-01
2.19E+03	1.67E-01
2.09E+03	1.66E-01
1.98E+03	1.65E-01
1.89E+03	1.63E-01
1.77E+03	1.62E-01
1.68E+03	1.60E-01
1.59E+03	1.59E-01
1.49E+03	1.56E-01
1.38E+03	1.54E-01
1.29E+03	1.52E-01
1.19E+03	1.49E-01
1.08E+03	1.46E-01
9.90E+02	1.43E-01
8.85E+02	1.39E-01
7.80E+02	1.34E-01
6.90E+02	1.29E-01
5.85E+02	1.23E-01
4.80E+02	1.15E-01
3.90E+02	1.05E-01
2.85E+02	9.19E-02
1.80E+02	7.22E-02
9.00E+01	4.70E-02
0.00E+00	-3.24E-03
-1.05E+02	-5.10E-02
-1.95E+02	-7.49E-02
-3.00E+02	-9.33E-02
-4.05E+02	-1.06E-01
-4.95E+02	-1.15E-01
-6.00E+02	-1.23E-01

-7.05E+02	-1.30E-01
-7.95E+02	-1.35E-01
-9.00E+02	-1.39E-01
-1.01E+03	-1.43E-01
-1.10E+03	-1.46E-01
-1.20E+03	-1.49E-01
-1.31E+03	-1.52E-01
-1.40E+03	-1.54E-01
-1.50E+03	-1.56E-01
-1.61E+03	-1.58E-01
-1.70E+03	-1.60E-01
-1.80E+03	-1.62E-01
-1.91E+03	-1.63E-01
-2.00E+03	-1.64E-01
-2.10E+03	-1.66E-01
-2.21E+03	-1.67E-01
-2.30E+03	-1.68E-01
-2.40E+03	-1.69E-01
-2.51E+03	-1.70E-01
-2.60E+03	-1.71E-01
-2.70E+03	-1.72E-01
-2.81E+03	-1.73E-01
-2.90E+03	-1.73E-01
-3.00E+03	-1.74E-01

S5:

-4.99500E+3	-1.23667E-1
-4.74500E+3	-1.23240E-1
-4.49500E+3	-1.22739E-1
-4.24500E+3	-1.22158E-1
-3.99500E+3	-1.21576E-1
-3.74500E+3	-1.20860E-1
-3.49500E+3	-1.20028E-1
-3.24500E+3	-1.19123E-1
-2.99500E+3	-1.18051E-1
-2.94500E+3	-1.17825E-1
-2.89500E+3	-1.17590E-1
-2.84500E+3	-1.17300E-1
-2.79500E+3	-1.17081E-1
-2.74500E+3	-1.16845E-1
-2.69500E+3	-1.16555E-1
-2.64500E+3	-1.16288E-1
-2.59500E+3	-1.16017E-1
-2.54500E+3	-1.15731E-1
-2.49500E+3	-1.15431E-1
-2.44500E+3	-1.15066E-1
-2.39500E+3	-1.14747E-1
-2.34500E+3	-1.14406E-1
-2.29500E+3	-1.14073E-1
-2.24500E+3	-1.13700E-1
-2.19500E+3	-1.13339E-1
-2.14500E+3	-1.12939E-1
-2.09500E+3	-1.12539E-1

-2.04500E+3	-1.12108E-1
-1.99500E+3	-1.11684E-1
-1.94500E+3	-1.11218E-1
-1.89500E+3	-1.10722E-1
-1.84500E+3	-1.10225E-1
-1.79500E+3	-1.09710E-1
-1.74500E+3	-1.09183E-1
-1.69500E+3	-1.08612E-1
-1.64500E+3	-1.08032E-1
-1.59500E+3	-1.07411E-1
-1.54500E+3	-1.06752E-1
-1.49500E+3	-1.06065E-1
-1.44500E+3	-1.05367E-1
-1.40000E+3	-1.04564E-1
-1.35000E+3	-1.03775E-1
-1.29500E+3	-1.02909E-1
-1.25000E+3	-1.02015E-1
-1.20000E+3	-1.01041E-1
-1.15000E+3	-1.00005E-1
-1.10000E+3	-9.89088E-2
-1.05000E+3	-9.77315E-2
-1.00000E+3	-9.64891E-2
-9.50000E+2	-9.50923E-2
-9.00000E+2	-9.36392E-2
-8.50000E+2	-9.20609E-2
-8.00000E+2	-9.03305E-2
-7.50000E+2	-8.84673E-2
-7.00000E+2	-8.64139E-2
-6.50000E+2	-8.41553E-2
-6.00000E+2	-8.16781E-2
-5.50000E+2	-7.88689E-2
-5.00000E+2	-7.57715E-2
-4.50000E+2	-7.22981E-2
-4.00000E+2	-6.83243E-2
-3.50000E+2	-6.38326E-2
-3.00000E+2	-5.85664E-2
-2.50000E+2	-5.25285E-2
-2.00000E+2	-4.53729E-2
-1.50000E+2	-3.68828E-2
-1.00000E+2	-2.67896E-2
-5.00000E+1	-1.48714E-2
0.00000E+0	-1.52019E-3
4.50000E+1	1.18893E-2
9.50000E+1	2.46363E-2
1.45000E+2	3.52508E-2
1.95000E+2	4.40386E-2
2.45000E+2	5.13567E-2
2.95000E+2	5.75388E-2
3.45000E+2	6.28712E-2
3.95000E+2	6.74420E-2
4.45000E+2	7.14877E-2
4.95000E+2	7.50070E-2
5.45000E+2	7.81937E-2
5.95000E+2	8.09907E-2
6.45000E+2	8.35098E-2
6.95000E+2	8.57804E-2
7.45000E+2	8.78406E-2
7.95000E+2	8.97508E-2
8.45000E+2	9.15031E-2
8.95000E+2	9.30938E-2
9.45000E+2	9.45757E-2
9.95000E+2	9.59867E-2
1.04000E+3	9.71976E-2
1.09500E+3	9.84041E-2
1.14000E+3	9.95387E-2
1.19000E+3	1.00569E-1
1.24500E+3	1.01573E-1
1.29500E+3	1.02461E-1
1.34500E+3	1.03349E-1
1.39500E+3	1.04144E-1
1.44000E+3	1.04929E-1

1.49500E+3	1.05664E-1
1.54500E+3	1.06367E-1
1.59500E+3	1.07037E-1
1.64500E+3	1.07658E-1
1.69500E+3	1.08239E-1
1.74500E+3	1.08817E-1
1.79000E+3	1.09356E-1
1.84500E+3	1.09894E-1
1.89000E+3	1.10390E-1
1.94500E+3	1.10887E-1
1.99500E+3	1.11342E-1
2.04000E+3	1.11781E-1
2.09000E+3	1.12211E-1
2.14000E+3	1.12627E-1
2.19500E+3	1.13038E-1
2.24500E+3	1.13441E-1
2.29500E+3	1.13783E-1
2.34500E+3	1.14136E-1
2.39000E+3	1.14487E-1
2.44000E+3	1.14784E-1
2.49000E+3	1.15084E-1
2.54500E+3	1.15422E-1
2.59000E+3	1.15686E-1
2.64000E+3	1.16048E-1
2.69000E+3	1.16307E-1
2.74000E+3	1.16555E-1
2.79000E+3	1.16804E-1
2.84000E+3	1.17093E-1
2.89000E+3	1.17333E-1
2.94000E+3	1.17548E-1
2.99000E+3	1.17797E-1
3.24000E+3	1.18901E-1
3.49000E+3	1.19844E-1
3.74000E+3	1.20693E-1
3.99000E+3	1.21478E-1
4.24000E+3	1.22174E-1
4.49000E+3	1.22757E-1
4.74000E+3	1.23380E-1
4.99000E+3	1.23875E-1
4.74000E+3	1.23390E-1
4.49000E+3	1.22787E-1
4.24000E+3	1.22165E-1
3.99000E+3	1.21470E-1
3.74000E+3	1.20681E-1
3.49000E+3	1.19821E-1
3.24000E+3	1.18867E-1
2.99000E+3	1.17795E-1
2.94000E+3	1.17548E-1
2.89000E+3	1.17280E-1
2.84000E+3	1.17024E-1
2.79000E+3	1.16785E-1
2.74000E+3	1.16514E-1
2.69000E+3	1.16248E-1
2.64000E+3	1.15941E-1
2.59000E+3	1.15663E-1
2.54000E+3	1.15314E-1
2.49000E+3	1.15024E-1
2.44000E+3	1.14709E-1
2.39000E+3	1.14392E-1
2.34000E+3	1.14100E-1
2.29000E+3	1.13700E-1
2.24000E+3	1.13354E-1
2.19000E+3	1.12988E-1
2.14000E+3	1.12556E-1
2.09000E+3	1.12155E-1
2.04000E+3	1.11714E-1
1.99000E+3	1.11265E-1
1.94000E+3	1.10846E-1
1.89000E+3	1.10355E-1
1.84000E+3	1.09852E-1
1.79500E+3	1.09356E-1

1.74500E+3	1.08780E-1
1.69000E+3	1.08223E-1
1.64000E+3	1.07618E-1
1.59000E+3	1.07020E-1
1.54500E+3	1.06337E-1
1.49500E+3	1.05655E-1
1.44500E+3	1.04929E-1
1.39000E+3	1.04106E-1
1.34000E+3	1.03319E-1
1.29500E+3	1.02463E-1
1.24500E+3	1.01577E-1
1.19000E+3	1.00568E-1
1.14500E+3	9.95499E-2
1.09500E+3	9.84598E-2
1.04500E+3	9.72704E-2
9.90000E+2	9.60330E-2
9.45000E+2	9.46323E-2
8.95000E+2	9.31491E-2
8.45000E+2	9.15737E-2
7.95000E+2	8.98680E-2
7.45000E+2	8.79661E-2
6.95000E+2	8.59194E-2
6.45000E+2	8.36421E-2
5.95000E+2	8.11791E-2
5.45000E+2	7.83683E-2
4.95000E+2	7.52659E-2
4.45000E+2	7.17209E-2
3.95000E+2	6.77863E-2
3.45000E+2	6.31983E-2
2.95000E+2	5.79442E-2
2.45000E+2	5.18171E-2
1.95000E+2	4.46278E-2
1.45000E+2	3.60589E-2
9.50000E+1	2.58019E-2
4.50000E+1	1.37131E-2
-5.00000E+0	3.54333E-4
-5.00000E+1	-1.33744E-2
-1.00000E+2	-2.60432E-2
-1.50000E+2	-3.64899E-2
-2.00000E+2	-4.51911E-2
-2.50000E+2	-5.24032E-2
-3.00000E+2	-5.84931E-2
-3.50000E+2	-6.37746E-2
-4.00000E+2	-6.83050E-2
-4.50000E+2	-7.22666E-2
-5.00000E+2	-7.57568E-2
-5.50000E+2	-7.88550E-2
-6.00000E+2	-8.16018E-2
-6.50000E+2	-8.41288E-2
-7.00000E+2	-8.63620E-2
-7.50000E+2	-8.84146E-2
-8.00000E+2	-9.02787E-2
-8.50000E+2	-9.20406E-2
-9.00000E+2	-9.35599E-2
-9.50000E+2	-9.50400E-2
-1.00000E+3	-9.64447E-2
-1.05000E+3	-9.76795E-2
-1.10000E+3	-9.88465E-2
-1.15000E+3	-9.99221E-2
-1.20000E+3	-1.00957E-1
-1.25000E+3	-1.01931E-1
-1.30000E+3	-1.02819E-1
-1.35000E+3	-1.03703E-1
-1.40000E+3	-1.04556E-1
-1.45000E+3	-1.05301E-1
-1.50000E+3	-1.06046E-1
-1.55000E+3	-1.06708E-1
-1.60000E+3	-1.07353E-1
-1.65000E+3	-1.08021E-1
-1.70000E+3	-1.08607E-1
-1.75000E+3	-1.09123E-1

-1.80000E+3	-1.09698E-1
-1.84500E+3	-1.10225E-1
-1.89500E+3	-1.10714E-1
-1.95000E+3	-1.11190E-1
-2.00000E+3	-1.11656E-1
-2.05000E+3	-1.12087E-1
-2.10000E+3	-1.12501E-1
-2.14500E+3	-1.12926E-1
-2.19500E+3	-1.13328E-1
-2.24500E+3	-1.13695E-1
-2.29500E+3	-1.14050E-1
-2.34500E+3	-1.14424E-1
-2.39500E+3	-1.14775E-1
-2.44500E+3	-1.15066E-1
-2.49500E+3	-1.15413E-1
-2.54500E+3	-1.15698E-1
-2.59500E+3	-1.15993E-1
-2.64500E+3	-1.16288E-1
-2.69500E+3	-1.16555E-1
-2.74500E+3	-1.16876E-1
-2.79500E+3	-1.17093E-1
-2.84500E+3	-1.17346E-1
-2.89500E+3	-1.17631E-1
-2.94500E+3	-1.17826E-1
-2.99500E+3	-1.18045E-1
-3.24500E+3	-1.19113E-1
-3.49500E+3	-1.19994E-1
-3.74500E+3	-1.20841E-1
-3.99500E+3	-1.21560E-1
-4.24500E+3	-1.22205E-1
-4.49500E+3	-1.22782E-1
-4.74000E+3	-1.23297E-1
-4.99000E+3	-1.23724E-1

S6:

-3.00E+03	-1.33E-01
-2.90E+03	-1.33E-01
-2.81E+03	-1.32E-01
-2.70E+03	-1.32E-01
-2.60E+03	-1.31E-01
-2.51E+03	-1.31E-01
-2.40E+03	-1.30E-01
-2.30E+03	-1.30E-01
-2.21E+03	-1.29E-01
-2.10E+03	-1.28E-01
-2.00E+03	-1.27E-01
-1.91E+03	-1.26E-01
-1.80E+03	-1.25E-01
-1.70E+03	-1.24E-01
-1.61E+03	-1.24E-01
-1.50E+03	-1.22E-01
-1.40E+03	-1.21E-01
-1.31E+03	-1.19E-01
-1.20E+03	-1.16E-01

-1.10E+03	-1.15E-01
-1.01E+03	-1.14E-01
-9.00E+02	-1.11E-01
-7.95E+02	-1.08E-01
-7.05E+02	-1.04E-01
-6.00E+02	-9.97E-02
-4.95E+02	-9.28E-02
-4.05E+02	-8.70E-02
-3.00E+02	-7.67E-02
-1.95E+02	-6.20E-02
-1.05E+02	-4.28E-02
0.00E+00	-2.39E-03
9.00E+01	4.05E-02
1.80E+02	6.05E-02
2.85E+02	7.58E-02
3.90E+02	8.65E-02
4.80E+02	9.34E-02
5.85E+02	9.96E-02
6.90E+02	1.04E-01
7.80E+02	1.08E-01
8.85E+02	1.11E-01
9.90E+02	1.14E-01
1.08E+03	1.16E-01
1.19E+03	1.18E-01
1.29E+03	1.20E-01
1.38E+03	1.21E-01
1.49E+03	1.23E-01
1.59E+03	1.24E-01
1.68E+03	1.25E-01
1.79E+03	1.26E-01
1.89E+03	1.27E-01
1.97E+03	1.28E-01
2.09E+03	1.29E-01
2.19E+03	1.29E-01
2.28E+03	1.30E-01
2.39E+03	1.31E-01
2.49E+03	1.31E-01
2.58E+03	1.32E-01
2.69E+03	1.32E-01
2.79E+03	1.33E-01
2.88E+03	1.33E-01
2.99E+03	1.34E-01
2.88E+03	1.33E-01
2.79E+03	1.33E-01
2.69E+03	1.32E-01

2.58E+03	1.32E-01
2.49E+03	1.31E-01
2.39E+03	1.30E-01
2.28E+03	1.30E-01
2.19E+03	1.29E-01
2.09E+03	1.29E-01
1.98E+03	1.28E-01
1.89E+03	1.27E-01
1.79E+03	1.26E-01
1.68E+03	1.25E-01
1.59E+03	1.24E-01
1.49E+03	1.23E-01
1.38E+03	1.21E-01
1.29E+03	1.20E-01
1.17E+03	1.18E-01
1.08E+03	1.16E-01
9.90E+02	1.14E-01
8.85E+02	1.11E-01
7.80E+02	1.08E-01
6.90E+02	1.04E-01
5.85E+02	9.96E-02
4.80E+02	9.32E-02
3.90E+02	8.66E-02
2.85E+02	7.60E-02
1.80E+02	6.06E-02
7.50E+01	4.04E-02
0.00E+00	-3.09E-03
-1.05E+02	-4.33E-02
-1.95E+02	-6.22E-02
-3.00E+02	-7.70E-02
-4.05E+02	-8.71E-02
-4.95E+02	-9.38E-02
-6.00E+02	-9.96E-02
-7.05E+02	-1.04E-01
-7.95E+02	-1.08E-01
-9.00E+02	-1.11E-01
-1.01E+03	-1.14E-01
-1.10E+03	-1.16E-01
-1.20E+03	-1.18E-01
-1.31E+03	-1.19E-01
-1.40E+03	-1.21E-01
-1.50E+03	-1.22E-01
-1.61E+03	-1.23E-01
-1.70E+03	-1.24E-01
-1.80E+03	-1.25E-01

-1.91E+03	-1.27E-01
-2.00E+03	-1.27E-01
-2.10E+03	-1.28E-01
-2.21E+03	-1.29E-01
-2.30E+03	-1.29E-01
-2.40E+03	-1.30E-01
-2.51E+03	-1.31E-01
-2.60E+03	-1.31E-01
-2.70E+03	-1.32E-01
-2.81E+03	-1.32E-01
-2.90E+03	-1.33E-01
-3.00E+03	-1.33E-01

S7:

-3.00E+03	-7.77E-02
-2.90E+03	-7.75E-02
-2.81E+03	-7.72E-02
-2.70E+03	-7.68E-02
-2.60E+03	-7.64E-02
-2.51E+03	-7.59E-02
-2.40E+03	-7.55E-02
-2.30E+03	-7.48E-02
-2.21E+03	-7.47E-02
-2.10E+03	-7.40E-02
-2.00E+03	-7.36E-02
-1.91E+03	-7.27E-02
-1.80E+03	-7.23E-02
-1.70E+03	-7.14E-02
-1.61E+03	-7.08E-02
-1.50E+03	-6.98E-02
-1.40E+03	-6.90E-02
-1.31E+03	-6.79E-02
-1.20E+03	-6.68E-02
-1.10E+03	-6.55E-02
-1.01E+03	-6.42E-02
-9.00E+02	-6.26E-02
-7.95E+02	-6.06E-02
-7.05E+02	-5.86E-02
-6.00E+02	-5.58E-02
-4.95E+02	-5.25E-02
-4.05E+02	-4.87E-02
-3.00E+02	-4.31E-02
-1.95E+02	-3.48E-02

-1.05E+02	-2.38E-02
0.00E+00	-1.63E-03
9.00E+01	2.22E-02
1.80E+02	3.42E-02
2.85E+02	4.28E-02
3.90E+02	4.87E-02
4.80E+02	5.26E-02
5.85E+02	5.61E-02
6.90E+02	5.88E-02
7.80E+02	6.09E-02
8.85E+02	6.26E-02
9.90E+02	6.46E-02
1.08E+03	6.57E-02
1.19E+03	6.72E-02
1.29E+03	6.84E-02
1.38E+03	6.94E-02
1.49E+03	7.01E-02
1.59E+03	7.12E-02
1.68E+03	7.18E-02
1.79E+03	7.26E-02
1.89E+03	7.34E-02
1.98E+03	7.38E-02
2.09E+03	7.44E-02
2.19E+03	7.48E-02
2.28E+03	7.54E-02
2.39E+03	7.59E-02
2.49E+03	7.64E-02
2.58E+03	7.68E-02
2.69E+03	7.74E-02
2.79E+03	7.75E-02
2.88E+03	7.80E-02
2.99E+03	7.83E-02
2.88E+03	7.81E-02
2.79E+03	7.76E-02
2.69E+03	7.72E-02
2.58E+03	7.67E-02
2.49E+03	7.64E-02
2.39E+03	7.60E-02
2.28E+03	7.53E-02
2.18E+03	7.50E-02
2.09E+03	7.43E-02
1.98E+03	7.39E-02
1.89E+03	7.31E-02
1.79E+03	7.24E-02
1.67E+03	7.16E-02

1.59E+03	7.11E-02
1.49E+03	7.00E-02
1.29E+03	6.81E-02
1.19E+03	6.71E-02
1.08E+03	6.56E-02
9.90E+02	6.45E-02
8.85E+02	6.26E-02
7.80E+02	6.09E-02
6.90E+02	5.88E-02
5.85E+02	5.61E-02
4.80E+02	5.25E-02
3.90E+02	4.89E-02
2.85E+02	4.28E-02
1.80E+02	3.43E-02
9.00E+01	2.25E-02
0.00E+00	-1.70E-04
-1.05E+02	-2.38E-02
-1.95E+02	-3.47E-02
-3.00E+02	-4.29E-02
-4.05E+02	-4.89E-02
-4.95E+02	-5.24E-02
-6.00E+02	-5.58E-02
-7.05E+02	-5.85E-02
-7.95E+02	-6.06E-02
-9.00E+02	-6.23E-02
-1.01E+03	-6.41E-02
-1.20E+03	-6.67E-02
-1.31E+03	-6.77E-02
-1.40E+03	-6.88E-02
-1.50E+03	-6.95E-02
-1.61E+03	-7.03E-02
-1.70E+03	-7.10E-02
-1.80E+03	-7.19E-02
-1.91E+03	-7.24E-02
-2.00E+03	-7.32E-02
-2.10E+03	-7.35E-02
-2.21E+03	-7.43E-02
-2.30E+03	-7.46E-02
-2.40E+03	-7.50E-02
-2.51E+03	-7.57E-02
-2.60E+03	-7.61E-02
-2.70E+03	-7.64E-02
-2.81E+03	-7.69E-02
-2.90E+03	-7.71E-02
-3.00E+03	-7.75E-02

Definitions:

SPIONs: Superparamagnetic Iron Oxide Nanoparticles

SPIONP: Superparamagnetic Iron Oxide Nanoparticle Polymer

D.I. Water: De-ionised water

SEM: Scanning electron microscopy

TEM: Transmission electron microscopy

CCD Camera: Charge-coupled devices Camera

VSM: Vibrating sample magnetometer

EDX: Energy-dispersive X-ray spectroscopy

FFT: Fast Fourier Transform

MRI: Magnetic Resonance Imaging

XRD: X-ray diffraction

List of References:

1. A.S.Teja, P.-Y. K., 2009. Progress in Crystal Growth and Characterization of Materials., p. 55.
2. Anon., 2007. Superparamagnetism: limits and applications. *Nanotechnol,* Volumn 7, pp. 1828-1836.
3. Chitose, N., Ueta, S., Seino, S. & Yamamoto, T., 2003. Radiolysis of aqueous phenol solutions with nanoparticles. 1. Phenol degradation and TOC removal in solutions containing TiO2 induced by UV, gamma-ray and electron beams Chemosphere. 50, p. 1007–1013.
4. Detlef Müller-Schultea, T. S.-R., 29 April 2005. *Thermosensitive magneticpolymer particles as contactless controllable drug carriers.* MagnaMedics GmbH, Martelenberger Weg 8, D-52066 Aachen, Germany,
5. GERCEK, H., January 2007. Poisson's ratio values for rocks. *International Journal of Rock Mechanics and Mining Sciences,* p. pp. 1–13.
6. J. I. Martín, J. N. K. L. J. L. V. a. I. K. S., January 2003. Ordered magnetic nanostructures: fabrication and properties. *Journal of Magnetism and Magnetic Materials,,* Volume 256(Issues 1-3), pp. Pages 449-501.
7. J.K.Oh, J., 2011. Iron Oxide-based Superparamagnetic polymeric nanomaterals: design, preparation and biomedical application. *Progress in Polymer Science,* pp. 36, 168-189.
8. Kodama, R. 1., 1999. *Magnetic nanoparticles. Journal of Magnetism and Magnetic Materials, 200(1-3),* pp. p.359-372..
9. L. Néel, C. R., 1949. Acad, Sci..
10. Livingston, J. D. 1., 1981. "A review of coercivity mechanisms". *Journal of Applied Physics 52: 2541–2545.,* Issue Bibcode 1981JAP....52.2544L. doi:10.1063/1.328996].
11. Lutz-f, S. S. H. A. K. L. P. U. C. R., 2006. One-pot synthesis of PEGylated ultrasmall iron-oxide nanoparticles and their in vivo evaluation as magnetic resonace imaging contrast agents. *Biomacromolecules 2006,* 7:3132-8.
12. M. Knobel, J. N., 2008. *Nanotechnol.,* 8,, pp. 2836-2857.

13. Mornet S, V. S. G. F. D. E., 2004. Magnetic nanoparticles design for medical diagnosis and therapy.. *J mater Chem,* 14:2161-75.
14. mullens, s.,Vibrating Sample Magnetometer. *Journal of Applied Physics,* Issue http://www.ebah.com.br/content/ABAAAe-y0AF/vibrating-sample-magnetometer.
15. Müller-Schulte, D., 2003.. *PCT application EP/05614,*.
16. Ni Xiaomin, S. X. Z. H. & Zhang Dongen, Y. D. Z. Q., 2004. *Studies on the one-steppreparation of iron nanoparticles in solution,* epartment of Chemistry, University of Science and Technology of China, Heifei, Anhui 230026, China:
17. Nora & Diallo, M. S., 2005-10-01;. Nanomaterials and Water Purification: Opportunities and ChallengesSavage. *Journal of Nanoparticle Research,* Vol 7(Doi: 10.1007/s11051-005-7523-5/ Issn:1388-0764), pp. page 331-342.
18. Nurmi, J. T. P. S. V. B. D. A. J. P. K. W. C. L. J. M. D. P. R. D. M., 2005. Characterization and properties of metallic iron nanoparticles: spectroscopy, electrochemistry and kinetics. *Environ. Sci. Technol,* 39, pp. 1221-1230.
19. Obare, S. O. & Meyer, G. J., 2004. Nanostructured Materials for Environmental Remediation of Organic Contaminants in Water. *Journal of Environmental Science and Health, Part A: Toxic/Hazardous Substances and Environmental Engineering,* 39(DOI:10.1081/ESE-200027010), pp. Pages: 2549-2582.
20. R. Nagarajan, T. Alan Hatton,, September 19, 2008. *Nanoparticles: Synthesis, Stabilization, Passivation, and Functionalization.* ISBN13: 9780841269699 eISBN: 9780841221390
21. S.FONER, 1959. Versatile and Sensitive Vibrating-Sample Magnetometer. p. Rev. Sci. Instrum 30 (7): 548–557..
22. Schmidt, H., 2001. Nanoparticles by chemical synthesis, processing to materials and innovative applications. *APPLIED ORGANOMETALLIC CHEMISTRY,* Issue DOI: 10.1002/aoc.169, p. 15: 331–343;.
23. Shih, W., 1931. phy6s. Rev. 38, 2051.
24. Vaseashta, A. & Marshall Univ., H. W., 2006. Nanoscale Materials, Devices, and Systems for Sensing, Detection, and Environmental Pollution Monitoring and Mitigation, Microelectronics. *25th International Conference on,,* Issue ISBN: 1-4244-0117-8.

List of Bibliography:

A.S.Teja, P.-Y. K., 2009. Progress in Crystal Growth and Characterization of Materials., p. 55.

Anon., 2007. Superparamagnetism: limits and applications. *Nanotechnol,* Volumn 7, pp. 1828-1836.

Chitose, N., Ueta, S., Seino, S. & Yamamoto, T., 2003. Radiolysis of aqueous phenol solutions with nanoparticles. 1. Phenol degradation and TOC removal in solutions containing TiO2 induced by UV, gamma-ray and electron beams Chemosphere. 50, p. 1007–1013.

Detlef Müller-Schultea, T. S.-R., 29 April 2005. *Thermosensitive magneticpolymer particles as contactless controllable drug carriers.* MagnaMedics GmbH, Martelenberger Weg 8, D-52066 Aachen, Germany,

GERCEK, H., January 2007. Poisson's ratio values for rocks. *International Journal of Rock Mechanics and Mining Sciences,* p. pp. 1–13.

J. I. Martín, J. N. K. L. J. L. V. a. I. K. S., January 2003. Ordered magnetic nanostructures: fabrication and properties. *Journal of Magnetism and Magnetic Materials,,* Volume 256(Issues 1-3), pp. Pages 449-501.

J.K.Oh, J., 2011. Iron Oxide-based Superparamagnetic polymeric nanomaterals: design, preparation and biomedical application. *Progress in Polymer Science,* pp. 36, 168-189.

Kodama, R. 1., 1999. *Magnetic nanoparticles. Journal of Magnetism and Magnetic Materials, 200(1-3),* pp. p.359-372..

L. Néel, C. R., 1949. Acad, Sci..

Livingston, J. D. 1., 1981. "A review of coercivity mechanisms". *Journal of Applied Physics 52: 2541–2545.*, Issue Bibcode 1981JAP....52.2544L. doi:10.1063/1.328996].

Lutz-f, S. S. H. A. K. L. P. U. C. R., 2006. One-pot synthesis of PEGylated ultrasmall iron-oxide nanoparticles and their in vivo evaluation as magnetic resonace imaging contrast agents. *Biomacromolecules 2006,* 7:3132-8.

M. Knobel, J. N., 2008. *Nanotechnol.,* 8,, pp. 2836-2857.

Mornet S, V. S. G. F. D. E., 2004. Magnetic nanoparticles design for medical diagnosis and therapy.. *J mater Chem,* 14:2161-75.

mullens, s.,Vibrating Sample Magnetometer. *Journal of Applied Physics,* Issue http://www.ebah.com.br/content/ABAAAe-y0AF/vibrating-sample-magnetometer.

Müller-Schulte, D., 2003.. *PCT application EP/05614,.*

Ni Xiaomin, S. X. Z. H. & Zhang Dongen, Y. D. Z. Q., 2004. *Studies on the one-steppreparation of iron nanoparticles in solution,* epartment of Chemistry, University of Science and Technology of China, Heifei, Anhui 230026, People's Republic of China;:

Nora & Diallo, M. S., 2005-10-01;. Nanomaterials and Water Purification: Opportunities and ChallengesSavage. *Journal of Nanoparticle Research,* Vol 7(Doi: 10.1007/s11051-005-7523-5/ Issn:1388-0764), pp. page 331-342.

Nurmi, J. T. P. S. V. B. D. A. J. P. K. W. C. L. J. M. D. P. R. D. M., 2005. Characterization and properties of metallic iron nanoparticles: spectroscopy, electrochemistry and kinetics. *Environ. Sci. Technol,* 39, pp. 1221-1230.

Obare, S. O. & Meyer, G. J., 2004. Nanostructured Materials for Environmental Remediation of Organic Contaminants in Water. *Journal of Environmental Science and Health, Part A: Toxic/Hazardous Substances and Environmental Engineering,* 39(DOI:10.1081/ESE-200027010), pp. Pages: 2549-2582.

R. Nagarajan, T. Alan Hatton,, September 19, 2008. *Nanoparticles: Synthesis, Stabilization, Passivation, and Functionalization.* ISBN13: 9780841269699 eISBN: 9780841221390

S.FONER, 1959. Versatile and Sensitive Vibrating-Sample Magnetometer. p. Rev. Sci. Instrum 30 (7): 548–557..

Schmidt, H., 2001. Nanoparticles by chemical synthesis, processing to materials and innovative applications. *APPLIED ORGANOMETALLIC CHEMISTRY,* Issue DOI: 10.1002/aoc.169, p. 15: 331–343;.

Shih, W., 1931. phy6s. Rev. 38, 2051.

Vaseashta, A. & Marshall Univ., H. W., 2006. Nanoscale Materials, Devices, and Systems for Sensing, Detection, and Environmental Pollution Monitoring and Mitigation, Microelectronics. *25th International Conference on,,* Issue ISBN: 1-4244-0117-8.

<New magnetic polymers> Masi, J.V. ; Univ. of Southern Maine, Gorham, ME Electrical Insulation Conference and Electrical Manufacturing Expo, 2007Issue Date : 22-24 Oct. 2007 On page(s): 352 - 355 Print ISBN: 978-1-4244-0446-9 References Cited: 4 INSPEC Accession Number: 10215071 Digital Object Identifier : 10.1109/EEIC.2007.4562641
http://ieeexplore.ieee.org/stamp/stamp.jsp?tp=&arnumber=4562641

Fabrication and properties of magnetic particles with nanometer dimensions
Charles J. O'Connor, Vladimir Kolesnichenko, Everett Carpenter, Claudio Sangregorio, Weilie Zhou, Amar Kumbhar, Jessica Sims and Fabrice Agnoli
Advanced Materials Research Institute, University of New Orleans, New Orleans, LA 70148, USA
Naval Research Lab, 4555 Overlook Avenue SE, Washington, DC 20375, USA
Universita' degli Studi di Firenze, Via Maragliano 75, 50144 Firenze, Italy
Received 18 July 2000; revised 29 November 2000; accepted 12 December 2000
Available online 10 July 2001
http://www.sciencedirect.com/science/article/pii/S0379677901003289

Particle size investigations of a multistep synthesis of PVA coated superparamagnetic nanoparticles

M. Chastellain, A. Petri, H. Hofmann

Powder Technology Laboratory, Swiss Federal Institute of Technology (EPFL), Lausanne, Switzerland

Received 22 August 2003; accepted 3 June 2004

Available online 24 July 2004

http://www.sciencedirect.com/science?_ob=MImg&_imagekey=B6WHR-4CXTW75-7-K&_cdi=6857&_user=126317&_pii=S0021979704005417&_origin=&_coverDate=10%2F15%2F2004&_sk=997219997&view=c&wchp=dGLbVzW-zSkzk&md5=1ccc90afa514e3e8cbc0486783c33afa&ie=/sdarticle.pdf

<Introduction to magnetism and magnetic materials>

0412386402 – 0412386305; Jiles, David; London : Chapman and Hall, 1991

<An Advantageous Fabrication Technology to Integrate Pressure Sensor into Multi-sensor for Micro Weather Station>

Cheng Pang 1,2, Zhan Zhao1, Jiangang Zhang Li Shi 2, Lidong Du 1,2, Zhen Fang and Yonghong Liu State Key Laboratory o/Transducer Technology, Institute o/Electronics, Chinese Academy o/Sciences, Beijing 100190, China Graduate University o/Chinese Academy o/Sciences, Beijing 100039, China

http://ieeexplore.ieee.org/stamp/stamp.jsp?tp=&arnumber=5068575

<Design, Fabrication and Testing of Nanoscale Gap Microlens Array Applied in Image Sensor> Xiangliang Jin1, 2*, Yicheng Zeng1; Faculty of Material and Photo-Electronic Physics, Xiangtan University, Xiangtan 411105, China; Superpix Micro Technology Company, Beijing, 100085, China

http://ieeexplore.ieee.org/stamp/stamp.jsp?tp=&arnumber=5460323

<Nanoscale Fabrication Using Thermal Lithography Technique With Blue Laser>

Chung Ping Liu, Yao Xian Huang, Che Chuan Hsu, Tsun Ren Jeng, and Jung Po Chen

Department of Electrical Engineering, Yuan Ze University, Chungli 320, Taiwan, R.O.C.Electronics and Optoelectronics Research Laboratories, Industrial Technology Research Institute,
Hsinchu 310, Taiwan, R.O.C.
http://ieeexplore.ieee.org/stamp/stamp.jsp?tp=&arnumber=4815973

<Fabrication and Characterization of EmergingNanoscale Memory>
SangBum Kim, Yuan Zhang, Byoungil Lee, Marissa Caldwell*, H.-S. Philip Wong
Department of Electrical Engineering, *Department of Chemistry Stanford University
Stanford, CA 94305, USA.
{kimsangb,zhangy,bilee,macaldwe,hspwong}@stanford.edu
http://ieeexplore.ieee.org/stamp/stamp.jsp?tp=&arnumber=5117686